

**APPLICATION OF GENETIC ALGORITHM TO  
OPTIMIZE MICROALGAE CULTIVATION CONDITIONS  
IN A LOCALLY ASSEMBLED FLAT PLATE  
PHOTOBIOREACTOR**

**BONFACE GODWIN MUKABANE**

**DOCTOR OF PHILOSOPHY  
(Energy Technology)**

**JOMO KENYATTA UNIVERSITY  
OF  
AGRICULTURE AND TECHNOLOGY**

**2024**

**Application of Genetic Algorithm to Optimize Microalgae Cultivation  
Conditions in a Locally Assembled Flat Plate Photobioreactor**

**Bonface Godwin Mukabane**

**A Thesis Submitted in Partial Fulfilment of the Requirements for the  
Degree of Doctor of Philosophy in Energy Technology of the Jomo  
Kenyatta University of Agriculture and Technology**

**2024**

## DECLARATION

This thesis is my original work and has not been presented for a degree in any other university

Signature.....Date.....

**Bonface Godwin Mukabane,**

This thesis has been submitted for examination with our approval as the University Supervisors

Signature.....Date.....

**Dr. Stephen N. Ondimu, PhD**  
**JKUAT, Kenya**

Signature.....Date.....

**Prof. Urbanus N. Mutwiwa, PhD**  
**JKUAT, Kenya**

Signature.....Date.....

**Dr. Paul Njogu, PhD**  
**JKUAT, Kenya**

Signature.....Date.....

**Dr. Benson B. Gathitu, PhD**  
**JKUAT, Kenya**

## **DEDICATION**

I dedicate this thesis to the Lord Jesus Christ and to my late mother for the sacrifice she did for our family. I further dedicate to my lovely wife, Deborah and children; Obuyanzi, Omulembe and Amaliah, who have been and continue to be a source of encouragement and hard work to my life.

## **ACKNOWLEDGEMENT**

My sincere thanks to the Almighty God for making this work a success. I also extend my warm regards to National Research fund (NRF) for granting me a research grant. Further, I acknowledge my supervisors: Dr. Stephen N. Ondimu, Prof. Urbanus N. Mutwiwa and Dr. Benson B. Gathitu, all from Agricultural and Biosystems Engineering Department (ABED), and Dr. Paul Njogu of The Institute of Energy and Environmental Technology (IEET), all of the Jomo Kenyatta University of Agriculture and Technology (JKUAT) for working tirelessly and closely with me, and critiquing this work and providing guidance, suggestions and encouragement throughout the research period. I also acknowledge Dr. Bilhah Eshton of The Technical University of Kenya (T-UK) for reviewing all my manuscripts.

I appreciate my colleagues from Nairobi Technical Training Institute (NTTI): Dr. Bancy Muruga, Dr. Odilia Salano and Dr. Margaret Mwangi, microbiologists, for guidance in isolation and characterization of the microalgae. I am also grateful to my colleague in the Department of Mechanical and Chemical Engineering of NTTI, Mr. Elijah Kamau Mwangi for guidance and assistance on use of MATLAB and SPSS. I also appreciate Hezron Kiprotich Bii, a technician of Medical Laboratory of NTTI and all technical staff in the School of Food Science and Technology (JKUAT), more specifically; Jessica Oruka and David Vodha. I also acknowledge my research assistants; Samuel Ouma, Hezron Kiprotich Bii and Dominic Magut.

I am forever indebted to my dear wife, Deborah and children; Obuyanzi, Omulembe and Amaliah, for support and understanding for the many hours I spent in my study room away from them. The list is endless and I want to thank those who contributed to the success of this work. To all, I say thank you very much and may the Good LORD bless you mightily.

## **TABLE OF CONTENTS**

<b>DECLARATION.....</b>	<b>ii</b>
<b>DEDICATION.....</b>	<b>iii</b>
<b>ACKNOWLEDGEMENT .....</b>	<b>iv</b>
<b>TABLE OF CONTENTS.....</b>	<b>v</b>
<b>LIST OF TABLES .....</b>	<b>xi</b>
<b>LIST OF FIGURES .....</b>	<b>xiv</b>
<b>SYMBOLS AND FORMULAE .....</b>	<b>xvii</b>
<b>LIST OF APPENDICES .....</b>	<b>xxiv</b>
<b>ACRONYMS AND ABBREVIATIONS.....</b>	<b>xxv</b>
<b>ABSTRACT.....</b>	<b>xxx</b>
<b>CHAPTER ONE .....</b>	<b>1</b>
<b>INTRODUCTION.....</b>	<b>1</b>
1.1 Background of the Study.....	1
1.2 Statement of the Problem .....	4
1.3 Justification .....	6
1.4 Hypotheses .....	8
1.5.1 Main Objective.....	8

1.5.2 Specific Objectives.....	8
1.6 Research Questions .....	9
1.7 Scope of Study .....	9
1.8 Limitations of the Study.....	9
<b>CHAPTER TWO .....</b>	<b>11</b>
<b>LITERATURE REVIEW.....</b>	<b>11</b>
2.1 Introduction.....	11
2.2 Microalgae as a Feedstock for Biodiesel Production.....	14
2.2.1 Species and Strains of Microalgae and Lipid Composition.....	16
2.2.2 Fatty Acid Profile of Various Microalgae Strains.....	18
2.2.3 Fatty Acid Methyl ester (FAME) Composition .....	19
2.3 Metabolic Pathways .....	20
2.4 Techniques for Producing Axenic Microalgal Cultures .....	22
2.4.1 Streak Plate Method.....	22
2.4.2 Dilution in Liquid Media .....	22
2.4.3 Fluorescence Activated Cell Sorting.....	24
2.4.4 Micromanipulation.....	25
2.4.5 Density Centrifugation.....	26

2.4.6 Ultra Violet Radiation .....	27
2.4.7 Addition of Antibiotics .....	27
2.5 Microalgae Cultivation Systems .....	28
2.6 Harvesting .....	31
2.6.1 Sedimentation.....	35
2.6.2 Flotation .....	35
2.6.3 Centrifugation .....	36
2.7 Pilot-Scale Microalgae Production .....	38
2.8 Challenges for Commercialization of Microalgal Biodiesel.....	38
2.9 Optimization.....	39
2.9.1 Genetic Algorithms .....	40
2.9.2 Simulated Annealing.....	47
2.9.3 Particle Swarm Optimization .....	53
2.9.4 Ant Colony Optimization.....	58
2.9.5 Optimization of Fuzzy Systems .....	64
2.9.6 Neural-Network-Based Optimization .....	69
2.10 Optimizing the Biomass Yield of Microalgae Using Genetic Algorithm.....	72
2.10.1 Genetic Algorithm Solver Options .....	72



2.11 Research Gaps .....	79
2.12 Conceptual Framework .....	81
<b>CHAPTER THREE .....</b>	<b>82</b>
<b>MATERIALS AND METHODS .....</b>	<b>82</b>
3.1 Introduction .....	82
3.2 Research Design .....	82
3.2.1 Experimental Design .....	82
3.3 Photobioreactor Tanks Design and Dimensions .....	83
3.4 Study Design .....	86
3.4.1 Computer Optimization Model for Simulating the Biomass Yield of Microalgae .....	86
3.4.2 Isolation and Characterization of Strains of Microalgae.....	96
3.4.3 Validation of the Performance of the Developed Computer Simulation Model .....	104
3.4.4 Investigation of the Effect of Light Wavelength and Strain on the Biomass and Lipid Yield .....	109
3.5 Statistical Analysis .....	110
<b>CHAPTER FOUR.....</b>	<b>111</b>
<b>RESULTS AND DISCUSSION .....</b>	<b>111</b>

4.1 Introduction.....	111
4.2 Computer Optimization Model for Simulating Microalgae Biomass Yield .....	111
4.2.1 Optimization Using Response Surface Methodology and Genetic Algorithm .....	113
4.3 Isolation and Characterization of Strains of Microalgae.....	133
4.3.1 Abiotic Properties of Water Samples Collected.....	133
4.3.2 Isolation.....	134
4.3.3 Comparison of Growth Pattern of Microalgal Isolates .....	135
4.4 Validation of the Performance of the Developed Computer Simulation Model..	138
4.4.1 Biomass Yield on Light Energy.....	138
4.4.2 Validation of the Optimization Model .....	141
4.4.3 Modification of the Optimization Model.....	143
4.5 Effect of Light Wavelength and Strain on the Biomass and Lipid Yield of Microalgae.....	143
4.5.1 Effect of Light Wavelength and Strain on the Biomass Yield of Microalgae.....	143
4.5.2 Effect of Light Wavelength and Strain on the Lipid Yield of Microalgae ...	150

<b>CHAPTER FIVE.....</b>	<b>156</b>
<b>CONCLUSIONS AND RECOMMENDATIONS.....</b>	<b>156</b>
5.1 Conclusions.....	156
5.2 Recommendations.....	157
5.2.1 Recommendations from the Study.....	157
5.2.2 Recommendations for Further Studies.....	157
<b>REFERENCES.....</b>	<b>159</b>
<b>APPENDICES.....</b>	<b>189</b>

## LIST OF TABLES

<b>Table 2.1:</b> Comparison of Some Sources of Biodiesel.....	15
<b>Table 2.2:</b> Lipid Content of Various Species of Microalgae.....	17
<b>Table 2.3:</b> A Comparison of Growing Microalgae in Open Ponds and Photobioreactors .....	31
<b>Table 2.4:</b> Maximum Removal Rates of Various Flocculants for the Removal of Algal Biomass .....	35
<b>Table 2.5:</b> Harvesting Methods, Effectiveness and Energy Requirements .....	37
<b>Table 2.6:</b> Research Gaps.....	79
<b>Table 3.1:</b> Lower and Upper Bounds of Optimization Model Variables .....	90
<b>Table 3.2:</b> Values for the GA Options.....	93
<b>Table 3.3:</b> Independent Variables and Their Levels in CCD .....	95
<b>Table 3.4:</b> Independent Variables and Their Levels in CCD with Outlier Removed .....	96
<b>Table 3.5:</b> Components of the MBL Medium .....	98
<b>Table 4.1:</b> Optimal Cultivation Conditions According to Equation 3.1 Using GA .....	112
<b>Table 4.2:</b> CCD Matrix with Simulated Biomass Yields.....	113
<b>Table 4.3:</b> Summary for Model Fit- Sequential Model Sum of Squares .....	114
<b>Table 4.4:</b> ANOVA for Response Surface Quadratic Model.....	115
<b>Table 4.5:</b> CCD Matrix with Simulated Biomass Yields and Outlier Removed .....	116

<b>Table 4.6:</b> Summary for Model Fit- Sequential Model Sum of Squares for Modified Data .....	117
<b>Table 4.7:</b> ANOVA for Response Surface Quadratic Model with Outlier Removed ...	118
<b>Table 4.8:</b> ANOVA for Reduced Quadratic Model .....	119
<b>Table 4.9:</b> Coefficients for the Reduced Quadratic Model in Terms of Coded factors	120
<b>Table 4.10:</b> CCD Matrix with Simulated and Predicted Biomass Yields .....	121
<b>Table 4.11:</b> Abiotic Properties of Water Samples before Sampling .....	133
<b>Table 4.12:</b> Growth Characteristics of the Microalgal Strains .....	137
<b>Table 4.13:</b> Biomass Yield for the Simulation and Experiment .....	139
<b>Table 4.14:</b> Validation of Model Results .....	141
<b>Table 4.15:</b> Correlation Results for the Model and Experimental Values .....	142
<b>Table 4.16:</b> Student's <i>t</i> -Test Results for Model Values .....	142
<b>Table 4.17:</b> Yield (g) of Microalgae under Different Light Wavelengths .....	144
<b>Table 4.18:</b> ANOVA Table for Microalgal Biomass Yield with Blocking .....	149
<b>Table 4.19:</b> ANOVA Table for Microalgal Biomass Yield without Blocking .....	150
<b>Table 4.20:</b> Lipids (%) Produced by Microalgae under Different Light Wavelengths .	150
<b>Table 4.21:</b> ANOVA Table for Lipid Yield under Different Light Wavelengths with Blocking .....	152

**Table 4.22:** ANOVA Table for Lipid Yield under Different Light Wavelengths without  
Blocking ..... 154

## LIST OF FIGURES

<b>Figure 2.1:</b> Serial Dilution Block Diagram .....	23
<b>Figure 2.2:</b> Fluorescence Activated Cell Sorting Method for Particle Separation Based on Differential Fluorescent Rendering of Cells in the Stream .....	25
<b>Figure 2.3:</b> Micromanipulation of an Enrichment Sample with a Capillary Micropipette to Obtain a Uni-Algal Culture .....	26
<b>Figure 2.4:</b> Simulated Annealing Procedure .....	52
<b>Figure 2.5:</b> Graphical Representation of the Aco Process in the Form of a Multi-Layered Network .....	59
<b>Figure 2.6:</b> Concept of Fuzzy Decision .....	67
<b>Figure 2.7:</b> Single Neuron and Its Output .....	70
<b>Figure 2.8:</b> Multilayer Feedforward Network .....	72
<b>Figure 3.1:</b> Illustration of the PBR System .....	84
<b>Figure 3.2:</b> Flat Plate Perspex Photobioreactor Used in the Study .....	85
<b>Figure 3.3:</b> MATLAB® Desktop Window .....	88
<b>Figure 3.4:</b> The Objective/Fitness MATLAB Function .....	88
<b>Figure 3.5:</b> Graphics User Interface for MATLAB® Showing Tool Bar for the “APP” Icon .....	89
<b>Figure 3.6:</b> Graphics User Interface for MATLAB® Showing the Optimization Tool .....	90
<b>Figure 3.7:</b> Graphics User Interface for MATLAB® Showing GA Solver .....	91

<b>Figure 3.8:</b> Graphics User Interface for MATLAB® Showing GA Solver Options .....	92
<b>Figure 3.9:</b> Experimental Setup for Initial Isolation Using Nutrient Agar and Peptone Water .....	99
<b>Figure 3.10:</b> Experimental Setup for Isolation by Serial Dilution Method in MBL.....	100
<b>Figure 3.11:</b> Experimental Setup for Maintaining Microalgae Stocks .....	101
<b>Figure 3.12:</b> Experimental Setup for the Determination of Growth of the Two Isolated Unialgal Microalgae and for Biomass Growth for Inoculation into PBRs .	103
<b>Figure 3.13:</b> Experimental Set-Up .....	105
<b>Figure 3.14:</b> Drying of Harvested Microalgae in a Biomass Greenhouse .....	107
<b>Figure 3.15:</b> Dried Microalgae Biomass .....	107
<b>Figure 4.1:</b> Results of Simulation Model Equation 3.1 .....	112
<b>Figure 4.2:</b> Normal Probability of Externally Studentized Residuals.....	123
<b>Figure 4.3:</b> A Graph of Predicted Microalgae Yield against Simulated Microalgae Yield .....	123
<b>Figure 4.4:</b> A Graph of Externally Studentized Residuals against Run Number.....	124
<b>Figure 4.5:</b> A Graph of Externally Studentized Residuals against Predicted Values ...	125
<b>Figure 4.6:</b> A Graph of Externally Studentized Residuals against Growth Rate.....	126
<b>Figure 4.7:</b> A Graph of Externally Studentized Residuals against Biomass Concentration .....	127



<b>Figure 4.8:</b> A Graph of Externally Studentized Residuals against Photon Flux Density .....	128
<b>Figure 4.9:</b> Contour Plot for Biomass Concentration against Growth Rate .....	130
<b>Figure 4.10:</b> Contour Plot for Photon Flux Density against Biomass Concentration ...	131
<b>Figure 4.11:</b> RSM Plot: Effect of Photon Flux Density and Biomass Concentration on Microalgae Yield.....	132
<b>Figure 4.12:</b> RSM Plot: Effect of Biomass Concentration and Growth Rate on Microalgae Yield.....	133
<b>Figure 4.13:</b> Microscope Images Showing Different Morphologies of the Microalgae Obtained at the End of the Isolation Process (X10-X100).....	135
<b>Figure 4.14:</b> Growth Pattern for Strains: <i>Chlorella Emersonii</i> and <i>Chlorella Vulgaris</i> .....	136
<b>Figure 4.15:</b> Growth Profile of Microalgae Strains under White Wavelength .....	144
<b>Figure 4.16:</b> Growth Profile of Microalgae Strains under Blue Wavelength .....	145
<b>Figure 4.17:</b> Growth Profile of Microalgae Strains under Red Wavelength .....	146

## SYMBOLS AND FORMULAE

<b>a</b>	Weighted Sum of Inputs
<b>A</b>	Illuminated Reactor Surface Area (m <sup>2</sup> ); Subset
<b>A</b>	Denotes Arcs Traveled by Ant <i>k</i> in Its Path from Home to Destination
<b><math>\alpha</math></b>	Degree of Significance of the Pheromones
<b>C</b>	Carbon
<b><i>c</i></b>	Fractional Value
<b><i>c</i><sub>1</sub></b>	Individual Learning Rate
<b><i>c</i><sub>2</sub></b>	Group Learning Rate
<b>CaCl<sub>2</sub>.2H<sub>2</sub>O</b>	Calcium Chloride Dihydrate
<b>CO<sub>2</sub></b>	Carbon Dioxide
<b>CoCl<sub>2</sub>.6H<sub>2</sub>O</b>	Hydrated Cobalt Chloride
<b>CuSO<sub>4</sub>.H<sub>2</sub>O</b>	Hydrated Copper Sulphate
<b><i>C</i><sub><i>x</i></sub></b>	Biomass Concentration (gL <sup>-1</sup> )
<b><i>E</i></b>	Energy of a System (Jmol <sup>-1</sup> )
<b><i>E</i><sub><i>i</i></sub></b>	Energy of State <i>x<sub>i</sub></i>
<b><math>\Delta E</math></b>	Change in Energy (Jmol <sup>-1</sup> )

$\Delta t$	Change in Time (Days)
$f(\mathbf{a})$	Sigmoid Function
$f_{best}$	Best Value of the Objective Function among the Paths Taken by the $N$ Ants
$f_{worst}$	Worst Value of the Objective Function among the Paths Taken by the $N$ Ants
$F_i$	Fitness
$\mathbf{f}_i$	Objective Function
$\text{FeCl}_3 \cdot \text{H}_2\text{O}$	Hydrated Iron Chloride
$F(X)$	Fitness Function
$f(X)$	Objective Function
$f(X_i)$	Objective Function of Design Point $X_i$
$\Delta \mathbf{f}$	Change in Functional Value
$G_{best}$	Historical Best Value of Any of the $N$ Particles
$g_i(X)$	Constraint
$g_j(X)$	Function
$g_j(x)$	Constraint
$g_j^{(l)}$	Lower Bound Value

$g_j^{(u)}$	Upper Bound Value
$G_j$	Fuzzy Interval to Which the Function $g_j(\mathbf{X})$ Should Belong
<b>HCL</b>	Hydrochloric Acid
$h_j(\mathbf{X})$	Constraint
<b>H<sub>2</sub>SO<sub>4</sub></b>	Sulphuric Acid
$i$	Iteration Number; Node
$i_{max}$	Maximum Number of Generations or Iterations
$j$	Node
$k$	Boltzmann's Constant; Ant
<b>K<sub>2</sub>HPO<sub>4</sub></b>	Potassium Hydrogen Phosphate
$l$	Total String Length
$L_k$	Length of Path Traveled by the $k^{th}$ Ant
$m$	Population Size
<b>MgSO<sub>4</sub>·7H<sub>2</sub>O</b>	Magnesium Sulphate Heptahydrate
<b>MnCl<sub>2</sub>·4H<sub>2</sub>O</b>	Hydrated Manganese Chloride
$N$	Number of Particles in a Swarm
$N_i^{(k)}$ node $i$	Set of Neighbourhood Nodes of Ant $k$ When Located at node $i$

$n$	Number of Iterations
$\mu$	Growth Rate ( $\text{h}^{-1}$ )
$\gamma$	Gamma
$\emptyset(X)$	Penalty Function
N	Nitrogen
<b>Na<sub>2</sub>EDTA</b>	diSodium Ethylenediaminetetraacetic Acid
<b>NaHCO<sub>3</sub></b>	Sodium Hydrogen Carbonate
<b>NaMoO<sub>4</sub>.2H<sub>2</sub>O</b>	Hydrated Sodium Molybdate
<b>NaNO<sub>3</sub></b>	Sodium Nitrate
<b>NaOH</b>	Sodium Hydroxide
<b>NH<sub>4</sub><sup>+</sup></b>	Ammonium Ions
$nq$	Total String Length
<b>NO<sub>3</sub><sup>-</sup></b>	Nitrate Ions
<b>Na<sub>2</sub>SiO<sub>3</sub>.9H<sub>2</sub>O</b>	Hydrated Sodium Silicate
<b>P</b>	Phosphorous
<b>P</b>	Parameter
$P_{best,j}$	Historical Best Value of $X_j(i)$
$p_c$	Crossover Probability

$p_i$	Probability of Selecting $i^{th}$ String
$P_{ij}^{(k)}$	Probability of Choosing $j$ as the Next Node
$p_m$	Mutation Probability
$P(E)$	Probability of Achieving Energy Level $E$
$PO_4^{3-}$	Phosphate Ions
$q$	String Length
$Q$	Constant
$\rho$	Pheromone Decay Factor or Evaporation Rate
$r_1, r_2$	Uniformly Distributed Random Numbers in the Range 0 and 1
$r_i$	Penalty Parameter Associated with $g_i(\mathbf{X})$
$R$	Correlation Coefficient
$R_j$	Penalty Parameter Associated with $h_j(\mathbf{X})$
$(s_f)_{max}$	Permissible value of standard deviation of fitness values of the population
$\tau_{ij}$	Pheromone Trail
$\tau_{ij}^{(old)}$	Pheromone Amount of the Previous Iteration left after Evaporation

$\Delta\tau^{(k)}$	Amount of Pheromone Dropped by $k^{th}$ Ant before Heading Back to Its Home Node
$\Delta\tau_{ij}^k$	Amount of Pheromone Deposited on Arc $ij$ by the Best Ant
$\theta$	Inertia Term/Weight
$\theta_{max}$	Initial Value of the Inertia Weight
$\theta_{min}$	Final Value of the Inertia Weight
$\sigma$	Stress ( $psi$ )
$\sigma_{max}$	Maximum Stress ( $psi$ )
$\mu_A$	Characteristic Function
$\mu_A(x), \mu_f(x), \mu_g(x)$	Membership Function
$\mu_D(x), \mu_s(x)$	Membership Function
$S$	Fuzzy Feasible Region
$T$	Temperature (K)
$T_d$	Doubling Time (Days)
$V$	Volume of the Reactor Content (L)
$V_{(j)}^{(i)}$	Velocity of Particle $j$ in Iteration $i$
$w_i$	Weight/Gain Associated with Input $i$

$x$	Generic Element; Depth of Crane Girder
$X$	Classical Crisp Set of Objectives or Universe
$X$	Design Vector
$X^*$	Optimum Value
$X_i$	Design Variable; Design Point (State)
$X^{(l)}$	Lower Bound of $X$
$X^{(u)}$	Upper Bound of $X$
$X_{(j)}^{(i)}$	Position of Particle $j$ in Iteration $i$
$\zeta$	A Parameter Used to Control the Scale of the Global Updating of the Pheromone
$Y$	Yield (gmolphotons <sup>-1</sup> )
<b>ZnSO<sub>4</sub>.7H<sub>2</sub>O</b>	Hydrated Zinc Sulphate



## LIST OF APPENDICES

<b>Appendix I:</b> Determination of Photosynthetic Efficiency .....	189
<b>Appendix II:</b> Analysis of Variance .....	191
<b>Appendix III:</b> Publications .....	194

## ACRONYMS AND ABBREVIATIONS

<b>ABED</b>	Agricultural and Biosystems Engineering Department
<b>ANOVA</b>	Analysis of Variance
<b>ATP</b>	Adenosine triphosphate
<b>CCD</b>	Central Composite Design
<b>CFPP</b>	Cold filter plugging point
<b>CSIRO</b>	Commonwealth Scientific and Industrial Organization
<b>DHA</b>	Docosahexaenoic Acid
<b>d. f.</b>	Degrees of freedom
<b>EA</b>	East Africa
<b>EDTA</b>	Ethylenediaminetetraacetic acid
<b>EIA</b>	Energy Information Administration
<b>EJ</b>	Exajoule
<b>EPA</b>	Eicosapentaenoic Acid
<b>FACS</b>	Fluorescence Activated Cell Sorting
<b>FAMES</b>	Fatty Acid Methyl Esters
<b>FAO</b>	Food and Agriculture Organization
<b>FFAs</b>	Free Fatty Acids

<b>FPPBR</b>	Flat Plate Photobioreactor
<b>FPPPBR</b>	Flat Plate Perspex Photobioreactor
<b>Ft</b>	Feet
<b>GA</b>	Genetic Algorithm
<b>GAs</b>	Genetic Algorithms
<b>GHG</b>	Greenhouse gases
<b>IBM</b>	International Business Machines
<b>IEA</b>	International Energy Agency
<b>IEET</b>	Institute of Energy and Environmental Technology
<b>ISO</b>	International Organization of Standards
<b>JKUAT</b>	Jomo Kenyatta University of Agriculture and Technology
<b>KATTI</b>	Kenya Association of Technical Training Institutions
<b><i>lb</i></b>	Pound
<b>LCA</b>	Life Cycle Assessment
<b>LED</b>	Light Emitting Diodes
<b>MATLAB</b>	Matrix Laboratory
<b>MAE</b>	Mean Absolute Error
<b>MAPE</b>	Mean Absolute Percentage Error

<b>MBL</b>	Marine Biological Laboratory
<b><math>M_{dw}</math></b>	Dry weight
<b>MS</b>	Mean square
<b>MSE</b>	Mean Square Error
<b><math>M_{toe}</math></b>	Million tons of oil equivalents
<b>NADP</b>	Nicotinamide adenine dinucleotide phosphate
<b>NRF</b>	National Research Fund
<b>NTTI</b>	Nairobi Technical Training Institute
<b>OD</b>	Optical density
<b>OECD</b>	Organization for Economic Cooperation and Development
<b>ORPs</b>	Open Raceway Ponds
<b>PAR</b>	Photosynthetically Active Radiation
<b>PASAE</b>	Pan African Society for Agricultural Engineers
<b>PBR</b>	Photobioreactor
<b>PBRs</b>	Photobioreactors
<b>PC</b>	Personal Computer
<b>PET</b>	Polyethylene terephthalate
<b><math>PFD_{in}</math></b>	Photon Flux Density ( $\mu\text{mol photons m}^{-2}\text{s}^{-1}$ )

<b>PSI</b>	Pounds per Square Inch
<b>PUFAs</b>	Polyunsaturated fatty acids
<b>PVC</b>	Polyvinyl chloride
<b>PVD</b>	Polyvinylpyrrolidone
<b>RAM</b>	Random Access Memory
<b>RCBD</b>	Randomized Complete Block Design
<b>REG</b>	Renewable Energy Group
<b>REN21</b>	Renewable Energy Policy Network for the 21 <sup>st</sup> Century
<b>RMSE</b>	Root Mean Square Error
<b>RSM</b>	Response Surface Methodology
<b>SA</b>	Simulated Annealing
<b>SD</b>	Standard deviation
<b>SDG</b>	Sustainable Development Goal
<b>SDGs</b>	Sustainable Development Goals
<b>SoBEE</b>	School of Biosystems and Environmental Engineering
<b>SPSS</b>	Statistical Package for Social Scientists
<b>SS</b>	Sum of squares
<b>T-UK</b>	Technical University of Kenya

<b>TVET</b>	Technical Vocation Education Training
<b>UK</b>	United Kingdom
<b>US</b>	United States
<b>USA</b>	United States of America
<b>USD</b>	United States Dollar
<b>UV</b>	Ultraviolet
<b>VIF</b>	Variance Inflation Factor
<b>VIS</b>	Visible

## ABSTRACT

The availability of more cost-effective sources of energy is a key driver of any economic development more so for a developing country like Kenya. The interest in biofuels is motivated by: the fluctuating oil prices and recognizing that the global fossil fuel reserves are exhausting fast; concern about fossil fuel emissions polluting the environment and resultant environmental change due to such emissions. Biodiesel, as a clean and renewable combustible, is a good alternative to replace mineral diesel. The main objective of this study was to apply Genetic Algorithm (GA) in the optimization of microalgae cultivation conditions in a locally assembled flat plate perspex photobioreactor (FPPPBR) at pilot plant scale. An optimization model was developed using GA to predict the biomass yield of microalgae incubated in a FPPPBR. Samples from which microalgae were isolated were collected aseptically in February 2021. Isolation was done by streaking, pour plate and serial dilution methods in Marine Biological Laboratory media at 27 °C, under continuous light intensity of 15  $\mu\text{mol photons m}^{-2}\text{s}^{-1}$ . The model was validated using the strain that possessed a higher growth rate incubated in FPPPBR under 400-700 nm wavelength. As the validation process was ongoing, the influence of light quality and type of strain on yield was being investigated concurrently. This was replicated thrice. The validation of the simulation model was done by comparing simulated and experimental data. The statistical parameters used were: mean square error (MSE), mean absolute percentage error (MAPE), mean absolute error (MAE), root mean square error (RMSE), correlation coefficient (R) and student's *t*-test. Statistical analyses were performed using IBM SPSS statistics 25 software, Design expert 13 and MATLAB R2016a. The simulation results produced optimum microalgae yield as:  $0.250715 \pm 0.001608 \text{ gmol photons}^{-1}$  and optimal cultivation conditions as; biomass concentration of  $0.1 \text{ gL}^{-1}$ , microalgae growth rate of  $0.0102 \text{ h}^{-1}$ , photon flux density of  $100 \mu\text{mol photons m}^{-2}\text{s}^{-2}$ , volume of reactor of 192 L and illuminated PBR surface area of  $2.16 \text{ m}^2$ . Two strains were obtained and investigated namely, *Chlorella emersonii* and *Chlorella vulgaris*, whose growth rate was found to be  $0.16 \text{ day}^{-1}$  and  $0.244 \text{ day}^{-1}$  respectively. The experimental biomass yield was  $0.438423 \pm 0.027122 \text{ gmol photons}^{-1}$  and the RMSE value for the optimization model was 0.1889, the MSE, MAE and MAPE were; 0.0357, 0.2717 and 42.67% respectively, R value of 0.231 and *t*-value of -165.091 at 5% level of significance. The *C. vulgaris* yielded;  $9.30 \pm 0.57 \text{ g}$ ,  $8.32 \pm 0.48 \text{ g}$  and  $7.78 \pm 0.67 \text{ g}$  under 400-700, 430-480 and 610-680 nm wavelength, respectively. The corresponding values for the *C. emersonii* were;  $5.88 \pm 0.26 \text{ g}$ ,  $5.46 \pm 0.20 \text{ g}$  and  $5.12 \pm 0.14 \text{ g}$ . The %lipids produced by the *C. vulgaris* were; 43.61, 35.87 and 34.56 respectively, under 430-480, 610-680 and 400-700 nm wavelengths. The *C. emersonii* yielded 33.50, 29.80 and 28.03 %lipids under 610-680, 430-480 and 400-700 nm wavelengths, respectively. *C. vulgaris* has potential for microalgae cultivation for biomass and biofuel production. A new optimization model was developed to predict microalgal biomass yield and the strains grown in this study produced the highest biomass under 400-700 nm wavelength. *C. vulgaris* produced highest lipids (43.61%) under 430-480 nm whereas *C. emersonii* yielded highest lipids (33.50%) under 610-680 nm. GA and RSM could be used to optimize microalgae cultivation conditions.

# CHAPTER ONE

## INTRODUCTION

### 1.1 Background of the Study

Increased interest in biofuels is mainly driven by the fluctuating oil prices and recognition of the fact that the global fossil fuel reserves are getting exhausted fast (Mata *et al.*, 2010; Martin, 2013; Behera *et al.*, 2015). Also, concerns about environmental pollution and resultant environmental change due to fossil fuel emissions, the requirements of the Paris Agreement of 2015 of “net zero emissions of carbon” as a long-term global goal between 2050 and 2100, the provision of alternative outlets for agricultural producers (Mukabane, 2015) and foreign exchange savings (Demirbas, 2008). Owing to endless and increasing combustion of fossil carbon, the amount of greenhouse gas, particularly CO<sub>2</sub> has increased (Höök & Tang, 2013). As a consequence, global warming and climate change are threatening food security, ecological stability and social welfare (Chisti, 2008; Christenson & Sims, 2011). Globally, biofuels development is to address energy security, poverty mitigation and economic development (Gheewala *et al.*, 2013). According to Mitchell (2011), biofuel production in Africa will increase national energy security and foreign exchange saving by reducing oil imports. Biofuels have the potential to provide socio-economic benefits like having industrial plants in rural areas, creating employment, encouraging other economic activities and influencing other related industries (Gilio & Moraes, 2016; Moraes *et al.*, 2016). The transportation and energy sector are the two leading sources globally, responsible for the generation of 20% and 60% of greenhouse gases (GHG) emissions, respectively (Stephens *et al.*, 2010; Khatiwada, 2013; International Energy Agency [IEA], 2015). It is projected that with the development of emerging economies the global consumption of energy will rise considerably and this will lead to more environmental devastation (Stephens *et al.*, 2010).

Sustainable development addresses humanity’s aspirations for an improved life. The Sustainable Development Goals (SDGs) guarantee a better and sustainable future for all,



balancing the economic, social and environmental development (Fonseca & Carvalho, 2019). Access to clean and affordable energy (SDG7) is an indispensable component of achieving other SDGs such as SDG1 (No poverty), SDG2 (Zero hunger), SDG3 (Good Health and well-being), SDG8 (Decent work and economic growth) and SDG13 (Climate action) (Fonseca *et al.*, 2020). SDG1 targets to end poverty, SDG2 to end hunger and realize food security, SDG3 to safeguard healthy lives, SDG8 to promote economic growth and fruitful employment, and SDG13 to take urgent action to combat climate change and its impacts (Fonseca *et al.*, 2020). Biofuels are anticipated to be clean and affordable sources of energy. Thus the production of biodiesel, a biofuel, will achieve SDG7 and thus simultaneously achieve the other SDGs (Machandi, 2021).

Global biofuel production has been increasing rapidly over the last decade, but the expanding biofuel industry has recently raised pertinent concerns. In particular, the sustainability of many first-generation biofuels, fuels made from edible sugars and starch, has been increasingly questioned over concerns such as reported displacement of food crops, effects on the environment and climate change (IEA, 2008). In general, there is growing consensus that if significant emissions reductions in the transport sector are to be achieved, biofuel technologies must become more efficient in terms of net lifecycle greenhouse gas emission reduction while at the same time be socially and environmentally sustainable. It is increasingly understood that most first-generation biofuels, with the exception of sugarcane ethanol, will likely have a limited role in the future transport fuel mix (IEA, 2008).

Biodiesel is a mixture of fatty acid alkyl monoesters derived from vegetable oils and fats. It can be used as a replacement of fossil oil derived diesel because of their structural similarity. Biodiesel, a major biofuel, is produced using vegetable oil, plant oil, and animal fat. Biodiesel is an alternative fuel for diesel and most diesel engines can use 100% biodiesel (Cheng, 2010). The main feedstock currently used for biodiesel production includes: soybean, canola seed, rapeseed, sunflower, palm, coconut, jatropha, karanja, used fried oil and animal fats (Khan *et al.*, 2009). A great challenge of using vegetable

oils for biodiesel production is the availability of crop land for oil production to produce enough biodiesel that significantly replaces the current fossil fuel consumption. Chisti (2007) estimated that it would take 24% of the existing crop land in the US to grow oil palm that is considered as a high yield oil crop or over three times of the current cropland in the US to grow soybean to produce enough biodiesel that would replace 50% of the transportation fuel in the US. There are research activities on using alternative oils such as waste oils from kitchens and restaurants and microalgal oils for biodiesel production. Miao and Wu (2006) studied biodiesel production from heterotrophic microalgal oil. Shah *et al.* (2007) investigated the utilization of restaurant waste oil as

a precursor for sophorolipid and biodiesel production. Zhang *et al.* (2003) evaluated the Biodiesel production from waste cooking oil including economic analysis. A great advantage of using microalgal oil over vegetable oils for biodiesel production is that the production of algal oil does not necessarily need cropland. Furthermore, it has a much higher oil yield per acre of land because the microalgae can be grown in 3 dimensions in photo-reactors (Cheng, 2010). However, a big challenge of biodiesel production using algal oil is that the cost of algal oil production is prohibitively high.

The cost of energy is a threat to Kenya's realization of Vision 2030 strategic plan, whereby Kenya wants to be a middle income nation by this period. Kenya's production energy mix include 52.1% of hydro, 32.5% of fossil fuels, 13.2% geothermal energy, 1.8% of biogas cogeneration, and 0.4% of wind. Gasoline, hydro and geothermal powers are unable to meet Kenya's energy demand. This coupled with fossil fuel price fluctuations due to political situation in producing countries may reduce Kenya's economic growth expectations. This is currently being worsened by the ongoing war between Russia and Ukraine. As a consequence nowadays, the tendency is to turn to biofuels to fill the gap between energy demand and supply.

Biofuels are divided into three categories (Larson, 2008; Luque *et al.*, 2008; Ahmad *et al.*, 2011):

- i. First-generation biofuels made largely from edible sugars and starches, such as sugar cane and corn.
- ii. Second-generation biofuels made from non-edible lignocellulosic materials, for example maize stover, wheat straw, saw dust, sugar cane bagasse and sweet sorghum bagasse.
- iii. Third-generation biofuels made from algae and microbes.
- iv. Fourth-generation-fuel cells.

Biofuels can also be classified as:

- i. Simple sugar based like those from sugar cane and sweet sorghum
- ii. Starch based –maize, cassava and microalgae
- iii. Lignocellulose based- stalks, straws, grass and other agricultural wastes
- iv. Microorganism based biodiesel

## **1.2 Statement of the Problem**

Kenya's demand for energy has increased to outstrip supply. This has continued to push the prices of fossil fuels and hydroelectricity higher up. The consequence of this is that it has led to the increase of prices of crucial goods and services thus lowering the standard of living of most Kenyans. If this trend continues, it will reduce economic and industrial growth hence jeopardizing the realization of Vision 2030. Sustainable production of renewable energy is being debated globally since it is increasingly understood that first generation biofuels, primarily produced from food crops and mostly oil seeds, compete for arable land, freshwater or biodiverse natural landscapes and are limited in their ability to achieve targets for biofuel production (Kalpesh *et al.*, 2012). Due to continuous and increasing combustion of fossil carbon, the amount of greenhouse gases has increased. As

a result, global warming and climate change are threatening ecological stability, food and nutritional security and social welfare (Chisti, 2008; Christenson & Sims, 2011). The transportation and energy sector are the two major sources responsible for the generation of 20% and 60% of greenhouse gases (GHG) emissions respectively; and it is expected that with the development of emerging economies, the global consumption of energy will rise considerably and this will lead to more environmental damage (Stephens *et al.*, 2010). These concerns have increased the interest in developing second and third generation biofuels such as lignocellulosics and microalgae, respectively, which potentially offer great opportunities in the longer term and do not need to compete for arable land and precious freshwater (Chisti, 2007; Schenk *et al.*, 2008).

The two main methods of infrastructure considered suitable for cultivation of microalgae are open raceway ponds (ORPs) and photobioreactors (PBRs) (Jorquera *et al.*, 2010). Photobioreactors are more generally used for growing microalgae for high value commodities or for experimental work at a small scale. However, they have been considered for producing algal biomass on a large scale as they are capable of providing optimal conditions for the growth of the microalgae (Jorquera *et al.*, 2010; Soratana & Landis, 2011). PBRs provide very high productivity rates compared to raceway ponds. The reason why PBRs however have not become widespread is due to the energy and cost intensity of production and operation. PBRs require a far higher surface area for the volume of algal broth compared to alternative infrastructure. Much higher volumes of material are therefore required which in turn necessitates a higher capital energy input and increases environmental impacts (Soratana & Landis, 2011). The biomass production cost should fall below 400 USD/ton for it to be economically viable which is very far from reported full-scale production costs (Bilad *et al.*, 2012). The costs depicted from a study on a medium-scale plant showed that the production costs of microalgal biomass is still 173 times higher than the targeted value (Acien *et al.*, 2012).

Optimization can be defined as the process of finding the conditions that give the maximum or minimum value of a function (Rao, 2009). In recent years, some optimization techniques that are conceptually different from the traditional mathematical programming

methods have been developed. These techniques are labeled as modern or nontraditional methods of optimization. Most of these techniques are based on certain characteristics and behavior of biological, molecular, swarm of insects, and neurobiological systems. These techniques are: 1. Genetic algorithms 2. Simulated annealing 3. Particle swarm optimization 4. Ant colony optimization 5. Fuzzy optimization and 6. Neural-network-based methods. These techniques are emerging as popular methods for the solution of complex engineering problems. Most require only the function values (and not the derivatives). The genetic algorithms are based on the principles of natural genetics and natural selection (Rao, 2009).

Countless practical optimum design problems are described by; mixed continuous–discrete variables, and discontinuous and nonconvex design spaces. If standard nonlinear programming methods are used for this type of problem, they will be inefficient, computationally expensive, and, in most cases, find a relative optimum that is closest to the starting point. Genetic algorithms (GAs) are well suited for solving such problems, and in most cases they can find the global optimum (minimum) solution with a high probability (Rao, 2009). Therefore to substantially lower the production costs, significant improvements should be applied by optimizing many different aspects of the cultivation process.

### **1.3 Justification**

One of the pillars of Kenya's Vision 2030 is economic development which cannot be achieved without a secure, reliable and sustainable energy source. The vision of the Kenya Government Biofuel Policy is to increase access to energy through sustainable biofuel production, and reduce dependence on fossil fuels by 25% in volume by the year 2030 (Kenya's energy policy, 2012).

In comparison with other sources, for example, animal fat, oleaginous grain crops and oil palm, there are remarkable advantages of biodiesel from microalgae as an alternative energy source for the future. Advantages include the following: (i) real growth rate and

oil productivity of microalgae per unit of land use are much higher than those of other biofuel crops; (ii) algae grow in a wide range of environments. Fresh, brackish and saline waters are ideal environments for growth of different algae species. Even in municipal and other types of wastewater, algae grow well by using inorganic ( $\text{NH}_4^+$ ,  $\text{NO}_3^-$ ,  $\text{PO}_4^{3-}$ ) as well as organic sources of nutrients (Wang *et al.*, 2008; Garbowski *et al.*, 2020; Metsoviti *et al.*, 2020; Alvarez *et al.*, 2021); (iii) microalgae absorb carbon dioxide photosynthetically and convert it into chemical energy and biomass. The removal of carbon dioxide from the atmosphere (and possibly industrial flue gases) may play an important role in global warming mitigation by replacing fossil fuel emissions (Sheehan *et al.*, 1998; Wang *et al.*, 2008). Producing 100 tons of algal biomass fixes roughly 183 tons of carbon dioxide from the atmosphere (Chisti, 2007); (iv) microalgae can provide raw materials for different types of fuels such as biodiesel, ethanol, hydrogen and/or methane which are rapidly biodegradable and may perform more efficiently than fossil fuels; (v) products extracted from algal biomass can be used as sources for organic fertilizers or high value products, such as omega-3 fatty acids, sterols, carotenoids and other pigments and antioxidants, and could be amenable to a zero waste biorefinery concept (Wang *et al.*, 2008). Therefore, microalgae have been regarded as possibly the only route to sustainable displacement of high proportions of fossil oil consumption.

This study therefore developed a computer optimization model to simulate the yield of microalgae in a flat plate photobioreactor. The data generated will assist in optimizing the growth conditions of microalgae at pilot plant scale, hence leading to optimum yields. Furthermore microalgae strains were isolated and characterized. This will help in identifying local strains of microalgae that have the potential for biomass and biodiesel production. Finally, the effect of white, blue and red wavelengths on the biomass and lipid yields of microalgae was investigated. Therefore the data obtained will be used to advise policy especially in a world faced by unpredictable and complex challenges on energy.

## **1.4 Hypotheses**

1. The results of biomass yield estimation using optimization model have no significant difference with experimentally produced yields of microalgae grown in a flat plate perspex photobioreactor.
2. There is no significant difference in specific growth rate and doubling time between strains of microalgae.
3. Light wavelength and strain of microalgae has no influence on biomass yields of microalgae grown in flat plate perspex photobioreactor.
4. Light wavelength and strain of microalgae has no effect on lipid yields of microalgae grown in flat plate perspex photobioreactor.

### **1.5.1 Main Objective**

To apply Genetic Algorithm in the optimization of microalgae cultivation conditions in a locally assembled flat plate perspex photobioreactor at pilot plant scale.

### **1.5.2 Specific Objectives**

The main objective was achieved via the following specific objectives:

1. To develop a computer optimization model to simulate the biomass yield of microalgae in a flat plate photobioreactor at pilot plant scale.
2. To isolate and characterize strains of microalgae from local aquatic ecosystems that can be used in biomass and lipid production.
3. To validate the performance of the developed computer simulation model using a flat plate perspex photobioreactor at pilot plant scale under white wavelength.
4. To investigate the effect of light of various wavelengths and strain on the biomass and lipid yield of microalgae grown in the flat plate perspex photobioreactor.

## **1.6 Research Questions**

1. Is there a significant difference between results of biomass yield estimation using optimization model and those experimentally produced of microalgae grown in a flat plate perspex photobioreactor?
2. Can strains of microalgae be isolated and characterized from local aquatic ecosystems for biodiesel production?
3. Does light wavelength and strain of microalgae have influence on biomass yields of microalgae grown in flat plate perspex photobioreactor?
4. Does light wavelength and strain of microalgae have effect on lipid yields of microalgae grown in flat plate perspex photobioreactor?

## **1.7 Scope of Study**

The study was confined to flat plate photobioreactors, and their application in the growing of microalgae at pilot plant level. Two strains used in this research namely; *C. emersonii* and *C. vulgaris* were isolated from water samples collected in local aquatic ecosystems. The isolated strains were grown in three PBRs using light with various wavelengths. The optimization model was validated by the biomass yield of the strain that had a higher growth rate and a shorter doubling time i.e., *C. vulgaris*, grown under white wavelength supplied by light emitting diodes (LEDs). The biomass and lipid yields produced under the different light wavelengths were then compared statistically.

## **1.8 Limitations of the Study**

The study sought to apply Genetic Algorithm in the optimization of microalgae cultivation conditions in a locally assembled flat plate perspex photobioreactor at pilot plant scale. There was no existing literature on optimization of microalgae cultivation systems using modern optimization methods especially GA. Furthermore, for every experimental run, approximately 600 litres of sterilized MBL media was required whereas the autoclave available could sterilize only a maximum of 12 litres of culture media at a time for 3 hours.



Last but not least, non-probability sampling was applied to collect water samples from local aquatic ecosystems.

## CHAPTER TWO

### LITERATURE REVIEW

#### 2.1 Introduction

According to International Energy (IEA) Statistics for the year 2010, the Africa and the World consumed 3.4 and 85.7 million barrels of petroleum fuel respectively. It is speculated that the current rate of consumption of the petroleum fuel is 2.7% of the reserves, and the petroleum stocks may be depleted within the next 50 years or so (Taufiqurrahmi & Bhatia, 2011). Use of petroleum fuel is considered to have a negative environmental impact. Petroleum is a mixture of a number of organic compounds and some of which are toxic. Combustion of petroleum hydrocarbons lead to a net increase in carbon dioxide, a factor assumed to be responsible for global warming and climate change (Kumar, 2015). Adequate energy supply, not only dramatically increases human capabilities and opportunities; they are integral to poverty alleviation and environmentally sound social and economic development (Ahuja & Tatsutani, 2009; Kamau *et al.*, 2015). The continuous reduction of fossil fuel reserves which are non-renewable source and limited in supply, global concern on climate change as well as threats to energy security have led to interest in the exploration, production and exploitation of biofuels in household and transport sector. Apart from that, as energy predicament is beginning to hit almost every part of the world due to rapid industrialization and population growth, the quest for renewable energy sources has become the key challenge in this century in order to stimulate a more sustainable energy development for the future. Renewable energy sources such as solar, wind, hydro, geothermal and energy from biomass and waste have been effectively developed and used by different nations to limit the use of fossil fuels (Lam & Lee, 2012). Nevertheless, based on a recent study from (IEA), only energy produced from combustible renewables and waste has the utmost potential among other renewable sources (IEA, 2010). From the report, combustible renewables and waste accounted for 10.0% of the total primary energy supply, compared to hydro energy 2.2% and other 0.7% (geothermal, solar, wind and heat). Hence, it was predicted that renewable

energy from combustible sources such as biodiesel will play a more critical role as an alternative renewable energy in the near future to further diversify the global energy sources. Biofuels production and use reduce reliance on fossil fuel and contribute to rural and sustainable development (Demirbas, 2008; Ben-Iwo *et al.*, 2016). Energy security, environmental concerns, foreign exchange and socio-economic well-being of rural people are some of the causes that have led to promotion of biofuels (Demirbas, 2008).

Global biofuel production has been increasing rapidly over the last decade, but the expanding biofuel industry has recently raised pertinent concerns. In particular, the sustainability of many first-generation biofuels; fuels made from food and feed crops and mainly vegetable oil, has been increasingly questioned over concerns such as reported displacement of food crops, effects on the environment and climate change (Cheng, 2010). In general, there is growing consensus that if significant emissions reductions in the transport sector are to be achieved, biofuel technologies must become more efficient in terms of net lifecycle greenhouse gas emission reduction while at the same time be environmentally and socially sustainable. It is increasingly understood that most first-generation biofuels, except sugarcane ethanol, will likely have a limited role in the future transport fuel mix (IEA, 2008).

Biodiesel is a mixture of fatty acid alkyl monoesters (FAMES) derived from vegetable fats and oils. It can be used as a replacement of fossil diesel because of their structural similarity. Biodiesel is currently being acknowledged as a green and alternative renewable diesel fuel that has attracted enormous interest from researchers, governments, and local and international traders. Some of the benefits of using biodiesel instead of fossil diesel are that it is a non-toxic fuel, is biodegradable and has lower emission of GHG when burned in diesel engine (Demirbas, 2009). Biodiesel is produced using vegetable oil, plant oil, and animal fat. Biodiesel is an alternative fuel for diesel and most diesel engines can use 100% biodiesel (Cheng 2010). The main feedstock currently used for biodiesel production includes palm oil, sunflower, rapeseed, soybean, and canola seed. A great challenge of using vegetable oils for biodiesel production is the availability of crop land for oil production to produce enough biodiesel that significantly replaces the current fossil

fuel consumption. Chisti (2007) estimated that it would take 24% of the existing crop land in the US to grow oil palm that is considered as a high yield oil crop or over three times of the current cropland in the US to grow soybean to produce enough biodiesel that would replace 50% of the transportation fuel in the US. Thus, second generation biodiesel derived from non-edible oils such as *Jatropha curcas* L. seem as an attractive alternative feedstock for the biodiesel industry. In fact, the use of jatropha oil in existing biodiesel plant does not require major alteration on the equipment and process flow, mainly because the oil has similar properties to edible oils. However, jatropha oil does contain higher concentration of free fatty acid (FFA) that may require an additional pre-treatment step. Another merit of using jatropha oil is that jatropha trees can grow easily on non-arable or wasteland. Nevertheless, regular irrigation, heavy fertilization and good management practices are required to ensure high oil yield (Lam *et al.*, 2009). Due to these weaknesses, the pursuit for a more sustainable biodiesel feedstock continues and now focuses on microalgae.

Several studies have been conducted on using alternative oils such as waste oils from restaurants and kitchens and microalgal oils for biodiesel production (Cheng 2010). Shah *et al.* (2007) investigated the utilization of restaurant waste oil as a precursor for sophorolipid and biodiesel production. Zhang *et al.* (2003) evaluated the Biodiesel production from waste cooking oil including economic analysis. Miao and Wu (2006) studied biodiesel production from heterotrophic microalgal oil. A great advantage of using microalgal oil over vegetable oils for biodiesel production is that the production of algal oil does not need cropland and has much higher oil yield per acre of land because the microalgae can be grown in 3 dimensions in photobioreactors (Cheng 2010). However, a big challenge of biodiesel production using algal oil is that the cost of algal oil production is extremely high (Cheng 2010). This review paper provides information on where we have come since the first research on algal cultivation and energy recovery was initiated, what is currently hampering the commercial application of the concept and where we need to go from here. Continued research will allow us to recover the maximum potential from

algal biomass which will provide an increasingly vital resource for use in the future as predicted by Oswald (2003).

## **2.2 Microalgae as a Feedstock for Biodiesel Production**

Microalgae are a diverse group of aquatic photosynthetic microorganisms that grow very fast and have the ability to yield large quantities of lipids adequate for biodiesel production (Li *et al.*, 2008; World Watch Institute (WWI), 2007). Algae as a potential source of fuel was initially investigated during the gas scare of the late 1970s (Li *et al.*, 2008). The National Renewable Energy Laboratory (NREL) in the United States started its algae feedstock studies in the late 1970s, but their research program was halted in 1996. Recent renewed interest has led the NREL to restart their research in algae (Donovan & Stowe, 2009). The potential for microalgae to provide biomass for biodiesel production is now widely accepted (Miguel *et al.*, 2010). Further, microalgae are recognized among the most efficient for this purpose, and some studies, for instance, by Chisti (2007), assert it is the “only source of biodiesel that has the potential to completely displace fossil diesel” (Table 2.1). The superiority of microalgae as a feedstock for biodiesel production compared with the other conventional oil crops such as soybeans are (Wu *et al.*, 2012):

(1) Microalgae have simple structures, but high photosynthetic efficiency with a growth doubling time as short as 24 h (Tredici, 2010). Moreover, microalgae can be grown all year round. (2) The species abundance and biodiversity of microalgae over a broad range of climates and geographic regions make seasonal and geographical restrictions much less of a concern compared with other lipid feedstock. Microalgae may be cultivated on fresh water, saltwater lakes with eutrophication, oceans, marginal lands, deserts, etc., hence reducing or eliminating the competition for land with conventional agriculture (Khan *et al.*, 2009) and opening economic opportunities in arid or salinity affected regions of the world (Schenk *et al.*, 2008). (3) Microalgae can effectively remove nutrients such as phosphorus and nitrogen, and heavy metals like lead, from wastewaters (Munoz & Guieysse, 2006). (4) Microalgae sequester a large amount of carbon dioxide from the atmosphere via photosynthesis, for example, the CO<sub>2</sub> fixation efficiency of *C. vulgaris*

was up to 260 mg.L<sup>-1</sup>.h<sup>-1</sup> in a membrane photobioreactor (Cheng *et al.*, 2006). Utilization of CO<sub>2</sub> from thermal power plants by large-scale microalgae production facilities can reduce a great deal of the greenhouse gas emissions blamed for global warming (Cheng *et al.*, 2006; Verawaty *et al.*, 2017). (5) The production and use of microalgae biodiesel contribute near zero net CO<sub>2</sub> and sulfur to the atmosphere. (6) Microalgae can produce a number of valuable products, such as proteins, polysaccharides, pigments, animal feeds, fertilizers etc. (Priyadarshani & Rath, 2012; Ting *et al.*, 2017). Furthermore, annual oil production from high-oil microalgae can be in the range of 58,700 to 136,900 litres per hectare (Chisti, 2007). If this microalgal oil is used for biodiesel production, it would take approximately 1.0 – 2.5% of the current cropland in the US to meet 50% of the US transportation fuel needs, which is much more feasible than the current oil crops (Cheng, 2010). In summary, microalgae are a largely untapped biomass resource for renewable energy production (Lam & Lee, 2012; Wu *et al.*, 2012).

However, commercialization of microalgae biomass and biofuel production is still facing significant obstacles due to high production costs and poor efficiency of the cultivation systems. In face of these challenges, researchers are undertaking profound efforts to improve microalgae biomass production and lipid accumulation and lower downstream processing costs (Wu *et al.*, 2012).

**Table 2.1: Comparison of Some Sources of Biodiesel**

<b>Crop</b>	<b>Oil yield (L.ha<sup>-1</sup>)</b>
<b>Corn</b>	172
<b>Soybean</b>	446
<b>Canola</b>	1,190
<b>Jatropha</b>	1,892
<b>Coconut</b>	2,689
<b>Oil palm</b>	5,950
<b>Microalgae (70% oil in biomass)</b>	136,900
<b>Microalgae (30% oil in biomass)</b>	58,700

Source: (Chisti, 2007)

From Table 2.1, it can be observed that microalgae yield more oil per tonne, hence researchers ought to focus on them to avoid competition with food and feed crops.

### **2.2.1 Species and Strains of Microalgae and Lipid Composition**

The lipid content of microalgae varies among different species and strains (Table 2.2) (Singh *et al.*, 2011 a, b). The lipid content of microalgae is usually in the range of 20% - 50% (dry basis) (Wu *et al.*, 2012), and can be as high as 80% under certain circumstances. Selecting high lipid content and fast-growing microalgae is an important step in the overall success of biodiesel production from microalgae (Wu *et al.*, 2012; Del Río *et al.*, 2015). Lipid content and lipid productivity are two different concepts. The former refers to lipid concentration within the microalgae cells without consideration of the overall biomass production. However, the latter takes in account both the lipid concentration within cells and the biomass produced by these cells. Therefore, lipid productivity is a more reasonable indicator of a strain's performance in terms of lipid production (Wu *et al.*, 2012).

**Table 2.2: Lipid Content of Various Species of Microalgae**

<b>Species</b>	<b>Lipid content (% dry weight)</b>
<i>Anabaena cylindrical</i>	4-7
<i>Botyococcus braunii</i>	25-80
<i>Chlamydomonas reinhardtii</i>	21
<i>C. emersonii</i>	28-32
<i>Chlorella protothecoides</i>	57.9
<i>Chlorella pyrenoidosa</i>	2
<i>Chlorella vulgaris</i>	14-22
<i>Cryptocodinium cohnii</i>	20
<i>Cylindrotheca</i> sp.	16-37
<i>Dunaliella bioculata</i>	8
<i>Dunaliella primolecta</i>	23
<i>Dunaliella salina</i>	6
<i>Dunaliella tertiolecta</i>	35.6
<i>Euglena gracilis</i>	14-20
<i>Hormidium</i> sp.	38
<i>Isochrysis</i> sp.	25-33
<i>Monallanthus salina</i>	> 20
<i>Nannochloris</i> sp.	30-50
<i>Nannochloropsis</i> sp.	31-68
<i>Neochloris oleoabundans</i>	35-54
<i>Nitzschia</i> sp.	45-47
<i>Phaeodactylum tricornutum</i>	20-30
<i>Pleurochrysis carterae</i>	30-50
<i>Porphyridium cruentum</i>	9-14
<i>Prymnesium parvum</i>	22-38
<i>Scenedesmus dimorphus</i>	16-40
<i>Scenedesmus obliquus</i>	12-14
<i>Schizochytrium</i> sp.	50-77
<i>Spirogyra</i> sp.	11-21
<i>Spirulina maxima</i>	6-7
<i>Spirulina platensis</i>	4-9
<i>Synechoccus</i> sp.	11
<i>Tetraselmis maculate</i>	8
<i>Tetraselmis sueica</i>	15-23

Source: (Singh *et al.*, 2011 a, b)

Based on data presented in Table 2.2 the promising strains for biodiesel production are: *Botyococcus braunii*, *C. emersonii*, *Chlorella protothecoides*, *Cylindrotheca* sp.,



Dunaliella tertiolecta, Hormidium sp., Nannochloris sp., Nannochloropsis sp., Nannochloropsis sp., Neochloris oleoabundans, Nitzschia sp., Pleurochrysis carterae, and Schizochytrium sp. Since some of the most productive strains/species as per Singh et al., (2011 a, b) are spread globally, it was thought necessary to isolate the strains locally and test their viability.

### **2.2.2 Fatty Acid Profile of Various Microalgae Strains**

In addition to increasing the oil content and productivity of microalgae, it is also crucial to improve the quality of the biodiesel produced (Abomohra *et al.*, 2016). Although the fatty acid profile does not appear to have a major impact on the transesterification biodiesel production process, it does affect the properties of the fuel produced (Abomohra *et al.*, 2016). For example, the high proportion of saturated fatty acids enhances the oxidative stability and cetane number of the biodiesel, but with poor low-temperature properties and it behaves as a coagulant at ambient temperatures. Conversely, biodiesel produced from feedstocks with high proportion of polyunsaturated fatty acids (PUFAs) shows good cold-flow properties but with lower cetane number and poor oxidative stability during prolonged storage (Abomohra *et al.*, 2016).

The most important fuel properties that evaluate the potential of biodiesel as a substitute of fossil diesel are: kinematic viscosity, specific gravity, cetane number, cold filter plugging point (CFPP) and iodine value (Knothe, 2010; Georgianna & Mayfield, 2012). High cetane number is one of the most important fuel indicators of easier engine start-up, low nitrous oxide emissions, thus environmentally friendly, and better combustion (Knothe, 2008; Mandotra *et al.*, 2014). The cetane number is frequently influenced by the structure of fatty acids, the saturated fatty acid content, and the length of the carbon chains in a fuel. Longer carbon chains associated with a higher saturated fatty acid content result in a higher cetane number (Ramadhas *et al.*, 2006). On the other hand, higher iodine values may result in the deposition of lubricant in the engine and polymerization of glycerides (Francisco *et al.*, 2010). The melting point of unsaturated fatty acids is always lower than that of saturated fatty acids. Therefore, when the oil contains mostly saturated FAMES

(very low iodine value), crystallization may occur at the engine operation temperature (Francisco *et al.*, 2010) leading to poor CFPP (Abomohra *et al.*, 2016).

Kinematic viscosity is directly related to the impinging distance, lubricity, atomization and burning efficiency of a liquid fuel (Cherng-Yuan & Yi-Wei, 2012). Biodiesel generally has a higher viscosity than mineral diesel, and thus has inferior atomization and spray, resulting in a larger mean liquid droplet diameter and a longer ignition delay (Hoekman *et al.*, 2012).

Density is an important parameter for diesel fuel injection systems. It is the weight of a unit volume of fluid. A higher density results in the delivery of a slightly greater mass of fuel since fuel injection equipment operates on a volume metering system (Giwa *et al.*, 2010).

### **2.2.3 Fatty Acid Methyl ester (FAME) Composition**

A systematic analysis of the FAME composition and comparative fuel properties is very important for species selection for biodiesel production (Islam *et al.*, 2013). The most common fatty acids of microalgae are Linolenic acid (octadecatrienoic- C18:3), Linoleic acid (octadecadienoic- C18:2), Oleic acid (octadecenoic- C18:1), Stearic acid (octadecanoic- C18:0), and Palmitic acid (hexadecanoic- C16:0) (Knothe, 2009). Most algae have only small amounts of eicosapentaenoic acid (EPA) (C20:5) and docosahexaenoic acid (DHA) (C22:6) (Knothe, 2009), however, in some species of particular genera these PUFAs can accumulate in appreciable quantities depending on cultivation conditions (Huerlimann *et al.*, 2010). In general, eustigmatophytes and diatoms make appreciable amounts of EPA, while dinoflagellates and haptophytes typically produce both EPA and DHA, with DHA being often dominant over EPA. It has been suggested that, the higher the degree of unsaturation of FAMEs of biodiesel, the higher the tendency of the biodiesel to oxidize (Islam *et al.*, 2013). There are, however, other parameters which also define the oxidation stability of the fuel, for instance free fatty acid content and natural anti-oxidant (Knothe, 2005; Lapuerta *et al.*, 2009 Hoekman

*et al.*, 2012). A good quality biodiesel should have a 5:4:1 mass fat acid ratio of C16:1, C18:1 and C14:0, as recommended by Schenk *et al.* (2008).

### **2.3 Metabolic Pathways**

Microalgae may use one or more of the three main metabolic pathways depending on carbon conditions and light: photoautotrophy, heterotrophy, and mixotrophy (Chojnacka & Noworyta, 2004). Most microalgae are capable of photoautotrophic growth. Photoautotrophic cultivation in open ponds is a simple and low-cost method for large-scale production; however, the biomass density is low because of contamination by other species or bacteria, limited light transmission and low organic carbon concentration (Greenwell, 2010). Commercially, growing microalgae for value-added products is usually conducted in open ponds (raceways) or closed photobioreactors (PBRs) under autotrophic (making complex organic nutritive compounds from simple inorganic sources by photosynthesis) or heterotrophic (cannot synthesize its own food) conditions at relatively warm temperature (20 – 30 °C) (Cheng, 2010; Lam & Lee, 2012). In autotrophic microalgal cultivation, the microalgae need sunlight (energy source), CO<sub>2</sub> (carbon source) and nutrients (P, N and minerals) for their photosynthesis and generate oxygen. The main difference of growing heterotrophic microalgae from autotrophic ones is the carbon source. The former requires organic carbon source such as glucose to support its growth. Normally autotrophic microalgae are grown for biodiesel production, mainly because they use CO<sub>2</sub> as their carbon source for growth (Cheng, 2010). Therefore, the whole cycle of growing microalgae for biodiesel production and combustion of biodiesel as fuel would generate zero net carbon dioxide emission to the atmosphere. However, sometimes heterotrophically grown microalgae can make much more oil than autotrophic ones. Miao and Wu (2006) reported the heterotrophic growth of *Chlorella protothecoides* resulted in a significant increase of oil content of microalgae from 14.5% under the original autotrophic growth to 55.2% (dry weight).

Heterotrophic cultivation has drawn increasing attention and it is regarded as the most practical and promising way to increase the productivity (Chen, 1996; Li *et al.*, 2007;

Doucha & Lívansky, 2012). Currently, research on heterotrophic cultivation of microalgae is mainly focused on *Chlorella* (Wu *et al.*, 2012). Cell densities as high 104.9 g.L<sup>-1</sup>(dry cell weight, *Chlorella pyrenoidosa*) have been reported (Wu & Shi, 2006). Microalgae can adapt to different organic matters such as sucrose, xylan, glycerol and organic acids in slurry after acclimatization (Heredia-Arroyo *et al.*, 2011). The ability of heterotrophic microalgae to utilize a wide variety of organic carbons provides an opportunity to reduce the overall cost of microalgae biodiesel production since these organic substrates can be found in the waste streams such as municipal and animal wastewaters, effluents from anaerobic digestion, food processing wastes, etc. (Wu *et al.*, 2012). On the basis of heterotrophic cultivation, researchers have carried out studies of mixotrophic cultivation which can greatly enhance the growth rate because it realizes the combined effects of photosynthesis and heterotrophy (Wu *et al.*, 2012). After examining the biomass and lipid productivities characteristics of fourteen microalgae, Park *et al.* (2012) found that lipid and biomass productivities were boosted by mixotrophic cultivation. Andrade and Costa (2007) studied the effects of molasses concentration and light levels on mixotrophic growth of *Spirulina platensis*, and found that biomass production was stimulated by molasses, which suggested that this industrial by-product could be used as a low-cost supplement for the growth of this species. Bhatnager *et al.* (2011) found that the mixotrophic growth of *Chlamydomonas globosa*, *Chlorella minutissima* and *Scenedesmus bijuga* resulted in 3-10 times more biomass production compared with that obtained under phototrophic growth conditions. The maximum lipid productivities of *Phaeodactylum tricorutum* in mixotrophic cultures with glucose, acetate and starch in medium were 0.053, 0.023 and 0.020 g.L<sup>-1</sup>.day<sup>-1</sup>, which were respectively, 4.6-, 2.0-, and 1.7-fold of those obtained in the corresponding photoautotrophic control cultures (Wang *et al.*, 2012).

Therefore, researchers should choose strains that use photoautotrophic metabolic pathway because they utilize carbon dioxide from the surrounding to synthesize their own food. In so doing, they act as carbon sink hence reducing the amount of CO<sub>2</sub> in the atmosphere which is responsible for global warming and climate change.

## **2.4 Techniques for Producing Axenic Microalgal Cultures**

### **2.4.1 Streak Plate Method**

Streaking is an enrichment process that is widely used to separate a strain from a mixture of microorganisms for further examination and identification. It begins by inserting a sterile inoculation loop into the liquid sample or pinching a morphologically different colony from the filter membrane surface using a sterile pin tool and a dissecting microscope. After that, the sample is distributed over a new agar plate using a specified pattern (Black, 2008). The area that is first inoculated will contain too many microorganisms to be able to select a single colony. As the metallic gadget travels to the next location, fewer cells are deposited. The goal is that by the last quadrant, cells are placed in such a way that they are far enough from one another and thus the colony is product of a single cell, i.e. pure isolate. At this stage, single microalgal species can be easily distinguished based mainly on morphological (size/shape/colour) differences of the colonies and the latter are again chosen and streaked until no additional microorganisms can be found in the successive agar plates (Black, 2008). A single colony from the agar plate should then be chosen and placed in a drop of sterile culture medium on a glass slide to ensure that the target microbe has been isolated and is pure (CSIRO, 2013). When a pure strain is obtained, it is pinched one final time and streaked on an agar slant for stock establishment.

The technique is based on the idea that each individual colony on the agar surface is the result of a single dividing cell. While it may appear trivial, this is not always the case, particularly with some microalgae whose growth is dependent on symbiotic relationships and cannot be separated without jeopardizing growth (Alanís, 2013).

### **2.4.2 Dilution in Liquid Media**

The serial dilution protocol is a technique for reducing the concentration of microscopic organisms or cells in a liquid sample. This will allow one of the higher dilution tubes to

become the growing medium for an axenic culture (Alanís, 2013). If a few distinct species are still present in high dilution tubes, additional methods can be used concurrently to produce pure cultures. It begins by setting up a series of test tubes with a certain volume of liquid media (i.e. 9 mL). From the concentrated inoculum, 1 mL is taken, diluted in the second test tube ( $10^{-1}$ ) and mixed. Then, 1 ml is taken from the first dilution and placed in the third test tube ( $10^{-2}$ ). This is repeated till all remaining tubes have been used; if ten test tubes were used then the last one will represent a  $10^{-10}$  dilution (Figure 2.1).

Lastly, only the most diluted tubes are cultured in specific pre-set conditions and microscopical observations are made after 2 – 4 weeks. In parallel, agar plates can be prepared by streaking a sample from each dilution. By doing this, the higher the dilution, the higher is the probability of getting individual colonies in the agar plate (Alanís, 2013).

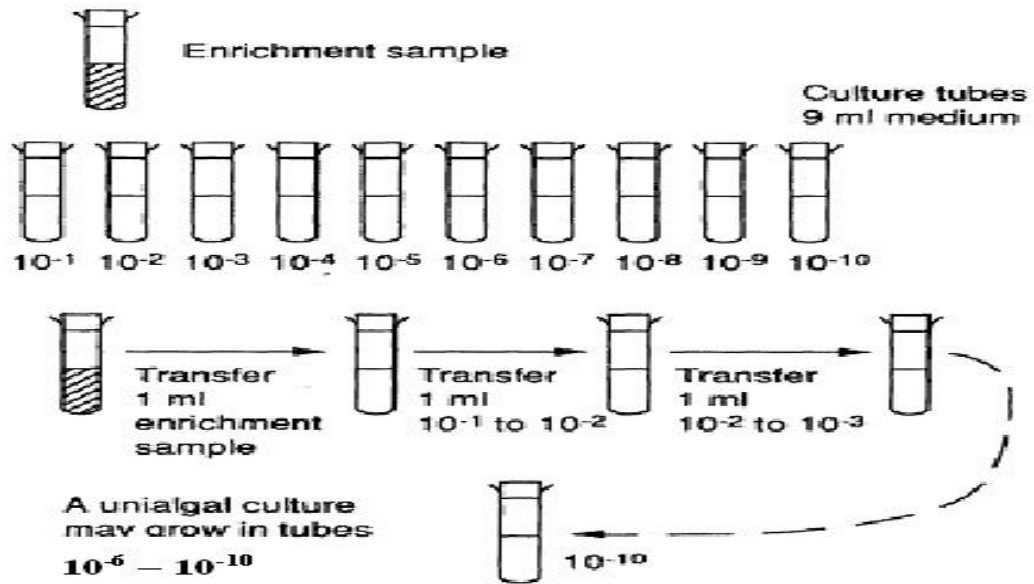


**Figure 2.1: Serial Dilution Block Diagram**

Source: (Alanís, 2013)

### **2.4.3 Fluorescence Activated Cell Sorting**

With the use of a laser beam and a fluid stream, single particles can have their many physical properties examined using a technique called flow cytometry. Particle size, granularity, and fluorescence intensity are a few examples of the characteristics that can be measured (Biosciences, 2000). Using the flow cytometry principle as a guide, Bonner *et al.* (1972) created the Fluorescence Activated Cell Sorting (FACS) system, which sorts living cells in a heterogeneous mixture one at a time according to their unique light scattering and fluorescent properties. Electrical signals are produced by the cells' fluorescence as they are successively passed via a laser beam. After that, the stream is changed to produce a sequence of drops with one cell in each that are all the same size downstream of the laser. The drops are given the proper electrostatic charges by the fluorescent signals, which allow them to flow between two charged plates and be deflected into the proper containers (Figure 2.2).

Despite being a very quick and effective way to isolate particular types of organisms from complex cell mixtures, cell sorters are generally costly and require a skilled, committed technician to operate efficiently. The acquisition of this equipment is not warranted in many laboratories where isolations are not performed frequently; therefore, alternative techniques must be used (Alanís, 2013).

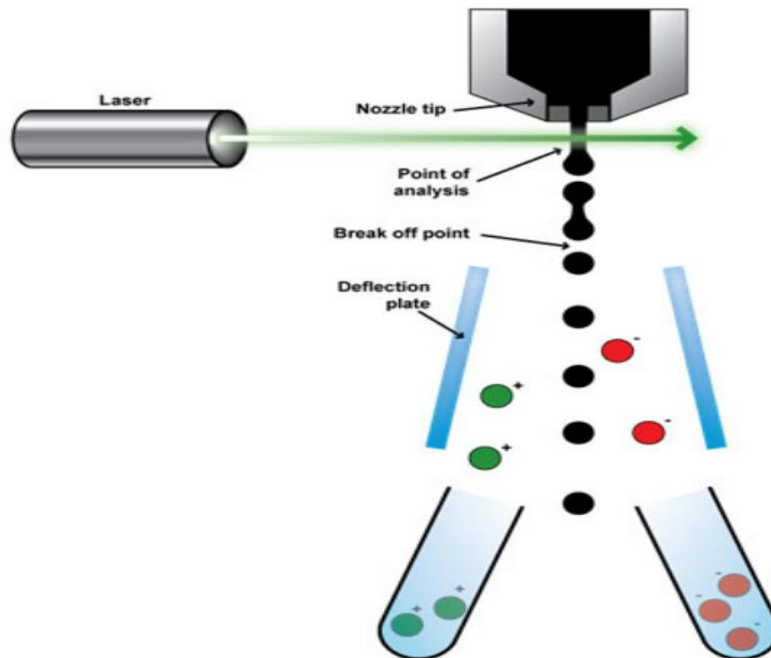


**Figure 2.2: Fluorescence Activated Cell Sorting Method for Particle Separation Based on Differential Fluorescent Rendering of Cells in the Stream**

Source: (ABCAM, 2013)

#### **2.4.4 Micromanipulation**

The initial step in the micromanipulation technique is to heat and pull out a micropipette from both ends of a capillary tube. The diameter of the narrow end must be at least twice that of the cell that is to be micromanipulated. Under a microscope, the researcher can extract a single cell from the enrichment medium by attaching a silicone tube to the thick end of the micropipette (Alanís, 2013). The sucking-obtained cell is then placed in a sterile medium drop. After sterilizing the micropipette, the cell is selected and moved to a fresh drop. To ‘wash’ the cell clean of bacteria, the procedure is repeated (Figure 2.3). Repeated washings of the cell can lower the likelihood of bacterial infection. Nonetheless, there is a greater chance of cell damage the more times a cell is handled. Therefore, the type of algae will determine the ideal number of washes. The cell is then finally put in culture



medium under the right circumstances to grow. This approach should produce axenic cultures (Alanís, 2013).

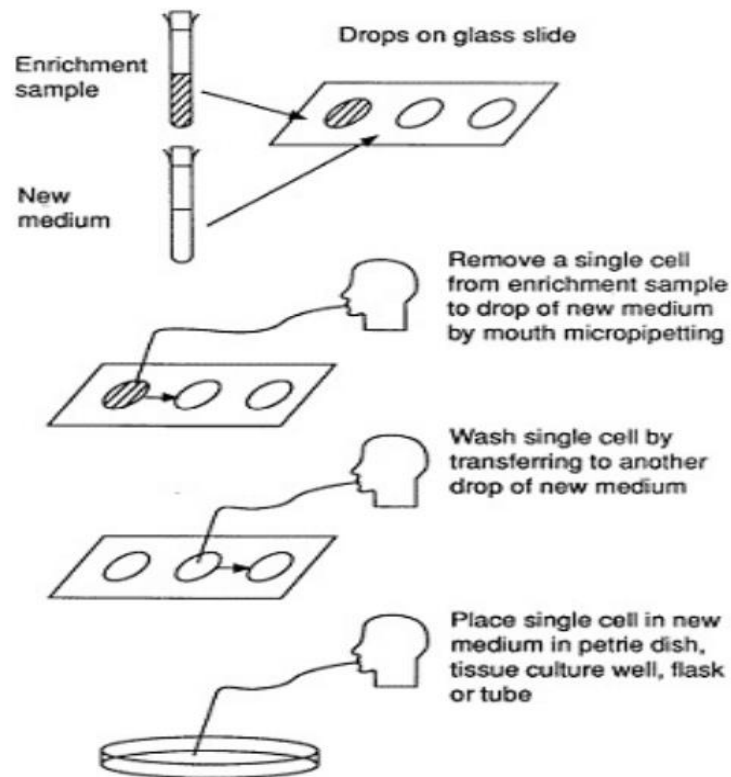


**Figure 2.3: Micromanipulation of an Enrichment Sample with a Capillary Micropipette to Obtain a Uni-Algal Culture**

Source: (Alanís, 2013)

### 2.4.5 Density Centrifugation

Microalgae separation was the first application of the technology (Whitelam *et al.*, 1983). Based on density gradient centrifugation in colloidal silica sol Percoll, it achieves separation through variations in the buoyant densities of the mixture's cells. The Percoll instrument was created by Pertoft *et al.* (1978) with the aim of achieving improved density separation in the field of biochemistry. By using density centrifugation, viruses, cells,

organelles, or cells can be isolated. Polyvinylpyrrolidone (PVP)-coated colloidal silica particles, measuring 15–30 nm in diameter (23% w/w), make up Percoll.

Percoll is not toxic to cells, and it also has low viscosity and low osmolarity (the number of osmoles of solute per litre of solution), which are two characteristics that make it a good choice for biological separation experiments, as shown by (Whitelam *et al.*, 1983). Cells separate into distinct bands at specific gradient locations following centrifugation. Fractionation can be used to readily separate the bands that the various cells formed if they are somewhat widely apart from one another. Furthermore, the scientists discovered that this approach has no effect on the photosynthetic activity and subsequent growth of microalgae (Whitelam *et al.*, 1983).

#### **2.4.6 Ultra Violet Radiation**

The majority of microalgae strains have a marginally higher UV radiation resistance than bacteria (Richmond, 2008). Therefore, pure algal culture devoid of bacterial contamination could be produced by subjecting the sample to ultraviolet (UV) irradiation, washing, diluting, and streaking it on selective agar.

#### **2.4.7 Addition of Antibiotics**

Obtaining microalgae isolates may need the use of antibiotics after all other basic microbiological isolation techniques have been exhausted. Since mutant clones may be created that do not always represent populations in the wild, this strategy is generally not advised when isolating strains that will be used for physiological or ecological investigations (Alanís, 2013).

Antibiotics directed against Gram (+) and/or Gram (–) bacteria that impede cell growth by blocking the synthesis of proteins or cell walls are frequently employed. Penicillin G and other members of the penicillin family are examples of cell wall inhibitors. The beta-lactam family of antibiotics causes the bacterial cell wall to become more permeable by rupturing it. Aminoglycosides, such as gentamycin, kanamycin, neomycin, and

streptomycin, work by permanently binding to bacterial ribosomes to impede protein synthesis. A few antifungal drugs that are utilized to isolate cyanobacteria are Nystatin ( $100 \mu\text{g mL}^{-1}$ ), cycloheximide ( $100 \mu\text{g mL}^{-1}$ ), and amphotericin B (Alanís, 2013).

## 2.5 Microalgae Cultivation Systems

The two key methods of infrastructure considered appropriate for cultivation of algae are open raceway ponds (ORPs) and photobioreactors (PBRs) (Jorquera *et al.*, 2010). Raceway ponds are analogous to oxidation ditches used in wastewater treatment systems being big, open basins of shallow depth and a length at least several times greater than that of the width. Raceway ponds are normally constructed using a concrete shell lined with polyvinyl chloride (PVC) with dimensions ranging from 10 to 100 m in length and 1 to 10 m in width with a depth of 10 to 50 cm (Jorquera *et al.*, 2010; Slade & Bauen, 2013). Photobioreactors are more generally used for growing microalgae for high value commodities or for experimental work at a small scale. However, they have been considered for producing algal biomass on a large scale as they are capable of providing optimal conditions for the growth of the microalgae (Jorquera *et al.*, 2010; Soratana & Landis, 2011). A closed reactor allows species to be protected from bacterial contamination, shallow tubing allows efficient light utilization, and bubbling  $\text{CO}_2$  offers high efficiency carbon uptake and water loss is lessened. PBRs provide very high productivity rates compared to raceway ponds (Table 2.3). In their life-cycle assessment (LCA) study, Jorquera *et al.* (2010) estimated volumetric productivity to be at least eight times higher in flat plate and tubular PBRs. The reason why PBRs however have not become widespread is due to the energy and cost intensity of production and operation. PBRs require a far higher surface area for the volume of algal broth compared to alternative infrastructure. Much higher volumes of material are therefore required which in turn necessitates a higher capital energy input and increases environmental impacts (Soratana & Landis, 2011). During operation, algal biomass must be kept in motion to provide satisfactory mixing and light exploitation. This increases productivity; however, it requires additional energy for pumping. So far in comparison to raceway ponds the benefits of PBRs do not outweigh the indispensable energy requirements identified in the

LCA study published by Jorquera *et al.* (2010). A net energy ratio (i.e., energy produced/energy consumed) of 8.34 has been reported for raceway ponds as compared to a net energy ratio of 4.51 and 0.20 for flat-plate and tubular photobioreactors, respectively (Jorquera *et al.*, 2010). It is likely that ponds will continue to provide the most effective infrastructure for algal cultivation due to their low impact design and low input energy requirement. PBRs will continue to be important however, for laboratory work, developing cultures and producing biomass with high economic value. As research continues it may also be possible to develop infrastructure that will provide the benefits of both PBRs and open ponds together (Aitken & Antizar-Ladislao, 2012).

The frequently studied process for algal biomass production is outdoor photoautotrophic cultivation, due to the straightforwardness of scalability and the added benefit of CO<sub>2</sub> sequestration. The primary bottleneck that limits the productivity of all photoautotrophic cultivation systems is the light penetration (Masojidek *et al.*, 2003; Perez-Garcia *et al.*, 2011) and absence of light at night (Edmundson & Huesemann, 2015). Light penetration is often poor inside PBRs and ORPs and the penetration further falls with increasing cell density and depth due to self-shading effects. Light/dark cycle is also inevitable for outdoor cultivation, and it was reported that respiratory effect at night causes a decrease in the biomass produced in the day period (Edmundson & Huesemann, 2015). In addition, the outdoor cultivation systems also suffer from inconsistent biomass productivity due to the fluctuations of light intensity and temperature across the day/night cycle and seasonal changes (De Bhowmick *et al.*, 2014; Perez-Lopez *et al.*, 2017). Furthermore, most common outdoor cultivation systems such as open raceway ponds frequently suffer from contamination problems. Due to the nature of open systems, it is nearly impossible to maintain a monoculture of a single target microalgal strain due to the high susceptibility of these systems to be contaminated with undesirable foreign species (Xu *et al.*, 2009). Initial capital investments are undoubtedly higher for photobioreactors, but they can provide higher overall productivity due to better contaminant management and improved utilization of photosynthetically active radiation, carbon dioxide and other nutrients (Sforza *et al.*, 2012). Cheng *et al.* (2006) constructed a 10 L photobioreactor integrated

with a hollow fiber membrane module which increased the gas bubbles retention time from 2 s to more than 20 s, increasing the CO<sub>2</sub> fixation rate of *C. vulgaris* from 80 to 260 mgL<sup>-1</sup>h<sup>-1</sup>. The design of closed systems must be carefully optimized for each individual microalgal strains, according to its specific physiological and growth characteristics. Apparently, major technical and economic challenges still prevent the selection of an optimal reactor type at the commercial scale (Kunjapur & Eldridge, 2010). Several researchers worldwide claim to possess technologies for the commercial production of biodiesel from microalgae, and many new companies have been recently developed (Grobbelaar, 2010; Singh & Gu, 2010; Zijffers *et al.*, 2010; Jo *et al.*, 2020). However, a number of technical challenges remain unresolved, including questions concerning large-scale microalgae recovery and oil separation processes. For these reasons, in spite of quite large scientific, technological and commercial interest, no industrial plants finalized to produce oil from microalgae are operated in the world (Singh & Gu, 2010). Microalgae cultivation systems work well at the laboratory and small pilot/demonstration levels, but the process feasibility has not been demonstrated for large scale production yet (Singh & Gu, 2010).

High volumetric productivities and high biomass yields on light used are required to decrease production system volumes and to lower production costs. This can be achieved by cultivating the microalgae in photobioreactors with a high surface to volume ratio, i.e., a short light path, such as panel reactors (Zijffers *et al.*, 2010). Panel photobioreactors have been demonstrated to be promising photobioreactors for the controlled cultivation of microalgae (Hu *et al.*, 1998b; Hu *et al.*, 1998c; Tredici & Zittelli, 1998; Degen *et al.*, 2001). Furthermore, such panels can be integrated in photobioreactors in which advanced optical engineering is used to dilute light (Gordon, 2002; Zijffers *et al.*, 2008). The flat-plate PBR has a large illuminated specific surface area, a short light path, a small site area requirement, and low energy consumption (Sierra *et al.*, 2008; Morweiser *et al.*, 2010).

**Table 2.3: A Comparison of Growing Microalgae in Open Ponds and Photobioreactors**

	<b>Raceway Pond</b>	<b>Photobioreactor</b>
<b>Estimated productivity</b>	11	27
<b>(g.m<sup>-2</sup>.day<sup>-1</sup>)</b>		
<b>Advantages</b>	Low energy Simple technology Inexpensive Well researched	Pure algal culture High volumetric productivity High controllability Small area required Concentrated biomass
<b>Disadvantages</b>	Low productivity Contamination Large area required High water use Dilute biomass	High energy Expensive Less researched

Source: (Cheng, 2010).

Thus, selection of an energy and cost-efficient production model could play a very vital role in achieving competitive biodiesel production. This comprises: (1) the selection of high lipid-producing algae, (2) suitable farming locations, (3) efficient cultivation and harvesting methods and (4) oil extraction procedures. Here, we focus on the third step, the optimization of cultivation conditions to maximize the microalgae yield in a flat plate photobioreactor at pilot scale relevant for commercial biodiesel production.

## **2.6 Harvesting**

As the biomass cannot be used efficiently at low concentrations in media, the first step in the biomass processing stage is harvesting the algae for subsequent processing (Chen *et al.*, 2010; Aitken & Antizar-Ladislao, 2012). The method to be used depends very much upon the type of algae which is under cultivation. Microalgae require more intensive harvesting methods in comparison to macroalgae, because of their cell size. Microalgae cells are small (normally in the range of  $\Phi$  2-70  $\mu\text{m}$ ) and the cell densities in culture broth are low (typically in the range of 0.3 – 5  $\text{gL}^{-1}$ ) (Wu *et al.*, 2012). Depending upon the

characteristics of microalgae (such as density and size) and the target products, often a series of harvesting methods is required to produce a final biomass below a desired moisture content (Wu *et al.*, 2012). Common methods of harvesting of algae are: gravity sedimentation, microfiltration, flotation, centrifugation, flocculation and electrophoresis (Grima *et al.*, 2003; Uduman *et al.*, 2010). Filtration using micro-filters is one of the most effective methods (Aitken & Antizar-Ladislao, 2012). This method of filtration uses a rotary drum covered with a filter to capture the biomass as the influent passes through from the centre outwards (Benemann *et al.*, 1980). Initial harvesting tests in the 1960s tested micro-filters but found that most of the algal cells simply passed through majority of the filter types (Golueke & Oswald, 1965). It was later suggested that micro-filtration was suitable for strains of algae with a cell size greater than 70  $\mu\text{m}$  and was not suitable for those species with cell sizes lower than 30  $\mu\text{m}$  (Brennan & Owende, 2010). The size of the opening in the filter mesh and that of biomass cells dictate what percentage of biomass is captured. The pore size also affects the amount of pressure required to facilitate the flow of water through the filter which eventually affect the amount of energy consumed (Uduman *et al.*, 2010). The concentration of the algae in suspension influences also the efficiency of removal as highly concentrated biomass will foul the filter very quickly leading to reduced performance and a requirement for backwashing. This increases energy consumption (Aitken & Antizar-Ladislao, 2012). If filtration is to be used, it is important that the method suits the species of algae which is being harvested; otherwise, the filtration will be ineffective and provide low yields of biomass (Aitken & Antizar-Ladislao, 2012). If the cultivated algal species allows for filtration (e.g., *Spirulina*, *Spirogyra*, *Coelastrum*), the filtration method can prove to be a very efficient and cost-effective method of harvesting (Aitken & Antizar-Ladislao, 2012). Mohn (1980) for instance found that gravity filtration using a microstainer and vibrating screen both provided good initial harvesting of *Coelastrum* up to a total suspended solid of 6% with low energy consumption (0.4 kWhm<sup>-3</sup>). Mohn (1980) also investigated pressure filtration of *Coelastrum* which provided even higher total solids of concentrate up to 27%, although requiring more than twice the energy. Clearly inexpensive and low energy harvesting of

biomass is possible with filtration, so long as the dominant algae being harvested is of a suitable cell size and optimal concentration level (Aitken & Antizar-Ladislao, 2012).

Flotation and sedimentation have been proven as viable options for harvesting algal biomass with no requirement for specific cell size (Aitken & Antizar-Ladislao, 2012). Both sedimentation and flotation rely on biomass density to facilitate the process. Both processes are aided by flocculation and flotation is aided further by bubbling (Aitken & Antizar-Ladislao, 2012). Sedimentation was considered a viable method of biomass removal in the 1960s due to its prominence in wastewater treatment and its low energy requirement (Golueke & Oswald, 1965). Due to the low specific gravity of algae, the settlement process is slow but, under certain conditions, the self-flocculation of some strains of algae is possible. Carbon and nutrient limitation and pH adjustment appear to be methods of auto-flocculation of algae which may provide a low-cost solution to the initial harvesting process (Benemann *et al.*, 1980; Spilling *et al.*, 2009). Recent studies have focused upon bio-flocculation which occurs as a result of using several bacteria or algal strains to flocculate with the desired algal biomass to allow settlement. Gutzeit *et al.* (2005) discovered that gravity sedimentation was possible using bacterial-algae flocs developed in wastewater for the removal of nutrients, and reported that the flocs of *C. vulgaris* were stable and settled quickly. Other approaches investigated the combined use of autoflocculating microalgae (*A. falcatus*, *Scenedesmus obliquus* and *T. suecica*) to allow for flocculation of non-flocculating oil-accumulating algae (*C. vulgaris* and *Neochloris oleoabundans*) (Salim *et al.*, 2011), which resulted in a faster sedimentation as well as a higher percentage of biomass harvested. This method of harvesting seems viable due to its low energy inputs and it does not rely on chemicals, thus allowing the water to be discharged or recycled without further treatment. However, it should be noted that this method of flocculation may not be suitable for all types of algae. Therefore, further research is required in this area (Aitken & Antizar-Ladislao, 2012).

Conventional methods of flocculation using flocculants common to wastewater treatment such as ferric chloride, alum, ferric sulphide, chitosan among other commercial products are likely to provide a more consistent and effective solution to flocculation (Aitken &



Antizar-Ladislao, 2012). Much research has been conducted upon the removal of algae using flocculants with varying degrees of success (Table 2.4). For instance, a complete removal of freshwater microalgae, *Chlorella* and *Scenedesmus*, using 10 mgL<sup>-1</sup> of polyelectrolytes while 95% removal using 3 mgL<sup>-1</sup> of polyelectrolytes has been reported (Golueke & Oswald, 1965). A comparative study where alum and ferric chloride were used as flocculants for three species of algal biomass (*C. vulgaris*, *I. galbana* and *C. stigmatophora*) indicated the low dosages of alum (25 mgL<sup>-1</sup>) and ferric chloride (11 mgL<sup>-1</sup>) were sufficient for optimal removal of *C. vulgaris*. Higher dosages of alum and ferric chloride were required for the removal of marine cultures *I. galbana* (225 mgL<sup>-1</sup> alum; 120 mgL<sup>-1</sup> ferric chloride) and *C. stigmatophora* (140 mgL<sup>-1</sup> alum; 55 mgL<sup>-1</sup> ferric chloride) (Sukenic *et al.*, 1988). It has also been reported that the combined use of chitosan at low concentrations (2.5 mgL<sup>-1</sup>) and ferric chloride provided much quicker flocculation of the algal cells, *Chlorella vulgaris*, *I. galbana* and *C. stigmatophora*, and reduced the requirement of ferric chloride (De Godos *et al.*, 2009). The use of chitosan as a flocculant for the removal of freshwater algae (*Spirulina*, *Oscillatoria* and *Chlorella*) and brackish algae (*Synechocystis*) has been investigated (Divakaran & Pillai, 2002), and chitosan has been found to be a very effective flocculant, at pH 7.0 and maximum concentrations of 15 mgL<sup>-1</sup>, removing about 90% of algal biomass. The use of conventional and polymeric flocculants for the removal of algal biomass in piggery wastewater has been recently investigated (De Godos *et al.*, 2009): ferric sulphate and ferric chloride were found to be effective flocculants at high doses (150–250 mgL<sup>-1</sup>) providing removal rates greater than 90%. Polymeric flocculants required less dosing (5–50 mgL<sup>-1</sup>), but provided lower biomass recoveries. Chitosan performed poorly at both low and high dosages for each of the algal species types with a maximum removal of 58% at a dose of 25 mgL<sup>-1</sup> for a conglomerate of *Chlorella* (Aitken & Antizar-Ladislao, 2012).

**Table 2.4: Maximum Removal Rates of Various Flocculants for the Removal of Algal Biomass**

<b>Flocculant</b>	<b>Algae</b>	<b>Removal (%)</b>	<b>Dosage (mgL<sup>-1</sup>)</b>	<b>Media type</b>	
<b>FeCl<sub>3</sub></b>	<i>Chlorella</i>	98	250	Piggery wastewater	
	<i>S. obliquus</i>	95	100		
<b>FeCl<sub>3</sub></b>	<i>Chlorococcum</i> sp.	90	150		
	<i>Chlorella</i>	90	250		
<b>Fe<sub>2</sub>(SO<sub>4</sub>)<sub>3</sub></b>	<i>S. obliquus</i>	98	150		
	<i>C. sorokiniana</i>	98	250		
<b>Chitosan</b>	<i>Spirulina, Oscillatoria,</i>	> 90	15		Nutrient media
	<i>Chlorella</i>				
<b>Polyelectrolyte</b>	<i>Chlorella, Scenedesmus</i>	95	3		Sewage
<b>(Puriflocs 601 &amp; 602)</b>					

**Source:** (Golueke & Oswald, 1965; Divakaran & Pillai, 2002; De Godos *et al.*, 2009)

### 2.6.1 Sedimentation

Sedimentation of algal biomass is a method of biomass removal but requires prior flocculation for high removal efficiencies. Sedimentation can be carried out with some species without flocculation, but removal efficiency is considered poor (Shelef *et al.*, 1984). Flocculation can be used to increase cell dimensions allowing improved sedimentation. If carried out in combination with flocculation, a sedimentation tank can provide a reliable solution for biomass recovery (Shelef *et al.*, 1984).

### 2.6.2 Flotation

Flotation was a method of harvesting considered in the 1960s (Golueke & Oswald, 1965), however the recoverability of biomass was found to be poor with a wide range of reagents tested. It has been reported that using dissolved air, flotation mixed algal species could be harvested up to a slurry of 6% total solids (Shelef *et al.*, 1984). Electro-flotation, which creates air bubbles through electrolysis which then attach to the algal cells, mixed algal

species could be harvested up to a slurry of 5%, but this approach required a significant energy input (Golueke & Oswald, 1963). Dispersed air flotation which uses froth or foam to capture the algal cells resulted also in similar results (Golueke & Oswald, 1963). Existing research indicates that flotation offers a quicker alternative to sedimentation following algal flocculation, but more energy is required and hence it is not cost competitive but provides a final product with lower total solids content (Aitken & Antizar-Ladislao, 2012).

### **2.6.3 Centrifugation**

Perhaps the most effective method of biomass removal, with very high recovery rates, is centrifugation (Golueke & Oswald, 1963; Rawat *et al.*, 2011). Compared with the other alternative methods, centrifugation was considered a feasible option in early algal biomass dewatering work in the 1960s (Aitken & Antizar-Ladislao, 2012). Golueke and Oswald (1963) investigated various methods of dewatering algae further to provide a biomass with sufficiently low moisture content. One of the method they looked at was centrifugation and three of the four centrifuges that they tested proved to be extremely effective producing a maximum removal of 79% and a biomass with solids content of 11.5% and maximum of 18.2%. Further research was conducted by Mohn (1980) in the area of harvesting algal biomass using centrifugation and he focused on suitability of algal strains, cost and energy use. Mohn found centrifuges to be very effective for the removal of *Scenedesmus* and *Coelastrum*, particularly the Westfalia self-cleaning plate separator and the Westfalia nozzle centrifuge (Mohn, 1980). This was in agreement with Golueke and Oswald. The centrifuges provided biomass with total solids content of 2%–22% with a minimum energy consumption of 0.9 kWhm<sup>-3</sup> (Mohn, 1980). Table 2.5 provides a summary of Mohn's findings indicating the possible harvesting methods, effectiveness, energy requirements and reliability of several harvesting methods. Mohn's (1980) results suggest filtration provides the best harvesting strategy in terms of high concentration of solids with low energy requirements.

**Table 2.5: Harvesting Methods, Effectiveness and Energy Requirements**

<b>Algae species</b>	<b>Harvesting method</b>	<b>%TSS of concentrate</b>	<b>Concentration factor</b>	<b>Energy Requirement kWh</b>	<b>Reliability</b>
<i>Coelastrum</i>	Gravity filtration	6	60	0.4	Good
<i>Coelastrum</i>	Pressure filtration	22-27	245	0.88	Very high
<i>Scenedesmus, Coelastrum, Proboscideum</i>	Centrifuge (Westfalia self-cleaning)	12	120	1	Very high
<i>Scenedesmus, Coelastrum, Proboscideum</i>	Centrifuge (Westfalia screw)	22	11	8	Very high

Source: (Mohn, 1980).

Even though centrifugation is an effective method of concentrating biomass, the energy requirements are much higher than that of filtration. However, clearly the choice of harvesting depends heavily upon the biomass type, if the cell size is large enough, then filtration is probably the most effective and economically viable option. Otherwise, it is likely that a process stream involving flocculation, sedimentation, flotation or centrifugation is necessary (Aitken & Antizar-Ladislao, 2012). There is little parallel between the effectiveness of common flocculants for harvesting algae in research conducted. It can be observed that there are many effective flocculants for algae removal however suggested optimal dosages vary significantly between studies. Ferric chloride can be considered a viable option potentially combined with chitosan to improve yield and reduce time and material input. Further research is necessary for individual scenarios to choose the most effective method of flocculation and consequent harvesting (Aitken & Antizar-Ladislao, 2012).

## **2.7 Pilot-Scale Microalgae Production**

There are numerous pilot-scale biodiesel production facilities using microalgal biomass in operation in the last few years (Cheng, 2010). Aurora Biofuels, Inc., a bioenergy firm in California, USA, has run a pilot microalgal biodiesel production facility in Florida, USA since 2007 ([www.americanfuels.info/2009/03/aurora-biofuels-pilot-algae-plant.html](http://www.americanfuels.info/2009/03/aurora-biofuels-pilot-algae-plant.html)). In this facility, microalgae with high oil content have been grown on seawater in open ponds on non-arable land. The company has developed efficient technologies in microalgae harvesting and oil extraction. Engineers and scientists at Old Dominion University built an algal farm to produce biodiesel in Virginia, USA in 2008 (Cheng, 2010). A one-acre open algal pond has been established to produce algal biomass for biodiesel production. Treated wastewater has been used to grow microalgae in the pond. Algal oil has been extracted from the biomass to produce 3,000 gallons of biodiesel fuel per year ([www.odu.edu/ao/news/index.php?todo=details&id=12031](http://www.odu.edu/ao/news/index.php?todo=details&id=12031)). Renewable Energy Group (REG), a biodiesel production company based in Iowa, USA developed a pilot-scale biodiesel production technology using the oil from a variety of microalgae in 2008 (Cheng, 2010). The pilot plant can produce a huge amount of high-quality biodiesel from microalgae. The company has developed a pretreatment technology that cleanses the crude oil from microalgae. The clean oil is then used for transesterification to produce biodiesel ([www.hydrocarbons-technology.com/projects/algae-biodiesel/](http://www.hydrocarbons-technology.com/projects/algae-biodiesel/)).

## **2.8 Challenges for Commercialization of Microalgal Biodiesel**

In principle, producing biodiesel from microalgae has been proven economically viable. The land area required to produce the same amount of oil from microalgae is only a small portion of that for oil crops. Biodiesel production from microalgal biomass or the advanced biodiesel technology has a potential for biofuel production to substitute fossil fuel without serious competition for arable land against food and feed production (Cheng, 2010). However, the prime challenge of the advanced biodiesel production is its high cost (Grobbelaar, 2013). The present microalgae production and the separation of the microalgal biomass from the growing media are too costly (Ruffing, 2011; Dutta *et al.*,

2014; Gerchman *et al.*, 2016; Tan *et al.*, 2020). An estimated cost to produce a kilogram of microalgal biomass with a mean oil content of 30% is \$2.95 and \$3.80 for photobioreactors and open ponds, respectively, assuming that carbon dioxide is available and free (Chisti, 2007). Taking account of 30% oil content in the microalgal biomass and the cost of oil extraction from the microalgae, the cost to produce a kilogram (approximately 1.14 liters) of crude microalgal oil is more than three times of that of producing a kilogram microalgal biomass (Cheng, 2010). This cost is much higher than vegetable oil production, e.g. the market price for crude palm oil which is possibly the cheapest vegetable oil was only \$0.52/liter in the US in 2006. It would be more discouraging if compared with mineral diesel production cost (the retail price of mineral diesel including taxes in the US in 2006 was only between \$0.66 and \$0.97 per liter) (Cheng, 2010). As of late 2008, Darzins (2008) indicated that seven US government laboratories, thirty US universities, and around sixty biofuels companies were conducting study in this area. Passionate efforts are also taking place in other parts of the world including (among many others) Australia, Europe, the Middle East, and New Zealand (Pienkos & Darzins, 2009).

## **2.9 Optimization**

Optimization is the act of finding the best result under given circumstances. In design, construction, and maintenance of any engineering system, engineers have to take many technological and managerial decisions at several stages. The ultimate goal of all such decisions is either to minimize the effort (input) required or to maximize the desired benefit (output). Since the effort required or the benefit desired in any practical situation can be written as a function of certain decision variables, optimization can be defined as the process of finding the conditions that give the maximum or minimum value of a function. Also, optimization can be taken to mean minimization since the maximum of a function can be found by seeking the minimum of the negative of the same function (Rao, 2009).

The classical methods of optimization are useful in finding the optimum solution of continuous and differentiable functions. These methods are analytical and make use of the techniques of differential calculus in locating the optimum points. Since some of the practical problems involve objective functions that are not continuous and/or differentiable, the classical optimization techniques have limited scope in practical applications. In recent years, some optimization techniques that are conceptually different from the traditional mathematical programming methods have been developed. These techniques are labeled as modern or nontraditional methods of optimization. Most of these techniques are based on certain characteristics and behavior of biological, molecular, swarm of insects, and neurobiological systems. These techniques are: 1. Genetic algorithms 2. Simulated annealing 3. Particle swarm optimization 4. Ant colony optimization 5. Fuzzy optimization and 6. Neural-network-based methods. These techniques are emerging as popular methods for the solution of complex engineering problems. Most require only the function values (and not the derivatives). The genetic algorithms are based on the principles of natural genetics and natural selection (Rao, 2009).

Countless practical optimum design problems are described by; mixed continuous–discrete variables, and discontinuous and nonconvex design spaces. If standard nonlinear programming methods are used for this type of problem, they will be inefficient, computationally expensive, and, in most cases, find a relative optimum that is closest to the starting point. Genetic algorithms (GAs) are well suited for solving such problems, and in most cases they can find the global optimum (minimum) solution with a high probability (Rao, 2009).

### **2.9.1 Genetic Algorithms**

Natural selection and natural genetics are the foundation of genetic algorithms. The genetic search process makes use of reproduction, crossover, and mutation—the fundamental components of natural genetics. The following are some ways that GAs vary from conventional optimization techniques (Rao, 2009):

1. The process is started using a population of points (trial design vectors) rather than a single design point. If the number of design variables is  $n$ , usually the size of the population is taken as  $2n$  to  $4n$ . Since several points are used as candidate solutions, GAs are less likely to get trapped at a local optimum.
2. GAs use only the values of the objective function. The derivatives are not used in the search procedure.
3. The design variables in GAs are expressed as binary variable strings that match the chromosomes in natural genetics. As a result, the search approach can be used to solve both discrete and integer programming issues. The string length for continuous design variables can be adjusted to reach any required resolution.
4. The objective function value corresponding to a design vector plays the role of fitness in natural genetics.
5. Every new generation of strings is created via crossover from the previous generation (old set of strings) and randomized parents selection. GAs are not just random search methods, even though they are randomized. In order to identify a new generation with higher fitness or an objective function value, they effectively explore new combinations using the knowledge at their disposal.

### **2.9.1.1 Representation of Design Variables**

The binary values 0 and 1 are used to denote the design variables in GAs. For example, if a design variable  $x_i$  is denoted by a string of length four (or a four-bit string) as 0 1 0 1, its integer (decimal equivalent) value will be  $(1) 2^0 + (0) 2^1 + (1) 2^2 + (0) 2^3 = 1 + 0 + 4 + 0 = 5$ . If each design variable  $x_i, i = 1, 2, \dots, n$  is coded in a string of length  $q$ , a design vector is represented using a string of total length  $nq$  (Rao, 2009).

### **2.9.1.2 Representation of Objective Function and Constraints**

Genetic algorithms aim to optimize a function known as the fitness function since they are predicated on the idea that the strongest organisms survive. GAs are therefore ideally suited to handle unconstrained maximization problems. The fitness function,  $F(\mathbf{X})$ , can



be taken to be same as the objective function  $f(\mathbf{X})$  of an unconstrained maximization problem so that  $F(\mathbf{X}) = f(\mathbf{X})$ . Prior to using the GAs, a minimization problem can be converted into a maximization problem. Typically, a nonnegative fitness function is selected. The transformation that is typically applied to change an unconstrained minimization issue into a fitness function is given by (Rao, 2009)

$$F(\mathbf{X}) = \frac{1}{1+f(\mathbf{X})} \quad \text{Equation 2.1}$$

It is evident that Equation (2.1) transforms the minimization problem into an analogous maximization problem rather than changing the location of the minimum of  $f(\mathbf{X})$ . A general constrained minimization problem can be stated as

Minimize  $f(\mathbf{X})$

subject to

$$g_i(\mathbf{X}) \leq 0, i = 1, 2, \dots, m \quad \text{Equation 2.2}$$

and

$$h_j(\mathbf{X}) = 0, j = 1, 2, \dots, p$$

With the use of the penalty function idea, this problem can be transformed into an equivalent unconstrained minimization problem as

$$\text{Minimize } \emptyset(\mathbf{X}) = f(\mathbf{X}) + \sum_{i=1}^m r_i (g_i(\mathbf{X}))^2 + \sum_{j=1}^p R_j (h_j(\mathbf{X}))^2 \quad \text{Equation 2.3}$$

Where  $r_i$  and  $R_j$  are the penalty parameters associated with the constraints  $g_i(\mathbf{X})$  and  $h_j(\mathbf{X})$  whose values are usually kept constant throughout the solution process. In Equation 2.3, the function  $\langle g_i(\mathbf{X}) \rangle$ , called the bracket function, is defined as

$$\langle g_i(\mathbf{X}) \rangle = \begin{cases} g_i(\mathbf{X}) & \text{if } g_i(\mathbf{X}) > 0 \\ 0 & \text{if } g_i(\mathbf{X}) \leq 0 \end{cases} \quad \text{Equation 2.4}$$

Generally speaking, it is believed that the penalty parameters connected to each inequality and equality requirement are the same constants as

$$r_i = r, \quad i = 1, 2, \dots, m \quad \text{and} \quad R_j = R, \quad j = 1, 2, \dots, p \quad \text{Equation 2.5}$$

Where  $r$  and  $R$  are constants. The fitness function,  $F(\mathbf{X})$ , to be maximized in the GAs can be obtained, similar to Equation 2.1, as

$$F(\mathbf{X}) = \frac{1}{1+\phi(\mathbf{X})} \quad \text{Equation 2.6}$$

Equations (2.3) and (2.4) show that the penalty will be proportional to the square of the amount of violation of the inequality and equality constraints at the design vector  $\mathbf{X}$ , while there will be no penalty added to  $f(\mathbf{X})$  if all the constraints are satisfied at the design vector  $\mathbf{X}$  (Rao, 2009).

### 2.9.1.3 Genetic Operators

A population of random strings representing many design vectors is the first step in the GAs' optimization problem solving process. The population size in GAs ( $n$ ) is usually fixed. Each string (or design vector) is evaluated to find its fitness value. The population (of designs) is operated by three operators—reproduction, crossover, and mutation—to produce a new population of points (designs). The new population is put through additional analysis to determine its fitness values and convergence of the process. In GAs, a generation is defined as one cycle of crossover, mutation, and reproduction together with the assessment of fitness values. The population is iteratively operated by the three operators, and the resulting new population is assessed for fitness values if the convergence requirement is not met. Until the convergence requirement is met and the process is stopped, it is repeated over a number of generations (Rao, 2009).

### 2.9.1.3.1 Reproduction

The first process that is used on a population to choose suitable strings (designs) to create a mating pool is reproduction. Because it chooses the best strings within the population, the reproduction operator is also known as the selection operator. Using a probabilistic process, the reproduction operator selects above-average strings from the current population and places additional copies of those strings in the mating pools. In a commonly used reproduction operator, a string is selected from the mating pool with a probability proportional to its fitness. Thus if  $F_i$  denotes the fitness of the  $i^{th}$  string in the population of size  $n$ , the probability for selecting the  $i^{th}$  string for the mating pool ( $p_i$ ) is given by (Rao, 2009)

$$p_i = \frac{F_i}{\sum_{j=1}^n F_j}; i = 1, 2, \dots, n \quad \text{Equation 2.7}$$

### 2.9.1.3.2 Crossover

The crossover operator is applied after reproduction. By sharing information between strings in the mating pool, crossover aims to create new strings. The majority of crossover operators include the random selection of two distinct strings (or designs) from the mating pool created by the reproduction operator and some portions of the strings are exchanged between the strings. In the commonly used process, known as a single-point crossover operator, a crossover site is selected at random along the string length, and the binary digits (alleles) lying on the right side of the crossover site are swapped (exchanged) between the two strings. The two strings selected for participation in the crossover operators are known as parent strings and the strings generated by the crossover operator are known as child strings (Rao, 2009).

### 2.9.1.3.3 Mutation

The primary operator used to generate new strings with improved fitness values for the upcoming generations is the crossover. The new strings with a particular tiny mutation

probability,  $p_m$ , are subjected to the mutation operator. The mutation operator changes the binary digit (allele's value) 1 to 0 and vice versa. The mutation operator can be implemented in a number of ways. In a single-point mutation, a random mutation site is chosen along the length of the string, and with a probability of  $p_m$ , the binary digit at that site is changed from 1 to 0 or 0 to 1. In the bit-wise mutation, each bit (binary digit) in the string is considered one at a time in sequence, and the digit is changed from 1 to 0 or 0 to 1 with a probability  $p_m$ . In terms of numbers, the procedure can be carried out as follows: A random number is generated, or selected, between 0 and 1. The binary digit is altered if the random integer is less than  $p_m$ . If not, Rao (2009) states that the binary digit remains unchanged.

It should be mentioned that the three operators; mutation, crossover, and reproduction, are easy to use. The crossover operator recombines the substrings of the mating pool's good strings to form strings (the next generation of the population), the mutation operator modifies the string locally, and the reproduction operator chooses good strings for the mating pool. By applying these three operators in turn, new generations with higher population average fitness values are produced. It has been discovered that the process converges to the objective function's optimal fitness value, even though the improvement in the strings' fitness over successive generations cannot be demonstrated mathematically.

Keep in mind that the reproduction operator in the following generation will remove any bad strings that are produced at any point during the process. Numerous optimization problems have been effectively resolved by GAs in the literature (Rao, 2009).

#### **2.9.1.4 Algorithm**

The following steps can be used to describe the computational procedure in optimizing the fitness function  $F(x_1, x_2, x_3, \dots, x_n)$  in the genetic algorithm (Rao, 2009):

1. A suitable string length  $l = ng$  is chosen to represent the  $n$  design variables of the design vector  $\mathbf{X}$ . Suitable values for the following parameters are assumed:

population size  $m$ , crossover probability  $p_c$ , mutation probability  $p_m$ , permissible value of standard deviation of fitness values of the population  $(s_f)_{max}$  to use as a convergence criterion, and maximum number of generations  $(i_{max})$  to be used as a second convergence criterion.

2. A random population of size  $m$  is generated each consisting of a string of length  $l = ng$ . The fitness values  $F_i, i = 1, 2, \dots, m$  of the  $m$  strings is then evaluated.
3. The process of reproduction is executed.
4. The crossover probability,  $p_c$ , is used to perform the crossover operation
5. The new generation of  $m$  strings is determined by the mutation process by applying the mutation probability  $p_m$ .
6. For each of the  $m$  strings in the new population, the fitness values  $F_i, i = 1, 2, \dots, m$ , are assessed. The standard deviation of the  $m$  fitness values is then calculated.
7. The process or algorithm's convergence is evaluated. If  $s_f \leq (s_f)_{max}$ , the process can be terminated as the convergence requirement is met. If not, proceed to step 8.
8. A test is conducted on the generation number. The procedure can be terminated if  $i = i_{max}$ , indicates that the calculations have been completed for the maximum number of generations that are permitted. If not, the generation number is set as  $i = i + 1$  and go to step 3 (Rao, 2009).

### **2.9.1.5 Advantages of Genetic Algorithms**

They can be summarized as (Mwakabuta & Sekar, 2008):

1. Works well with discrete or continuous variables.
2. Conducts multiple simultaneous searches across a large sample of the search surface.
3. Handles a considerable amount of variables.
4. Offers a list of the best variables rather than simply one answer.
5. Optimizes variables with incredibly intricate cost surfaces.

6. The variables might be encoded so that the encoded variables are used for optimization.
7. Uses analytical functions, experimental data, or data created numerically.

### **2.9.2 Simulated Annealing**

The simulation of thermal annealing of solids heated to critical temperatures forms the basis of the simulated annealing (SA) technique. The atoms in a metal move freely with regard to one another when it is heated to a high temperature, causing it to become molten. However, when the temperature drops, atoms' motions become more constrained. Atoms tend to become more organized as the temperature drops, eventually forming crystals with the least amount of internal energy (Rao, 2009). The rate of cooling is the primary determinant of the crystal formation process. The molten metal may not be able to reach the crystalline state if its temperature is lowered quickly; instead, it may form a polycrystalline state with a higher energy state than the crystalline state. Rapid cooling can induce internal material flaws in engineering applications. In order to ensure appropriate solidification with a highly ordered crystalline form that corresponds to the lowest energy state (internal energy), the temperature of the heated solid (molten metal) needs to be reduced at a slow and regulated rate. Annealing is the term for this gradual cooling process (Rao, 2009).

#### **2.9.2.1 Procedure**

The simulated annealing method simulates the process of slow cooling of molten metal to attain the minimum function value in a minimization problem. By introducing and regulating a temperature-like parameter, the cooling phenomena of the molten metal is reproduced by the use of Boltzmann's probability distribution principle. According to the relation, the energy ( $E$ ) of a system in thermal equilibrium at temperature  $T$  is distributed probabilistically, as per the Boltzmann's probability distribution (Rao, 2009).

$$P(E) = e^{-E/kT} \quad \text{Equation 2.8}$$

where  $P(E)$  represents the probability of achieving the energy level  $E$ , and  $k$  is called the Boltzmann's constant. Equation (2.8) demonstrates that at high temperatures the system has nearly a uniform probability of being at any energy state; however, at low temperatures, the system has a small probability of being at a high-energy state. This suggests that the temperature  $T$  can be adjusted to regulate the simulated annealing algorithm's convergence when the search process is considered to follow Boltzmann's probability distribution. In the context of function minimization, Metropolis *et al.* (1953) method of implementing Boltzmann's probability distribution in simulated thermodynamic systems can also be applied (Rao, 2009).

In the case of function minimization, let the current design point (state) be  $\mathbf{X}_i$ , with the corresponding value of the objective function given by  $f_i = f(\mathbf{X}_i)$ . Similar to the energy state of a thermodynamic system, the energy  $E_i$  at state  $\mathbf{X}_i$  is given by

$$E_i = f_i = f(\mathbf{X}_i) \quad \text{Equation 2.9}$$

Then, according to the Metropolis criterion, the probability of the next design point (state)  $\mathbf{X}_{i+1}$  depends on the difference in the energy state or function values at the two design points (states) given by

$$\Delta E = E_{i+1} - E_i = \Delta f = f_{i+1} - f_i \equiv f(\mathbf{X}_{i+1}) - f(\mathbf{X}_i) \quad \text{Equation 2.10}$$

The new state or design point  $\mathbf{X}_{i+1}$  can be found using the Boltzmann's probability distribution:

$$P[E_{i+1}] = \min\{1, e^{-\Delta E/kT}\} \quad \text{Equation 2.11}$$

The Boltzmann's constant serves as a scaling factor in simulated annealing and, as such, can be chosen as 1 for simplicity. Note that if  $\Delta E \leq 0$ , Equation (2.11) gives  $P[E_{i+1}] = 1$  and hence the point  $\mathbf{X}_{i+1}$  is always accepted. This is a logical choice in the context of

minimization of a function because the function value at  $\mathbf{X}_{i+1}$ ,  $f_{i+1}$ , is better (smaller) than at  $\mathbf{X}_i$ ,  $f_i$ , and hence the design vector  $\mathbf{X}_{i+1}$  must be accepted. On the other hand, when  $\Delta E > 0$ , the function value  $f_{i+1}$  at  $\mathbf{X}_{i+1}$  is worse (larger) than the one at  $\mathbf{X}_i$ . According to most conventional optimization procedures, the point  $\mathbf{X}_{i+1}$  cannot be accepted as the next point in the iterative process. Nevertheless, the probability of accepting the point  $\mathbf{X}_{i+1}$ , in spite of its being worse than  $\mathbf{X}_i$  in terms of the objective function value, is finite (although it may be small) according to the Metropolis criterion, (Metropolis *et al.*, 1953). Note that the probability of accepting the point  $\mathbf{X}_{i+1}$

$$P[E_{i+1}] = \{e^{-\Delta E/kT}\} \quad \text{Equation 2.12}$$

is not same in all situations. As can be seen from Equation (2.12), this probability depends on the values of  $\Delta E$  and. If the temperature  $T$  is large, the probability will be high for design points  $\mathbf{X}_{i+1}$  with larger function values (with larger values of  $\Delta E = \Delta f$ ). Thus at high temperatures, even worse design points  $\mathbf{X}_{i+1}$  are likely to be accepted because of larger probabilities. However, if the temperature  $T$  is small, the probability of accepting worse design points  $\mathbf{X}_{i+1}$  (with larger values of  $\Delta E = \Delta f$ ) will be small. Thus as the temperature values get smaller (that is, as the process gets closer to the optimum solution), the design points  $\mathbf{X}_{i+1}$  with larger function values compared to the one at  $\mathbf{X}_i$  are less likely to be accepted (Rao, 2009).

### 2.9.2.2 Algorithm

The SA algorithm can be summarized as follows: Starting with an initial design vector  $\mathbf{X}_1$  (iteration number  $i = 1$ ) and a high value of temperature  $T$ . A new design point is generated randomly in the vicinity of the current design point and the difference in function values is found (Rao, 2009):

$$\Delta E = \Delta f = f_{i+1} - f_i \equiv f(\mathbf{X}_{i+1}) - f(\mathbf{X}_i) \quad \text{Equation 2.13}$$



If  $f_{i+1}$  is smaller than  $f_i$  (with a negative value of  $\Delta f$ ), point  $\mathbf{X}_{i+1}$  is accepted as the next design point. Otherwise, when  $\Delta f$  is positive, then point  $\mathbf{X}_{i+1}$  is accepted as the next design point only with a probability  $e^{-\Delta E/kT}$ . This means that if the value of a randomly generated number is larger than  $e^{-\Delta E/kT}$ , the point  $\mathbf{X}_{i+1}$  is accepted; otherwise, the point  $\mathbf{X}_{i+1}$  is rejected. This completes one iteration of the SA algorithm. If the point  $\mathbf{X}_{i+1}$  is rejected, then the process of generating a new design point  $\mathbf{X}_{i+1}$  randomly in the vicinity of the current design point, evaluating the corresponding objective function value  $f_{i+1}$ , and deciding to accept  $\mathbf{X}_{i+1}$  as the new design point, based on the use of the Metropolis criterion, Equation (2.12), is continued. To simulate the attainment of thermal equilibrium at every temperature, a predetermined number ( $n$ ) of new points  $\mathbf{X}_{i+1}$  are tested at any specific value of the temperature  $T$  (Rao, 2009).

Once the number of new design points  $\mathbf{X}_{i+1}$  tested at any temperature  $T$  exceeds the value of  $n$ , the temperature  $T$  is reduced by a prespecified fractional value  $c$  ( $0 < c < 1$ ) and the whole process is repeated. The procedure is assumed to have converged when the current value of temperature  $T$  is sufficiently small or when changes in the function values ( $\Delta f$ ) are observed to be sufficiently small.

The initial temperature  $T$ , the number of iterations  $n$  prior to lowering the temperature, and the temperature reduction factor  $c$  are critical decisions that affect how well the SA algorithm converges. For example, more temperature reductions are needed for convergence if the initial temperature  $T$  is too high. However, the search procedure can be insufficient if the starting temperature is set too low, since it might not fully explore the design space to find the global minimum prior to convergence (Rao, 2009). The impact of the temperature reduction factor  $c$  is similar. A value of  $c$  that is excessively high (like 0.8 or 0.9) necessitates excessive computing work in order to reach convergence. However, using a value of  $c$  that is too small (e.g., 0.1 or 0.2) could cause the temperature to drop more quickly and prevent a full investigation of the design space in order to find the global minimum solution. Similar to this, a high value for  $n$  will increase the computing effort required to reach a quasiequilibrium condition at any temperature.

Conversely, a smaller value of  $n$  could lead to either a local minimum or an early convergence (since the design space for the global minimum would not have been sufficiently explored) (Rao, 2009). Sadly, there is not a single set of values for  $T$ ,  $n$ , and  $c$  that will be ideal for every situation. Nonetheless, there are several rules that can be followed while choosing these values. The average value of the objective function calculated at several randomly chosen sites in the design space can be used to determine the beginning temperature  $T$ . Depending on the available computer power and the required level of solution accuracy, the number of iterations ( $n$ ) can be selected between 50 and 100. For a reasonable temperature reduction strategy (also known as the cooling schedule), the temperature reduction factor  $c$  can be selected between 0.4 and 0.6.

In the literature, more intricate cooling schedules based on predicted mathematical convergence rates have been applied to solve challenging real-world optimization issues (Atiquillah & Rao, 1995). The selection of the starting temperature  $T$ , the number of iterations  $n$  at any given temperature, and the temperature reduction factor (or cooling rate)  $c$  remain an art and typically require a trial-and-error process to find suitable values for solving any particular type of optimization problems, despite all the research being done on SA algorithms. The SA procedure is shown as a flowchart in Figure 2.4.

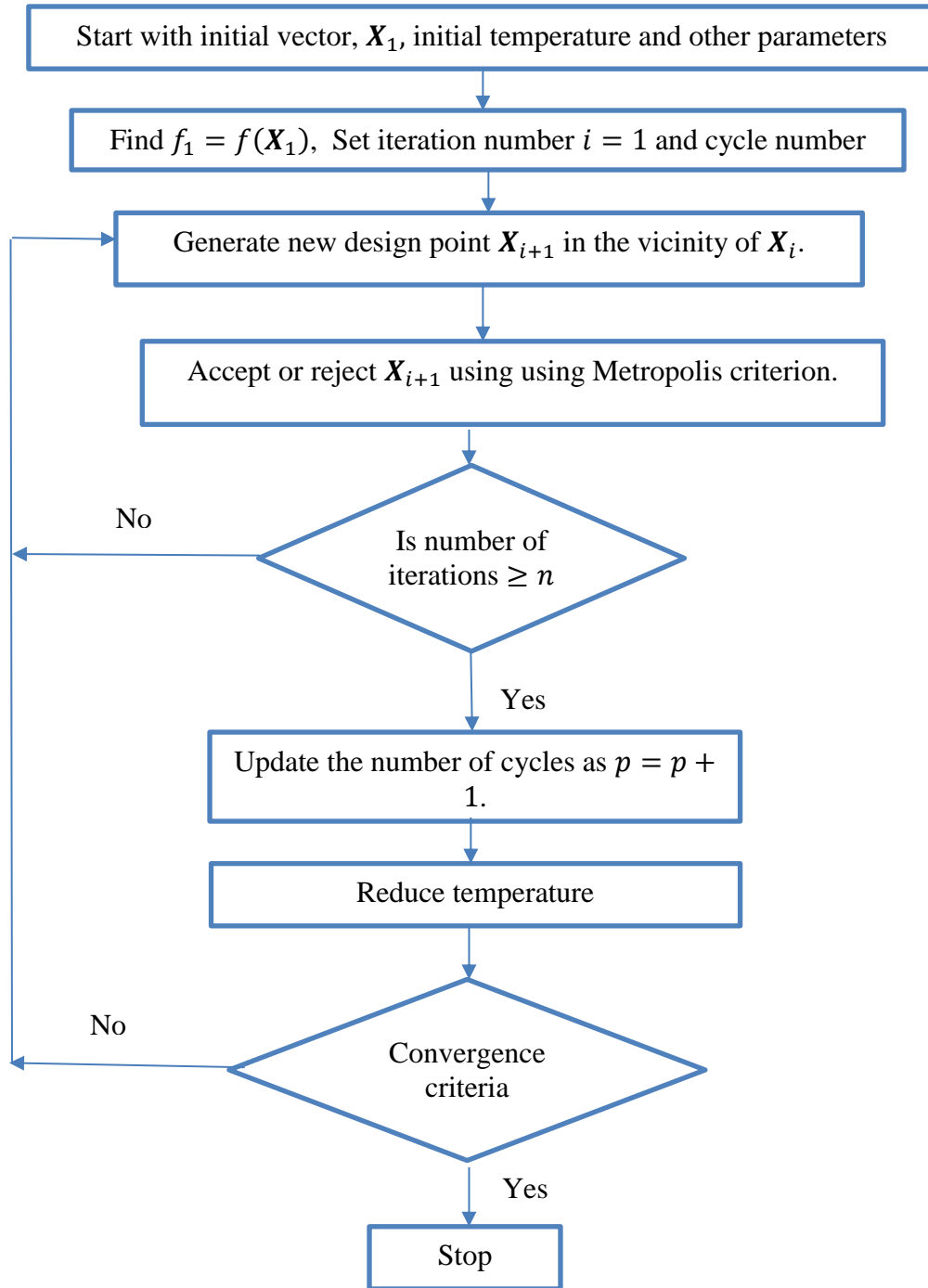


**Figure 2.4: Simulated Annealing Procedure**

Source: (Rao, 2009)

### **2.9.2.3 Features of the SA Method**

Some of the features of simulated annealing are as follows (Rao, 2009):

1. The initial assumptions have no effect on the quality of the eventual solution; the only possible effect is that a worse starting design may require more computational work.
2. The convergence or transition characteristics are independent of the functions' continuity or differentiability due to the discrete nature of the function and constraint assessments.
3. The feasible space's convexity has no bearing on the convergence.
4. The design variables need not be positive.
5. Discrete, continuous, or mixed-integer problems can all be resolved using this method.
6. Similar to evolutionary algorithms, an equivalent unconstrained function must be defined for issues with behavior restrictions (along with lower and upper bounds on the design variables).

### **2.9.3 Particle Swarm Optimization**

The behavior of a colony or swarm of insects, such as ants, termites, bees, and wasps; a flock of birds; or a school of fish, serves as the basis for particle swarm optimization (PSO). According to Rao (2009), the PSO algorithm emulates the actions of these social creatures. The term "particle" refers to things like a bird in a flock or a bee in a colony. A swarm's individual particles act in a distributed manner, drawing on both their individual intelligence and the collective intelligence of the group. Because of this, even if a particle in the swarm is located far away, the other particles will be able to follow the good path to food promptly if one of them finds it. Swarm intelligence-based optimization techniques are referred to as behaviorally inspired algorithms, whereas genetic algorithms are considered evolution-based procedures. Kennedy and Eberhart (1995) were the first to propose the PSO algorithm.

Inside the framework of multivariable optimization, it is presumed that the swarm possesses a fixed or determined size, with every particle initially situated at random points inside the multidimensional design space. It is considered that every particle possesses two attributes: a position and a velocity. Every particle roams around the design space, remembering the optimal location it finds for the food source or objective function value. The particles exchange information, or good positions, with one another and modify their respective velocities and positions in response to the information they get about the good locations.

The actions of a flock of birds is used as an illustration. Even though each bird is only somewhat intelligent, they all adhere to the same basic principles (Rao, 2009):

1. It makes an effort to avoid getting too close to other birds.
2. It follows the general path taken by other birds.
3. It makes an effort to find the "average position" among the other birds in the flock, avoiding large gaps.

Therefore, a combination of three straightforward elements determines how the flock or swarm behaves:

1. Cohesion: remain unified.
2. Separation: Keep your distance from each other.
3. Alignment: adhere to the flock's main heading.

The PSO was created using the following model as a foundation (Rao, 2009):

1. A single bird instantly notifies the others of its location when it finds food or a target, or when it reaches the maximum of the objective function.
2. All other birds, though not directly, move toward the target or food (or the maximum of the objective function).
3. Every bird has a portion of its own autonomous thought process in addition to its past memory.

As a result, the model mimics a random search for the objective function's highest value throughout the design space. Consequently, the birds approach the target (or maximum of the objective function) gradually over a large number of iterations.

### 2.9.3.1 Computational Implementation of PSO

Let's look into an unrestricted maximizing problem:

$$\text{Maximize } f(\mathbf{X})$$

$$\text{With } \mathbf{X}^{(l)} \leq \mathbf{X} \leq \mathbf{X}^{(u)} \quad \text{Equation 2.13}$$

where  $\mathbf{X}^{(l)}$  and  $\mathbf{X}^{(u)}$  denote the lower and upper bounds on  $\mathbf{X}$ , respectively. The following stages can be used to implement the PSO process (Rao, 2009):

1. It is assumed that the swarm has a size of  $N$  particles. The swarm must be assumed to be lower in size in order to minimize the total number of function evaluations required in order to discover a solution. However, if the swarm size is too small, it can take longer to discover a solution or, in certain situations, it might not find one at all. As a compromise, a size of 20 to 30 particles is typically assumed for the swarm.
2. Initial population of  $\mathbf{X}$  is generated in the range  $\mathbf{X}^{(l)}$  and  $\mathbf{X}^{(u)}$  randomly as  $\mathbf{X}_1, \mathbf{X}_2, \dots, \mathbf{X}_N$ . Hereafter, for convenience, the particle (position of)  $j$  and its velocity in iteration  $i$  are denoted as  $\mathbf{X}_j^{(i)}$  and  $\mathbf{V}_j^{(i)}$ , respectively. Thus the particles generated initially are denoted  $\mathbf{X}_1(0), \mathbf{X}_2(0), \dots, \mathbf{X}_N(0)$ . The vectors  $\mathbf{X}_j(0)$  ( $j = 1, 2, \dots, N$ ) are called particles or vectors of coordinates of particles (similar to chromosomes in genetic algorithms). The objective function values corresponding to the particles are evaluated as  $f[\mathbf{X}_1(0)], f[\mathbf{X}_2(0)], \dots, f[\mathbf{X}_N(0)]$ .

3. Calculations are made regarding particle velocities. Every particle will have a velocity and travel to the ideal location. All particle velocities are initially assumed to be zero. The iteration number is set as  $i = 1$ .
4. In the  $i^{\text{th}}$  iteration, the following two important parameters used by a typical particle  $j$  are calculated:
  - (a) The historical best value of  $\mathbf{X}_j(i)$  (coordinates of  $j^{\text{th}}$  particle in the current iteration  $i$ ),  $P_{best,j}$ , with the highest value of the objective function,  $f[\mathbf{X}_j(i)]$ , encountered by particle  $j$  in all the previous iterations. The historical best value of  $\mathbf{X}_j(i)$  (coordinates of all particles up to that iteration),  $G_{best}$ , with the highest value of the objective function  $f[\mathbf{X}_j(i)]$ , encountered in all the previous iterations by any of the  $N$  particles.
  - (b) The velocity of particle  $j$  in the  $i^{\text{th}}$  iteration is calculated as follows:

$$\begin{aligned} \mathbf{V}_j(i) = & \mathbf{V}_j(i - 1) + c_1 r_1 [P_{best,j} - \mathbf{X}_j(i - 1)] \\ & + c_2 r_2 [G_{best} - \mathbf{X}_j(i - 1)]; j = 1, 2, \dots, N \end{aligned} \quad \text{Equation 2.14}$$

Where  $c_1$  and  $c_2$  are the cognitive (individual) and social (group) learning rates, respectively, and  $r_1$  and  $r_2$  are uniformly distributed random numbers in the range 0 and 1. The parameters  $c_1$  and  $c_2$  denote the relative importance of the memory (position) of the particle itself to the memory (position) of the swarm. The values of  $c_1$  and  $c_2$  are usually assumed to be 2 so that  $c_1 r_1$  and  $c_2 r_2$  ensure that the particles would overfly the target about half the time.

- (c) The position or coordinate of the  $j^{\text{th}}$  particle in  $i^{\text{th}}$  iteration is calculated as

$$\mathbf{X}_j(i) = \mathbf{X}_j(i - 1) + \mathbf{V}_j(i); j = 1, 2, \dots, N \quad \text{Equation 2.15}$$

Where a time step of unity is assumed in the velocity term in Equation (2.15). The objective function values corresponding to the particles are then evaluated as  $f[\mathbf{X}_1(i)], f[\mathbf{X}_2(i)], \dots, f[\mathbf{X}_N(i)]$ .

5. Next, the existing solution's convergence is examined. The approach is considered to have converged if all particle positions converge to the same set of values. If the convergence criterion is not satisfied, step 4 is repeated by updating the iteration number as  $i = i + 1$ , and by computing the new values of  $P_{best,j}$  and  $G_{best}$ . The iterative process is continued until all particles converge to the same optimum solution (Rao, 2009).

### 2.9.3.2 Improvement to the Particle Swarm Optimization method

It was discovered that, in most cases, the particle velocities increase too quickly, skipping the objective function's maximum (Rao, 2009). Therefore, to lower the velocity, an inertia term,  $\theta$ , is introduced. Typically, as the iterative process advances, the value of  $\theta$  is supposed to vary linearly from 0.9 to 0.4. The velocity of the  $j^{th}$  particle, with the inertia term, is assumed as

$$\mathbf{V}_j(i) = \theta \mathbf{V}_j(i - 1) + c_1 r_1 [P_{best,j} - \mathbf{X}_j(i - 1)] + c_2 r_2 [G_{best} - \mathbf{X}_j(i - 1)]; j = 1, 2, \dots, N \quad \text{Equation 2.16}$$

When compared to the original PSO algorithm with Equation (2.14), the swarm was able to converge more precisely and efficiently, thanks to the introduction of the inertia weight  $\theta$  by Shi and Eberhart (1999). Equation (2.16) represents a formulation of adapting velocity that enhances its ability to be fine-tuned during solution search. A larger value of  $\theta$  encourages global exploration, while a smaller value encourages local search, as seen by equation (2.16). Therefore, a high value of  $\theta$  causes the algorithm to fail in finding the genuine optimality since it constantly explores new areas without doing much local search. In order to accelerate convergence to the true optimum, a linearly decreasing inertia weight has been employed to strike a balance between global and local exploration:



$$\theta(i) = \theta_{max} - \left( \frac{\theta_{max} - \theta_{min}}{i_{max}} \right) i \quad \text{Equation 2.17}$$

where  $\theta_{max}$  and  $\theta_{min}$  are the initial and final values of the inertia weight, respectively, and  $i_{max}$  is the maximum number of iterations used in PSO. The values of  $\theta_{max} = 0.9$  and  $\theta_{min} = 0.4$  are commonly used (Rao, 2009).

## 2.9.4 Ant Colony Optimization

### 2.9.4.1 Basic Concept

The cooperative behavior of actual ant colonies, which can determine the quickest route from their nest to a food supply, serves as the foundation for ant colony optimization (ACO). Dorigo and his colleagues created the technique in the early 1990s (Colorini *et al.*, 1992; Dorigo *et al.*, 1996). The optimization problem can be represented as a multilayered graph, as illustrated in Figure 2.5, where the number of layers corresponds to the number of design variables and the number of nodes within a given layer to the number of discrete values allowed for the associated design variable. This approach explains the ACO process. As a result, a design variable's allowable discrete value is linked to each node. A problem with six design variables and eight allowable discrete values for each design variable is shown in Figure 2.5 (Rao, 2009).

The following is an explanation of the ACO process: Let us say there are  $N$  ants in the colony. In each cycle or iteration, the ants begin at the home node, move through the layers from the first layer to the last or final layer, and finish at the destination node. As per Equation (2.18), each ant can choose only one node per layer based on the state transition rule. A potential solution is represented by the nodes that an ant has chosen to visit along its way (Rao, 2009).

For example, Figure 2.5 displays thick lines that represent an ant's typical journey. The solution  $(x_{12}, x_{23}, x_{31}, x_{45}, x_{56}, x_{64})$  is represented by this path. After the path is finished, the ant deposits some pheromone on the path based on the local updating rule given by

Equation (2.19). Equations (2.18) and (2.19) of the global updating rule are used to update the pheromones on the globally optimal path when every ant has completed their path (Rao, 2009).

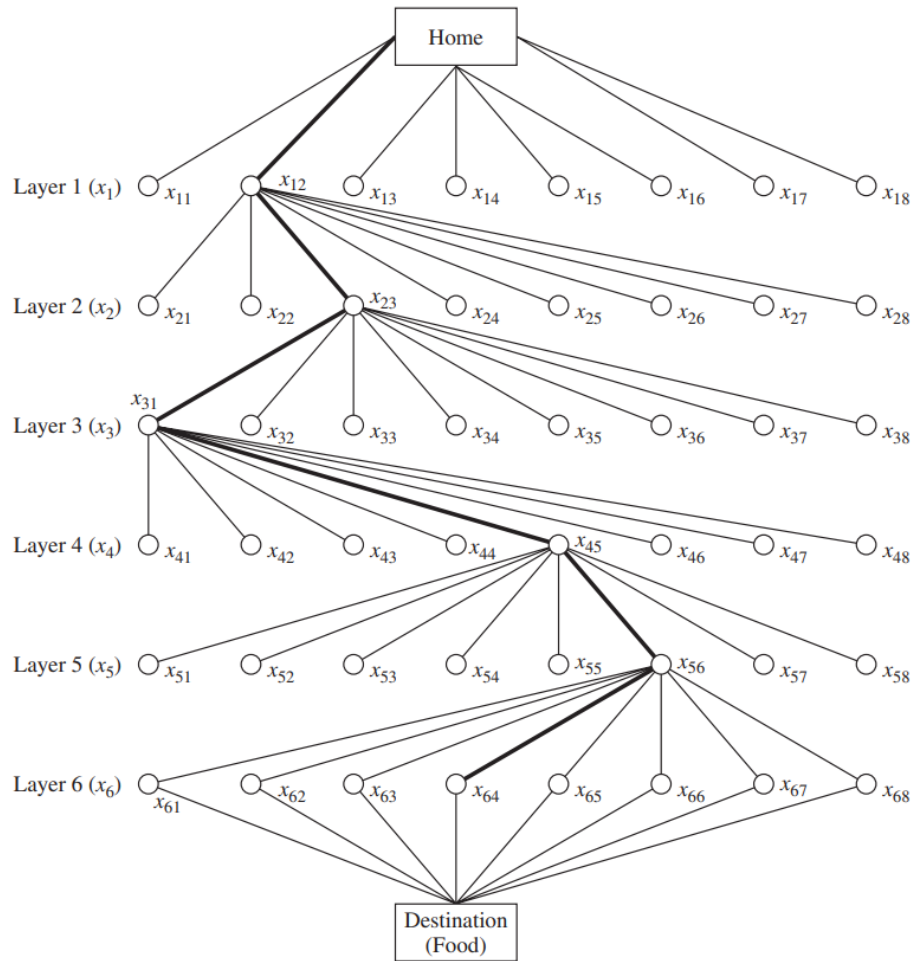


**Figure 2.5: Graphical Representation of the Aco Process in the Form of a Multi-Layered Network**

Source: (Rao, 2009)

At the onset of the optimization procedure (that is, during iteration 1), an equal quantity of pheromone is initialized for each edge or ray. Because of this, in iteration 1, every ant

begins at the home node and ends at the destination node, where they choose a node at random from each layer. If a better solution is not found in a predetermined number of consecutive cycles or iterations, or if the predetermined maximum number of iterations is reached, the optimization process is discontinued. The elements of the ideal solution vector are the values of the design variables indicated by the nodes on the path with the greatest concentration of pheromone. Generally speaking, all ants follow the same optimal (converged) path at the optimal solution (Rao, 2009).

#### 2.9.4.2 Ant searching behaviour

An ant  $k$ , when located at node  $i$ , uses the pheromone trail  $\tau_{ij}$  to compute the probability of choosing  $j$  as the next node (Rao, 2009):

$$P_{ij}^{(k)} = \begin{cases} \frac{\tau_{ij}^\alpha}{\sum_{j \in N_i^{(k)}} \tau_{ij}^\alpha} & \text{if } j \in N_i^{(k)} \\ 0 & \text{if } j \notin N_i^{(k)} \end{cases} \quad \text{Equation 2.18}$$

where  $\alpha$  represents the degree of significance of the pheromones and  $N_i^{(k)}$  designates the set of neighborhood nodes of ant  $k$  when located at node  $i$ . The neighborhood of node  $i$  comprises all the nodes directly connected to node  $i$  except the predecessor node (i.e., the last node visited before  $i$ ). This will hinder the ant from returning to the same node visited immediately before node  $i$ . Until it reaches the goal node—the food node—an ant moves from node to node (Rao, 2009).

#### 2.9.4.3 Path retracing and pheromone updating

Upon visiting an arc, the  $k^{th}$  ant drops  $\Delta\tau^{(k)}$  of pheromone before heading back to its home node (reverse node). According to Rao (2009), the pheromone value  $\tau_{ij}$  on the traversed arc  $(i, j)$  is updated as follows:

$$\tau_{ij} \leftarrow \tau_{ij} + \Delta\tau^{(k)} \quad \text{Equation 2.19}$$

The likelihood that the approaching ants will choose this arc will rise due to the pheromone's growth (Rao, 2009).

#### 2.9.4.4 Pheromone Trail Evaporation

After an ant  $k$  moves to the next node, the pheromone evaporates from all the arcs  $ij$  according to the relation (Rao, 2009)

$$\tau_{ij} \leftarrow (1 - p)\tau_{ij}; \forall (i, j) \in A \quad \text{Equation 2.20}$$

where  $p \in (0, 1)$  is a parameter and  $A$  denotes the segments or arcs traveled by ant  $k$  in its path from home to destination. The search process is aided by the exploration of alternative routes due to the drop in pheromone strength. This encourages the removal of bad path selection decisions. This aids in limiting the highest value that the pheromone trails can achieve. An iteration is a full cycle that includes the movement of ants, the evaporation and deposit of pheromones. When every ant has returned to its home node, or nest, the pheromone data is updated in accordance with the relation (Rao, 2009)

$$\tau_{ij} = (1 - \rho)\tau_{ij} + \sum_{k=1}^N \Delta\tau_{ij}^{(k)} \quad \text{Equation 2.21}$$

where  $\rho \in (0, 1)$  is the evaporation rate (also known as the pheromone decay factor) and  $\Delta\tau_{ij}^k$  is the amount of pheromone deposited on arc  $ij$  by the best ant  $k$ . The aim of pheromone update is to increase the pheromone value associated with good or promising paths. The pheromone deposited on arc  $ij$  by the best ant is taken as

$$\Delta\tau_{ij}^k = \frac{Q}{L_k} \quad \text{Equation 2.22}$$

Where  $Q$  is a constant and  $L_k$  is the length of the path traveled by the  $k^{th}$  ant (in the case of the travel from one city to another in a traveling salesman problem). Equation (2.22) can be implemented as (Rao, 2009)

$$\Delta\tau_{ij}^{(k)} = \begin{cases} \frac{\zeta f_{best}}{f_{worst}}; & \text{if } (i,j) \in \text{global best tour} \\ 0; & \text{otherwise} \end{cases} \quad \text{Equation 2.23}$$

Where  $f_{worst}$  is the worst value and  $f_{best}$  is the best value of the objective function among the paths taken by the  $N$  ants, and  $\zeta$  is a parameter used to control the scale of the global updating of the pheromone. The larger the value of  $\zeta$ , the more pheromone deposited on the global best path, and the better the exploitation ability. The purpose of Equation (2.23) is to provide a greater amount of pheromone to the tours (solutions) with better objective function values.

#### 2.9.4.5 Algorithm

The following is a summary of the ACO algorithm's step-by-step process for resolving a minimization problem (Rao, 2009):

1. An appropriate number of ants in the colony ( $N$ ) is assumed. A set of permissible discrete values for each of the  $n$  design variables is assumed. The permissible discrete values of the design variable  $x_i$  are denoted as  $x_{i1}, x_{i2}, \dots, x_{ip}$  ( $i = 1, 2, \dots, n$ ). Equal amounts of pheromone  $\tau_{ij}^{(1)}$  are initially assumed along all the arcs or rays (discrete values of design variables) of the multilayered graph shown in Figure 2.2. The superscript to  $\tau_{ij}$  signifies the iteration number. For simplicity,  $\tau_{ij}^{(1)} = 1$  can be assumed for all arcs  $ij$ . The iteration number is set as  $l = 1$ .
2. (a) The probability ( $p_{ij}$ ) of selecting the arc or ray (or the discrete value)  $x_{ij}$  is calculated as

$$p_{ij} = \frac{\tau_{ij}^{(l)}}{\sum_{m=1}^p \tau_{im}^{(l)}}; i = 1, 2, \dots, n; j = 1, 2, \dots, p \quad \text{Equation 2.24}$$

which is the same as Equation (2.18) with  $\alpha = 1$ . A larger value can also be used for  $\alpha$ .

(b) The specific path (or discrete values) chosen by the  $k^{th}$  ant can be determined using random numbers generated in the range (0, 1). For this, the cumulative probability ranges can be found associated with different paths of Figure 2.2 based on the probabilities given by Equation (2.24). The specific path chosen by ant  $k$  will be determined using the roulette-wheel selection process in step 3(a).

3. (a)  $N$  random numbers are generated  $r_1, r_2, \dots, r_N$  in the range (0, 1), one for each ant. The discrete value or path assumed by ant  $k$  is determined for variable  $i$  as the one for which the cumulative probability range [found in step 2(b)] includes the value  $r_i$ .

(b) Step 3(a) is repeated for all design variables  $n_i = 1, 2, \dots, n$ .

(c) The objective function values are assessed corresponding to the complete paths (design vectors  $\mathbf{X}^{(k)}$  or values of  $x_{ij}$  chosen for all design variables  $i = 1, 2, \dots, n$  by ant  $k, k = 1, 2, \dots, N$ ):

$$f_k = f(\mathbf{X}^{(k)}); k = 1, 2, \dots, N \quad \text{Equation 2.25}$$

The best and worst paths are determined among the  $N$  paths chosen by different ants using Equations (2.26) and (2.27):

$$f_{best} = \min_{k=1,2,\dots,N} \{f_k\} \quad \text{Equation 2.26}$$

$$f_{worst} = \max_{k=1,2,\dots,N} \{f_k\} \quad \text{Equation 2.27}$$

4. The convergence of the process is then verified. The process is assumed to have converged if all  $N$  ants take the same best path. If convergence is not realized, it is assumed that all the ants return home and start again in search of food. The new iteration number is set as  $l = l + 1$ , and the pheromones on different arcs updated (or discrete values of design variables) as

$$\tau_{ij}^{(l)} = \tau_{ij}^{(old)} + \sum_k \Delta \tau_{ij}^{(k)} \quad \text{Equation 2.28}$$

where  $\tau_{ij}^{(old)}$  denotes the pheromone amount of the previous iteration left after evaporation, which is taken as

$$\tau_{ij}^{(old)} = (1 - \rho)\tau_{ij}^{(l-1)} \quad \text{Equation 2.29}$$

and  $\Delta\tau_{ij}^{(k)}$  is the pheromone deposited by the best ant  $k$  on its path and the summation extends over all the best ants  $k$  (if multiple ants take the same best path). Note that the best path involves only one arc  $ij$  (out of  $p$  possible arcs) for the design variable  $i$ . The evaporation rate or pheromone decay factor  $\rho$  is assumed to be in the range 0.5 to 0.8 and the pheromone deposited  $\Delta\tau_{ij}^{(k)}$  is computed using Equation (2.23).

With the new values of  $\tau_{ij}^{(l)}$ , one goes to step 2. Steps 2, 3, and 4 are repeated until the process converges, that is, until all the ants choose the same best path. In some cases, the iterative process is terminated after completing a prespecified maximum number of iterations ( $l_{max}$ ) (Rao, 2009).

### 2.9.5 Optimization of Fuzzy Systems

In traditional designs, the optimization problem is expressed precisely in mathematical terms. Nevertheless, the design data, objective function, and constraints are stated in vague and linguistic terms in many real-world problems. For instance, the statement, “This beam carries a load of 1000 *lb* with a probability of 0.8” is not precise because of randomness in the material properties of the beam. Conversely, the statement, “This beam carries a large load” is imprecise because of the fuzzy meaning of “large load” (Rao, 2009). In the same vein, when designing a machine component optimally, the induced stress ( $\sigma$ ) is constrained by an upper bound value ( $\sigma_{max}$ ) as  $\sigma \leq \sigma_{max}$ . If  $\sigma_{max} = 30,000 \text{ psi}$ , it implies that a design with  $\sigma = 30,000 \text{ psi}$  is acceptable whereas a design with  $\sigma = 30,001 \text{ psi}$  is not acceptable (Rao, 2009).

On the other hand, designs with  $\sigma = 30,000 \text{ psi}$  and  $30,001 \text{ psi}$  do not differ significantly. It seems more sensible to have a phase of transition from total permission to total impermission. This suggests that the constraint should be expressed in fuzzy terms. Systems incorporating ambiguous and imprecise information can be modeled and designed using fuzzy theories (Rao, 1987; Rao *et al.*, 1992; Dhingra *et al.*, 1992).

### 2.9.5.1 Fuzzy Set Theory

Let  $X$  be a classical crisp set of objects, called the *universe*, whose generic elements are designated by  $x$ . Membership in a classical subset  $A$  of  $X$  can be viewed as a characteristic function  $\mu_A$  from  $X$  to  $[0, 1]$  such that (Rao, 2009)

$$\mu_A = \begin{cases} 1 & \text{if } x \in A \\ 0 & \text{if } x \notin A \end{cases} \quad \text{Equation 2.30}$$

The set  $[0, 1]$  is called a *valuation set*. A set  $A$  is called a fuzzy set if the valuation set is allowed to be the whole interval  $[0, 1]$ . The fuzzy set  $A$  is characterized by the set of all pairs of points represented as

$$A = \{x, \mu_A(x)\}, \quad x \in X \quad \text{Equation 2.31}$$

Where  $\mu_A(x)$  is known as the *membership function* of  $x$  in  $A$ . The closer the value of  $\mu_A(x)$  is to 1, the more  $x$  belongs to  $A$ . For example, let  $X = \{62 \ 64 \ 66 \ 68 \ 70 \ 72 \ 74 \ 76 \ 78 \ 80\}$  be possible temperature settings of the thermostat ( $^{\circ}\text{F}$ ) in an air-conditioned building. Then the fuzzy set  $A$  of “comfortable temperatures for human activity” may be defined as (Rao, 2009)

$$A = \left\{ \begin{array}{l} (62, 0.2), (64, 0.5), (66, 0.8), (68, 0.95), (70, 0.85), (72, 0.75), \\ (74, 0.6), (76, 0.4), (78, 0.2), (80, 1.0) \end{array} \right\} \quad \text{Equation 2.32}$$



Where a grade of membership of 1 implies complete comfort and 0 implies complete discomfort. In general, if  $X$  is a finite set,  $\{x_1, x_2, \dots, x_n\}$  the fuzzy set on  $X$  can be expressed as

$$A = \mu_A(x_1)|_{x_1} + \mu_A(x_2)|_{x_2} + \dots + \mu_A(x_n)|_{x_n} = \sum_{i=1}^n \mu_A(x_i)|_{x_i} \quad \text{Equation 2.33}$$

Or in the limit,  $A$  can be expressed as

$$A = \int_x \mu_A(x)|_x \quad \text{Equation 2.34}$$

### 2.9.5.2 Optimization of fuzzy systems

Conventional optimization techniques focus on choosing the design variables that maximize an objective function while meeting the specified constraints. This definition of optimization needs to be updated for fuzzy systems. A design (decision) can be seen as the intersection of the fuzzy objective and constraint functions since in a fuzzy system, the membership functions characterize the objective and constraint functions (Rao, 2009). For illustration, the objective function considered was: “The depth of the crane girder ( $x$ ) should be substantially greater than 80 in.” This can be represented by a membership function, such as

$$\mu_f(x) = \begin{cases} 0 & \text{if } x < 80 \text{ in.} \\ [1 + (x - 80)^{-2}]^{-1}, & \text{if } x \geq 80 \text{ in.} \end{cases} \quad \text{Equation 2.35}$$

Let the constraint be “The depth of the crane girder ( $x$ ) should be in the vicinity of 83 in.” This can be explained by a membership function of the type

$$\mu_g(x) = [1 + (x - 83)^4]^{-1} \quad \text{Equation 2.36}$$

Then the design (decision) is described by the membership function,  $\mu_D(x)$ , as (Rao, 2009)

$$\begin{aligned} \mu_D(x) &= \mu_f(x) \wedge \mu_g(x) \\ &= \begin{cases} 0 & \text{if } x < 80 \text{ in.} \\ \min\{[1 + (x - 80)^{-2}]^{-1}, [1 + (x - 83)^4]^{-1}\} & \text{if } x \geq 80 \text{ in.} \end{cases} \end{aligned} \quad \text{Equation 2.37}$$

This relationship is shown in Figure 2.6.

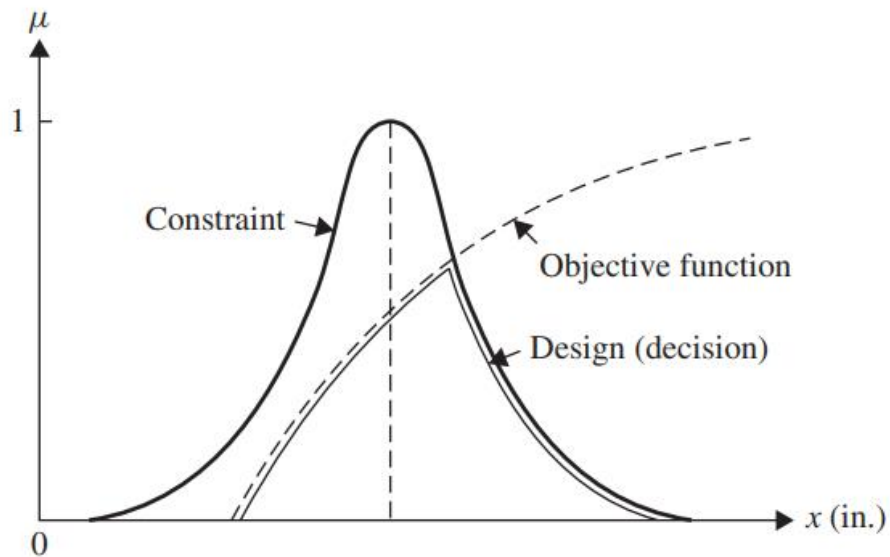


**Figure 2.6: Concept of Fuzzy Decision**

Source: (Rao, 1987)

Typically, the traditional optimization problem is expressed as follows:

Find  $\mathbf{X}$  which minimizes  $f(\mathbf{X})$

subject to

$$g_j^{(l)} \leq g_j(x) \leq g_j^{(u)}, \quad j = 1, 2, \dots, m \quad \text{Equation 2.38}$$

Where the superscripts  $l$  and  $u$  denote the lower and upper bound values, respectively. The optimization problem of a fuzzy system is stated as follows:

Find  $\mathbf{X}$  which minimizes  $f(\mathbf{X})$

subject to

$$g_j(\mathbf{X}) \in G_j, \quad j = 1, 2, \dots, m \quad \text{Equation 2.39}$$

where  $G_j$  denotes the fuzzy interval to which the function  $g_j(\mathbf{X})$  should belong. Thus the fuzzy feasible region,  $S$ , which denotes the intersection of all  $G_j$ , is defined by the membership function (Rao, 2009)

$$\mu_S(\mathbf{X}) = \min_{j=1,2,\dots,m} \{ \mu_{G_j}[g_j(\mathbf{X})] \} \quad \text{Equation 2.40}$$

Since a design vector  $\mathbf{X}$  is considered viable when  $\mu_S(\mathbf{X}) > 0$ , the optimum design is characterized by the maximum value of the intersection of the objective function and the feasible domain:

$$\mu_D(\mathbf{X}^*) = \max \mu_D(\mathbf{X}), \quad \mathbf{X} \in D \quad \text{Equation 2.41}$$

where

$$\mu_D(\mathbf{X}) = \min \{ \mu_f(\mathbf{X}), \min_{j=1,2,\dots,m} \mu_{G_j}[g_j(\mathbf{X})] \} \quad \text{Equation 2.42}$$

### 2.9.5.3 Computational procedure

The membership functions of  $f$  and  $g_j$  can be used to find the solution of a fuzzy optimization problem. In real-world scenarios, the membership functions are constructed with the help and collaboration of seasoned engineers in specific cases. Based on the anticipated fluctuations of the objective and constraint functions, linear membership

functions are frequently employed in the absence of additional information. Once the membership functions are known, the problem can be posed as a crisp optimization problem as (Rao, 2009)

Find  $\mathbf{X}$  and  $\lambda$  which maximize  $\lambda$

subject to

$$\lambda \leq \mu_f(\mathbf{X})$$

$$\lambda \leq \mu_{g_j}^{(l)}(\mathbf{X}), \quad j = 1, 2, \dots, m$$

$$\lambda \leq \mu_{g_j}^{(u)}(\mathbf{X}), \quad j = 1, 2, \dots, m \quad \text{Equation 2.43}$$

### 2.9.6 Neural-Network-Based Optimization

The nervous system's extraordinary computing capacity to address perception-related issues in the face of copious amounts of sensory data has been linked to its parallel processing ability. In recent years, optimization problems have been solved with neural computing algorithms (Berke & Hajela, 1992; Dhingra & Rao, 1992). A neural network is a massively parallel network of interconnected basic processors, or neurons, where each neuron computes an output that is propagated to the output nodes after accepting a set of inputs from other neurons. As a result, the individual neurons, network connectivity, weights corresponding to the connections between neurons, and activation function of each neuron can all be used to characterize a neural network. An input vector is mapped by the network from one space to another. Although not stated, the mapping is learned (Rao, 2009).

For example, a single neuron is shown in Figure 2.7. The neuron accepts a set of  $n$  inputs,  $x_i$ ,  $i = 1, 2, \dots, n$ , from its adjacent neurons and a bias whose value is equal to 1. Each input has a weight (gain)  $w_i$  associated with it. The weighted sum of the inputs determines

the state or activity of a neuron, and is given by  $a = \sum_{i=1}^{n+1} w_i x_i = \mathbf{W}^T \mathbf{X}$ , where  $\mathbf{X} = \{x_1 x_2 \dots x_n 1\}^T$ . A simple function is now used to provide a mapping from the

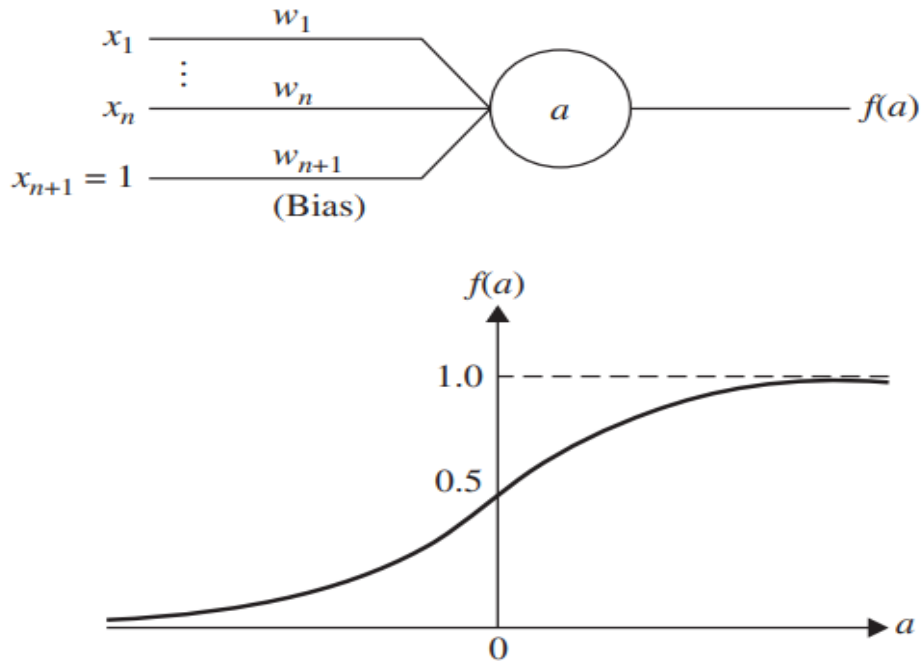


**Figure 2.7: Single Neuron and Its Output**

Source: (Dhingra and Rao, 2009)

$n$ -dimensional space of inputs into a one-dimensional space of the output, which the neuron sends to its neighbors. The output of a neuron is a function of its state and can be denoted as  $f(a)$ . Ordinarily, no output will be produced except the activation level of the node exceeds a threshold value. The output of a neuron is generally described by a sigmoid function as (Rao, 2009)

$$f(a) = \frac{1}{1+e^{-a}} \quad \text{Equation 2.44}$$

which is shown graphically in Figure 2.4. Both big and tiny input signals can be handled by the sigmoid function. The available gain is represented by the slope of the

function  $f(a)$ . A neuron can be thought of as a distinct processor that runs in parallel with other neurons as its output is solely dependent on its inputs and the threshold value. Finding values for the weights  $w_i$  that result in the best possible association between the neural network's inputs and outputs is the learning process (Rao, 2009).

Numerous neural network topologies have been developed to mimic the fundamental properties of a single neuron, including the Hopfield and Kohonen networks. The amount of neurons in the network, the kind of threshold functions, the connectivities between the different neurons, and the learning processes all vary between these architectures.

Figure 2.8 depicts a typical architecture called the multilayer feedforward network. The unidirectional feedforward communication links between the neurons are represented by the arcs in this picture. Each of these connections has a weight or gain that regulates the output that flows through it. Depending on whether a given neuron is excitatory or inhibitory, the weight may be positive or negative. The strengths of the various interconnections (weights) act as repositories for knowledge representation contained in the network (Rao, 2009).

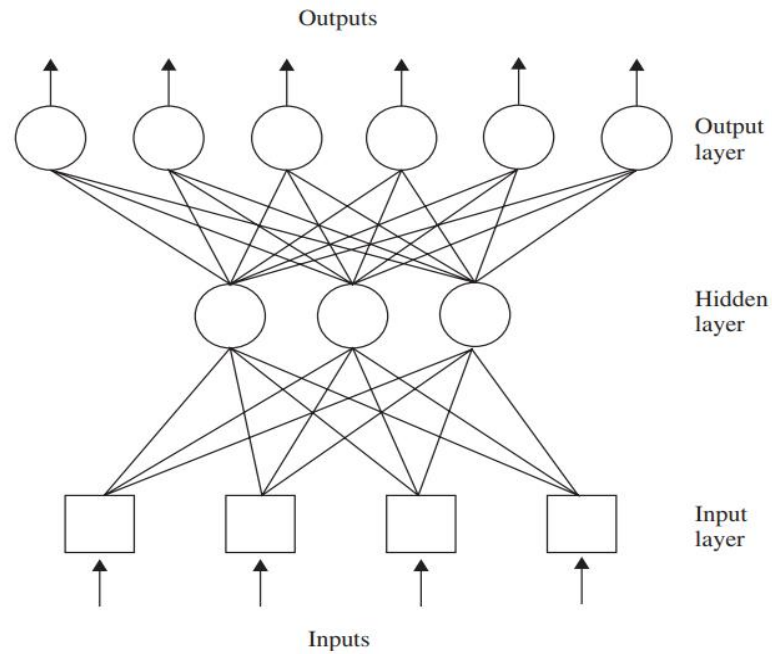


**Figure 2.8: Multilayer Feedforward Network**

Source: (Dhingra & Rao, 1992)

## **2.10 Optimizing the Biomass Yield of Microalgae Using Genetic Algorithm**

### **2.10.1 Genetic Algorithm Solver Options**

#### **2.10.1.1 Population Options**

- i. Population type- Specifies the type of the input to the fitness function.
- ii. Population size- Specifies how many individuals there are in each generation.
- iii. Creation function- Specifies the function that creates the initial population.
- iv. Initial population enables you to specify an initial population for the genetic algorithm. If you do not specify an initial population, the algorithm creates one using the creation function.
- v. Initial scores enables you to specify scores for the initial population.

- vi. Initial range specifies lower and upper bounds for the entries of the vectors in the initial population for the uniform creation function (R2016a).

### **2.10.1.2 Fitness Scaling**

The scaling function converts raw fitness scores returned by the fitness function to values in a range that is suitable for the selection function. The scaling function specifies the function that performs the scaling.

- i. Rank scales the raw scores based on the rank of each individual, rather than its score. The rank of an individual is its position in the sorted scores. The rank of the fittest individual is 1, the next fittest is 2 and so on.
- ii. Proportional makes the expectation proportional to the raw fitness score.
- iii. Top scales the individuals with the highest fitness values equally.
- iv. Shift linear scales the raw scores so that the expectation of the fittest individual is equal to a constant, which can be specified as the maximum survival rate, multiplied by the average score.
- v. Custom enables you to write your own scaling function (R2016a).

### **2.10.1.3 Selection**

The selection function chooses parents for the next generation based on their scaled values for the fitness scaling function.

- i. Stochastic uniform lays out a line in which each parent corresponds to a section of the line of length proportional to its expectation. The algorithm moves along the line in steps of equal size, one step for each parent. At each step, the algorithm allocates a parent from the section it lands on.
- ii. Remainder assigns parents deterministically from the integer part of each individual's scaled value and then uses roulette selection on the remaining fractional part.



- iii. Uniform select parents at random from a uniform distribution using the expectations and number of parents.
- iv. Shift linear scales the raw scores so that the expectation of the fittest individual is equal to a constant, which can be specified as maximum survival rate multiplied by the average score.
- v. Roulette simulates a roulette wheel with the area of each segment proportional to its expectation. The algorithm then uses a random number to select one of the sections with a probability equal to its area.
- vi. Tournament selects each parent by choosing individuals at random, the number of which can be specified by Tournament size, and then choosing the best individual out of the set to be a parent.
- vii. Custom enables one to write one's own selection function (R2016a).

#### **2.10.1.4 Reproduction**

Reproduction options determine how the GA creates children at each new generation.

- i. Elite count specifies the number of individuals that are guaranteed to survive to the next generation. Set Elite count to be a positive integer less than or equal to population size.
- ii. Crossover fraction specifies the fraction of the next generation that crossover produces. Mutation produces the remaining individuals in the next generation. Set crossover fraction to be a fraction between 0 and 1 (R2016a).

#### **2.10.1.5 Mutation**

Mutation functions make small random changes in the individuals in the population, which provide genetic diversity and enable the genetic algorithm to search a broader space.

- i. Constraint dependent chooses Gaussian if there are no constraints or otherwise Adaptive feasible. These choices ensure that feasible parents give rise to feasible children, where feasibility is with respect to bounds and linear constraints.
- ii. Gaussian adds a random number to each vector entry of an individual. This random number is taken from Gaussian distribution centered on zero. The standard deviation of this distribution can be controlled with two parameters. The Scale parameter determines the standard deviation at the first generation. The Shrink parameter controls how standard deviation shrinks as generation go by. If the Shrink parameter is 0, the standard deviation is constant. If the Shrink parameter is 1, the standard deviation shrinks to 0 linearly as the last generation is reached.
- iii. Uniform is a two-step process. First, the algorithm selects a fraction of the vector entries of an individual for mutation, where each entry has the same probability as the mutation rate of being mutated. In the second step, the algorithm replaces each selected entry by a random number selected uniformly from the range for that entry.
- iv. Adaptive feasible randomly generates directions that are adaptive with respect to the last successful or unsuccessful generation. A step length is chosen along each direction so that linear constraints and bounds are satisfied.
- v. Custom enables one to write one's own mutation function that satisfies any constraints specified (R2016a).

#### **2.10.1.6 Crossover**

Crossover combines two individuals, or parents, to form a new individual, or child, for the next generation.

- i. Constraint dependent chooses Scattered when there are no linear constraints, and chooses Intermediate when there are linear constraints. These choices

ensure that feasible parents give rise to feasible children, where feasibility is with respect to bounds and linear constraints.

- ii. Scattered creates a random binary vector. It then selects the genes where the vector is a 1 from the first parent, and the genes where the vector is a 0 from the second parent, and combines the genes to form the child.
- iii. Single point chooses a random integer  $n$  between 1 and number of variables, and selects the vector entries numbered less than or equal to  $n$  from the first parent, selects genes numbered greater than  $n$  from the second parent, and concatenates these entries to form the child.
- iv. Two point selects two random integers  $m$  and  $n$  between 1 and number of variables. The algorithm selects genes numbered less than or equal to  $m$  from the first parent, selects genes numbered from  $m+1$  to  $n$  from the second parent, and selects numbered greater than  $n$  from the first parent. The algorithm then concatenates these genes to form a single gene.
- v. Intermediate creates children by a random weighted average of the parents.
- vi. Heuristic creates children that randomly lie on the line containing the two parents, a small distance away from the parent with the better fitness value, in the direction away from the parent with the worse fitness value.
- vii. Arithmetic creates children that are a random arithmetic mean of two parents, uniformly on the line between the parents.
- viii. Custom enables one to write one's own crossover function that specifies any constraints specified (R2016a).

### **2.10.1.7 Migration**

Is the movement of individuals between subpopulations, which the algorithm creates if the population size is set to be a vector of length greater than 1. Every so often, the best individuals from one subpopulation replace the worst individuals in another subpopulation. Migration is controlled by the following parameters:

- i. Direction – specifies the direction in which migration can take place.

- ii. Fraction controls how many individuals move between subpopulations
- iii. Interval controls how many generations pass between migrations. If you set interval to 20, for instance, migration between subpopulations takes place every 20 generations (R2016a).

### **2.10.1.8 Stopping Criteria**

Stopping criteria determines what causes the algorithm to terminate.

- i. Generations-specifies the maximum number of iterations the generic algorithm performs.
- ii. Time limit-specifies the maximum time in seconds the GA runs before stopping.
- iii. Fitness limit- If the best fitness value is less than or equal to the value of fitness limit, the algorithm stops.
- iv. Stall generations- If the average change in the fitness function value over stall generations is less than function tolerance, the algorithm stops.
- v. Stall time limit- If there is no improvement in the best fitness value for an interval of time in seconds specified by stall time limit, the algorithm stops.
- vi. Stall test- Determines whether the definition of “stall” is average change over the last stall generations, or is the geometric weighted average change, where the geometric weighting factor is  $(1/2)^N$  for N generations from the end.
- vii. Function tolerance- If the average change in the fitness function value over stall generations is less than function tolerance, the algorithm stops.
- viii. Constraint tolerance- Tolerance for the maximum nonlinear constraint violation (R2016a).

### **2.10.1.9 Plot Functions**

Plot functions enable one to plot various aspects of the GA as it is executing. Each one draws in a separate axis on the display window.

- i. Plot interval- specifies the number of generations between successive updates of the plot.
- ii. Best fitness- plots the best function value in each generation versus iteration number.
- iii. Distance- plots the average distance between individuals at each generation.
- iv. Best individual- plots the vector entries of the individual with the best fitness function value in each generation.
- v. Expectation- plots the expected number of children versus the raw scores at each generation.
- vi. Genealogy- plots the genealogy of individuals. Lines from one generation to the next are colour-coded. Red lines indicate mutation children. Blue lines indicate crossover children whereas black one indicate elite individuals.
- vii. Range- plots the minimum, maximum and mean fitness function values in each generation.
- viii. Scores- plots the scores of the individuals at each generation.
- ix. Score diversity- plots a histogram of the scores at each generation.
- x. Selection-plots a histogram of the parents. This shows which parents are contributing to each generation (R2016a).

#### **2.10.1.10 Display to Command Window**

Level of display specifies the amount of information displayed in the MATLAB<sup>®</sup> command window when the algorithm is run.

- i. Off- Display no output.
- ii. Iterative-Display information at each iteration of the algorithm.
- iii. Diagnose-Display information at each iteration. In addition, the diagnostic lists some problem information and the options that are changed from the defaults.
- iv. Final- Display only the reason for stopping at the end of the run (R2016a).

## 2.11 Research Gaps

To improve the economics of microalgal biodiesel production, more research and development are compulsory to reduce the costs of growing microalgae and the separation of microalgal biomass from the growth media, and to competently control culture contamination when grown in open ponds. The research and development efforts probably need to focus on the following areas as illustrated in Table 2.6.

**Table 2.6: Research Gaps**

S/NO.	Literature	Findings	Research Gap
1	Chisti, 2007	Oil-rich microalgal species can be enhanced through cultivation and genetic engineering to increase the oil content in their biomass without compromising the biomass production rate	Selection and development of high-yield, oil-rich microalgae
2	Chisti, 2007	Most microalgae prefer to grow at the temperatures of 20-30 °C. When the temperature is higher than 30 °C, which happens very frequently during the sunny days in photobioreactors, heat exchangers have to be operated to cool down the microalgal culture to sustain a high microalgae growth	Enhancement of the tolerance oil-rich microalgae to high and/or low temperatures
3	Chisti, 2007	When microalgae grow under autotrophic conditions, they produce oxygen that dissolves in water to yield a super saturated dissolved oxygen concentration in the media, sometimes 4-5 times of the air saturation value. A combination of high dissolved oxygen with intense sunlight impedes the growth of the microalgae and destroys the microalgal cells	Enhancement of the tolerance of oil-rich microalgae to the high concentration of oxygen
4	Chisti, 2007	In open pond microalgae production, the contamination of wild algae and bacteria is very challenging. If the growth media is contaminated by wild algae and/or bacteria, the wild algae and bacteria will devour the nutrients	Improvement of the competitiveness of oil-rich microalgae against wild algae and bacteria

<b>S/NO.</b>	<b>Literature</b>	<b>Findings</b>	<b>Research Gap</b>
		in the media and significantly diminish the yield of the desired microalgae	
5	Chisti, 2007	When microalgae grow in tubular photobioreactors, some of them stick on the wall of the tubes, significantly decreasing the penetration of light to the growth media and resulting in a lower yield of the microalgal biomass. Cost-effective materials which inhibit the microalgae from attaching to the surface should be explored to maintain a high growth rate of the microalgae	Improvement of the engineering of the microalgae growth systems
6	Chisti, 2007	Harvesting microalgal biomass contributes markedly to the total costs of the biomass production. Current technologies ordinarily involve coagulation, filtration and centrifugation, which are costly	Development of cost-effective microalgae harvesting systems
7	Chisti, 2007	Microalgal biomass contains lipids (oil), carbohydrates, proteins and other minor components such as minerals and vitamins. Oil is used for biodiesel production. Other constituents can be processed into value-added products. After oil extraction, the residues which are rich in carbohydrates, proteins and minor nutrients can be used to produce animal feed. They can also be utilized for biogas production through anaerobic digestion. Special high-value organic chemicals could be extracted from the residues and should be explored to increase the revenue of the microalgae-to-biodiesel process. All these byproducts have capabilities to improve the economics of the microalgae-to-biodiesel process	Application of the biorefinery model to microalgal biodiesel production system

The present study therefore capitalizes on some of the gaps presented here. In particular, the improvement of the engineering of the microalgae cultivation systems where GA as one of the modern optimization techniques, is employed to solve the growth inefficiencies in photobioreactors

## 2.12 Conceptual Framework

The conceptual framework is as shown in Figure 2.9.

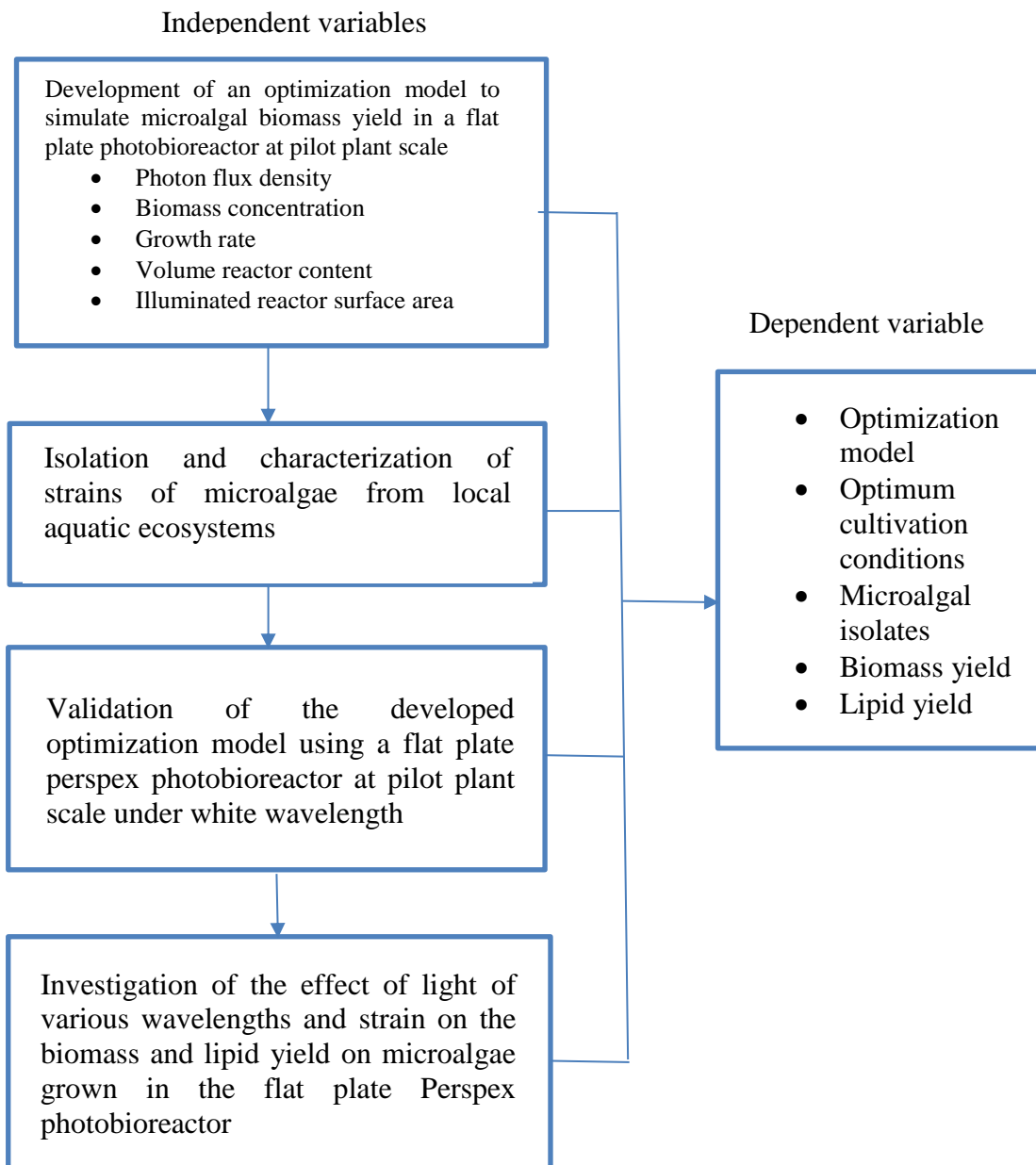


**Figure 2.9: Conceptual Framework**



## **CHAPTER THREE**

### **MATERIALS AND METHODS**

#### **3.1 Introduction**

In this chapter, the materials and methods used to meet the research objectives have been presented. Initially the experimental design and PBR tank design and dimensions are presented. Then, the study design is presented which is divided into four sections: The first section describes the development of a computer optimization model to simulate the biomass yield of microalgae in a flat plate photobioreactor at pilot plant scale; The second section describes the isolation and characterization of strains of microalgae from local aquatic ecosystems that can be used in biomass and lipid production; The third section describes the validation of the performance of the developed computer simulation model using a flat plate perspex photobioreactor at pilot plant scale under white wavelength; And the last section describes the determination of the effect of light of various wavelengths and strain on the biomass and lipid yield of microalgae grown in the flat plate perspex photobioreactor. Finally the chapter ends with presentation of data analysis and presentation methods.

#### **3.2 Research Design**

The study adopted experimental design to test the hypotheses.

##### **3.2.1 Experimental Design**

The experimental design consisted of a randomized complete block design (RCBD) with three replications.

### 3.3 Photobioreactor Tanks Design and Dimensions

A vertical flat-plate PBR set up was designed and built by Ondimu *et al.* (2019) at the Agricultural and Biosystems Engineering Department (ABED) of the School of Biosystems and Environmental Engineering (SoBEE) of JKUAT. The PBRs are three in number and made up of transparent materials (Perspex) for maximum utilization of light energy, as shown in Figures 3.1 and 3.2. Perspex was chosen for construction due to its favourable optical and mechanical properties: light transmittance of >92%, minimal light diffraction and intensity loss, refractive index of 1.92, tensile strength of >62 MPa, softening temperature of >110 °C (Ojo *et al.*, 2015). The thickness of the panel is 10 mm and total effective internal volume of each PBR is 216 L (120 cm long, 20 cm wide and 90 cm high). The mixing in the culture is ensured by an air- flux fed through two quarter inch tubes placed through the top and held at the bottom of each PBR by a weight of concrete wrapped in a white polythene bag and connected to a 6 W air pump. Light is continuously provided by 12, 10 W (6 on each side) light emitting diodes (LEDs) (MDL Ltd, China) with the first tank having white (400-700 nm) LEDs, second tank, red (610-680 nm) LEDs and finally the third one with blue (430-480) LEDs. The source of power was the National grid or eighteen, 200 W solar panels connected to six 12 V solar batteries.

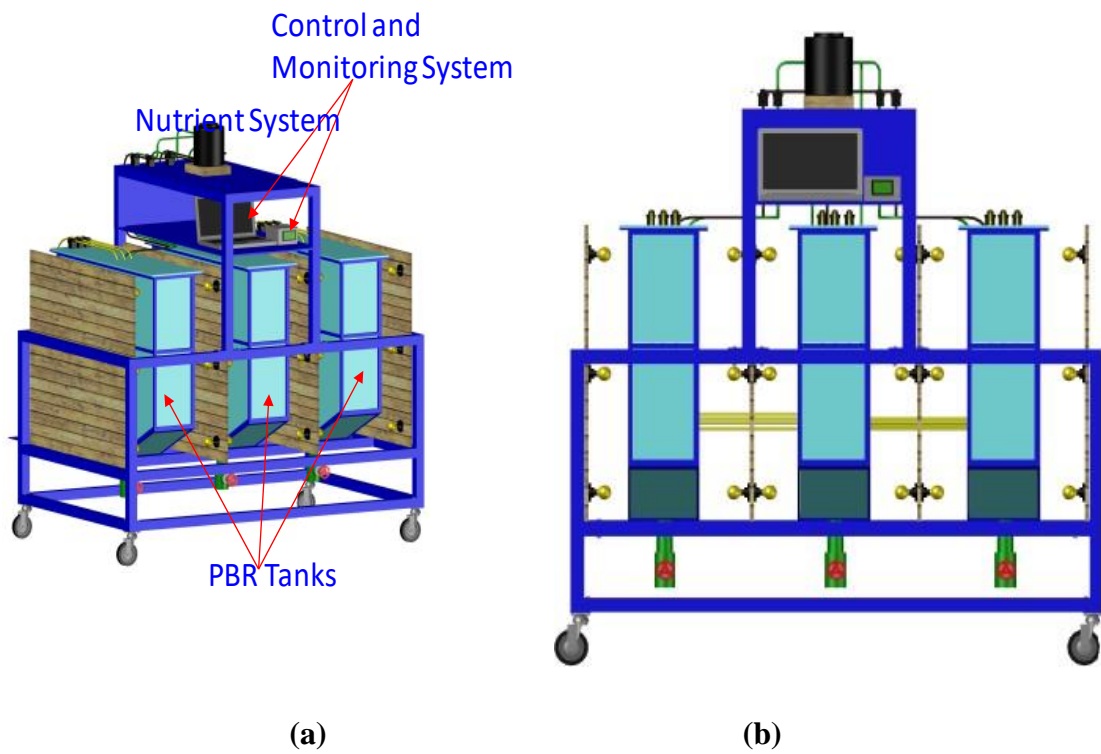


**Figure 3.1: Illustration of the PBR System**

a: Pictorial representation, b: Front view

Source: (Ondimu *et al.*, 2019)



**Figure 3.2: Flat Plate Perspex Photobioreactor Used in the Study**

The pH, content's temperature and ambient temperature at the end of the loop are measured using sensors (pH meter (SKU:SENo161, ELECbEE, China); Temperature sensor (DPH7, China)), connected to a control-transmitter unit (Arduino Me 2560, Crison Instruments, Spain), in turn connected to a PC control unit, allowing complete monitoring and control of the facility.

### **3.4 Study Design**

The study was divided into four broad areas;

- i. Development of a computer optimization model to simulate the biomass yield of microalgae in a flat plate photobioreactor at pilot plant scale,
- ii. Isolation and characterization of strains of microalgae from local aquatic ecosystems that can be used in biomass and lipid production,
- iii. Validation of the performance of the developed computer simulation model using a flat plate perspex photobioreactor at pilot plant scale under white wavelength,
- iv. Determination of the effect of light of various wavelengths and strain on the biomass and lipid yield of microalgae grown in the flat plate perspex photobioreactor.

#### **3.4.1 Computer Optimization Model for Simulating the Biomass Yield of Microalgae**

There are a number of variables that determine the biomass yield of microalgae. These are: light intensity, light duration, light wavelength (quality), pH of culture medium, temperature, strain of microalgae, rate of mixing, biomass concentration, nutrients, vitamins and trace elements, etc. It is therefore important to develop a computer optimization model to simulate the yield of microalgal biomass. This will assist in determining the optimal cultivation conditions by experimenting with equations. This is cost-effective and saves on time, compared with experimenting with actual equipment. The knowledge generated will help microalgae researchers and producers in scaling up microalgae production from laboratory scale to pilot scale and eventually commercial production.

##### **3.4.1.1 Optimization Model for Simulating the Biomass Yield of Microalgae**

The optimization model for biomass yield is given by equation 3.1 (Zijffers *et al.*, 2010),

$$Y = \frac{(C_x \cdot \mu \cdot V)}{(PFD_{in} \cdot A \cdot 3600 \cdot 10^{-6})} \left( gmolphotons^{-1} \right) \quad \text{Equation 3.1}$$

Where  $Y$  is the yield in  $gmolphotons^{-1}$

$C_x$  is the biomass concentration in  $gL^{-1}$

$V$  is the volume of the reactor content in L

$\mu$  is the growth rate per hour

$A$  is the illuminated reactor surface area in  $m^2$

$PFD_{in}$  is the photon flux density in  $\mu molphotonsm^{-2}s^{-1}$

A program in Matrix Laboratory (MATLAB R2016a) programming language was developed to simulate the microalgae biomass yield,  $Y$ . The input variables in the simulation of  $Y$  are  $C_x$ ,  $\mu$ ,  $V$ ,  $A$  and  $PFD_{in}$ . Inputs  $A$  and  $V$  were obtained from the designed and fabricated FPPPBR in the School of Biosystems and Environmental Engineering (SoBEE) of JKUAT. The  $PFD_{in}$  on the reactor surface was measured using a quantum sensor (RS485, BGT Technology Co., Ltd, Beijing, China). The values of  $A$  and  $V$  are constant as per the FPPPBR design and are  $2.16 m^2$  and  $192 L$ , respectively.

#### **3.4.1.2 Computer Model to Simulate Biomass Yield of Microalgae using Genetic Algorithm**

To simulate the biomass yield of microalgae, the optimization model, equation 3.1, had to be written in the editor window (Figure 3.3) of MATLAB® as a function MATLAB file (Figure 3.4), and the objective function was made negative because it is a maximization as the Global Optimization Tool Box of MATLAB® does minimization.

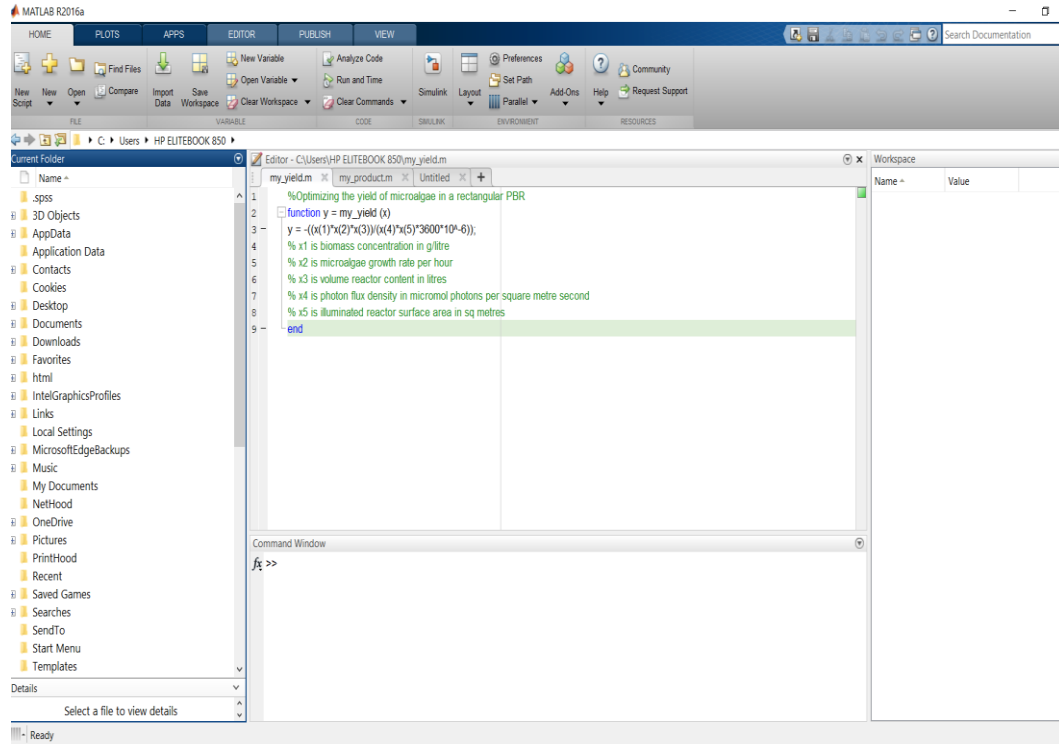


**Figure 3.3: MATLAB® Desktop Window**

Then click on the “APP” icon on the menu bar and Figure 3.5 will appear. After it appears, click on the optimization icon and Figure 3.6 will appear that has various options for solvers and click on “GA” and Figure 3.7 will show up.

```

%Optimizing the yield of microalgae in a rectangular PBR
function y = my_yield (x)
y = -((x(1)*x(2)*x(3))/(x(4)*x(5)*3600*10^-6));
% x1 is biomass concentration in g/litre
% x2 is microalgae growth rate per hour
% x3 is volume reactor content in litres
% x4 is photon flux density in micromol photons per square metre second
% x5 is illuminated reactor surface area in sq metres
end

```

**Figure 3.4: The Objective/Fitness MATLAB Function**

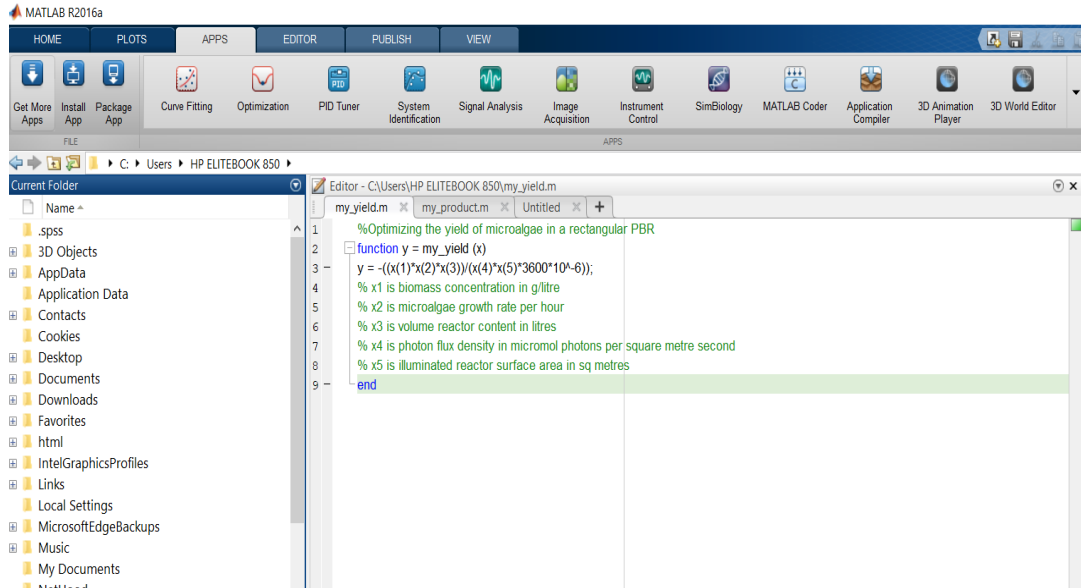


**Figure 3.5: Graphics User Interface for MATLAB® Showing Tool Bar for the “APP” Icon**

Figure 3.7 has spaces where the fitness function or objective function has to be filled starting with a handle “@” and also the number of variables in the optimization model. Also spaces for constraints are available. Whether linear inequalities, linear equalities, bounds, nonlinear constraint function and integer variable indices. Once these are filled, as summarized in Table 3.1, one goes to “options” Figure 3.8 and fills them also.



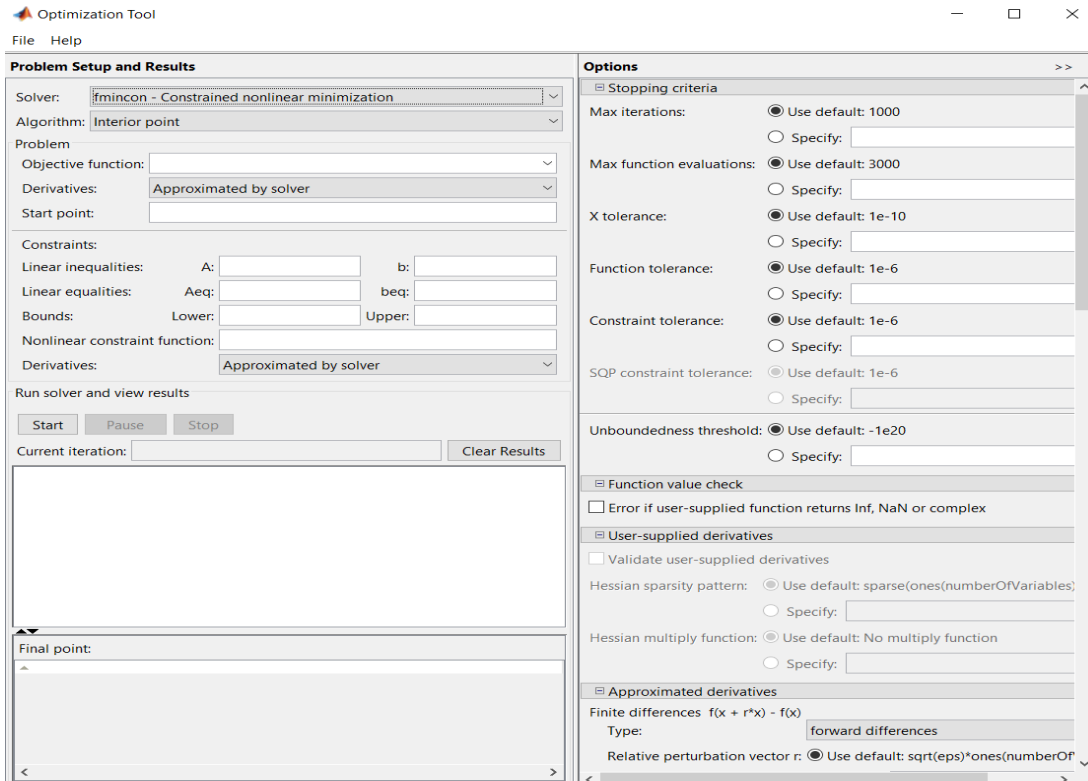


**Figure 3.6: Graphics User Interface for MATLAB® Showing the Optimization Tool**

**Table 3.1: Lower and Upper Bounds of Optimization Model Variables**

Symbol	Variable	Lower bound	Upper bound	Units	Reference
X1	Biomass Concentration	0.001	0.1	$\text{gL}^{-1}$	From current study
X2	Microalgae growth rate	0.0067	0.0102	$\text{h}^{-1}$	From current study
X3	Volume of reactor content	192	192	L	From the FPPBR
X4	Photon flux density	100	300	$\mu\text{molphotonsm}^{-2}\text{s}^{-1}$	Alanís, (2013), From the FPPBR
X5	Illuminated reactor surface area	2.16	2.16	$\text{m}^2$	From the FPPBR

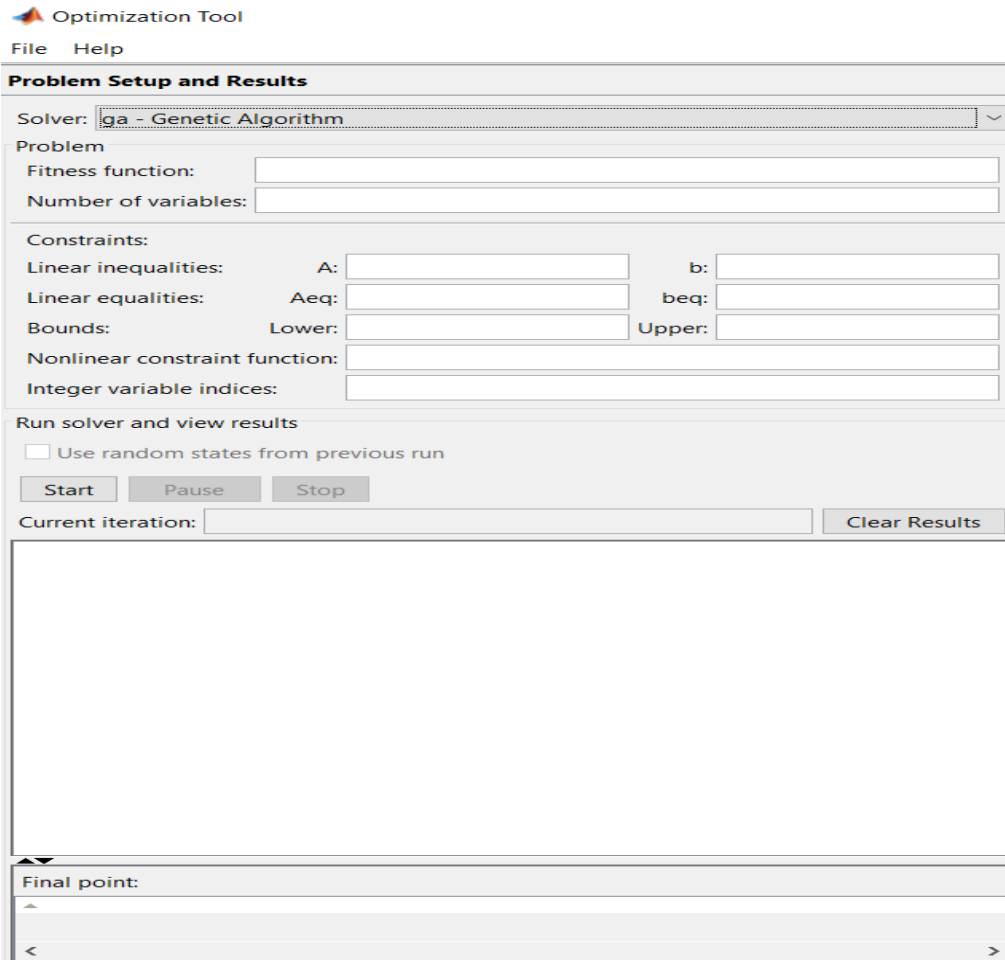


**Figure 3.7: Graphics User Interface for MATLAB® Showing GA Solver**

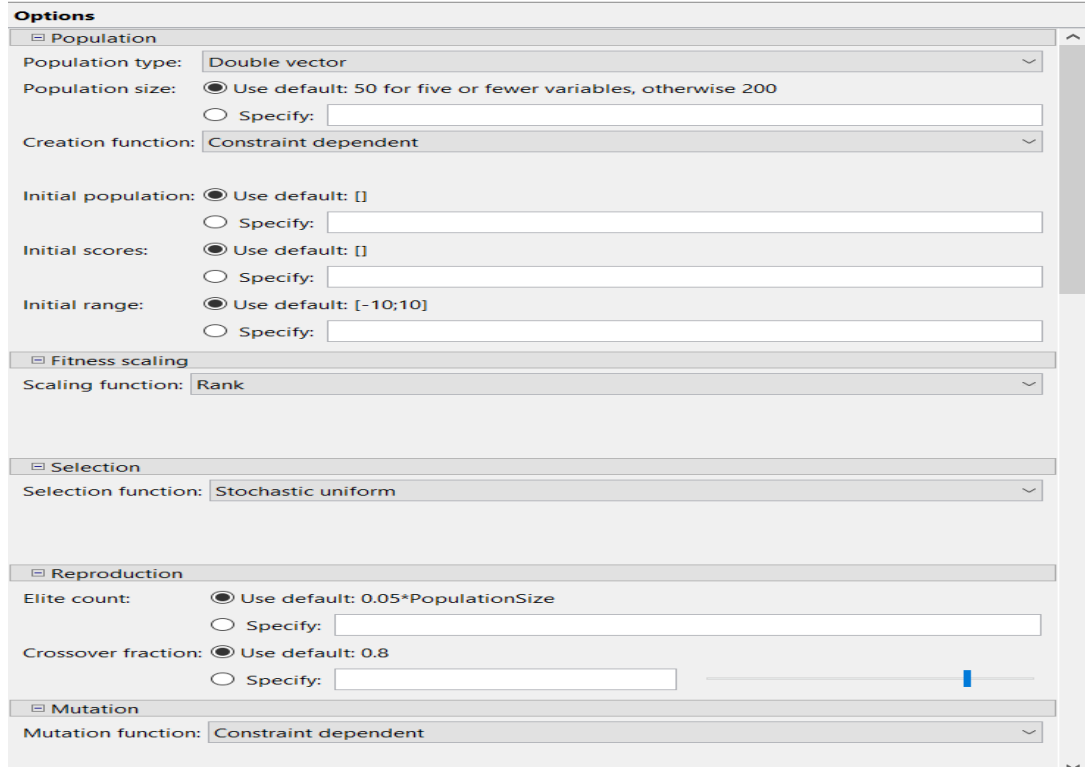


**Figure 3.8: Graphics User Interface for MATLAB® Showing GA Solver Options**

The options chosen are as shown in Table 3.2. Then run solver by clicking on the ‘Start’ icon in Figure 3.7 and execution is done. But remember the file having the function ‘my\_yield.m’ (Figure 3.4) should be on the path line or current directory in the MATLAB desktop for it to be executed.

**Table 3.2: Values for the GA Options**

<b>S/No.</b>	<b>OPTION</b>	<b>CHOICE</b>
1	Population type	Double vector
2	Population size	50
3	Creation function	Constraint dependent
4	Initial population	[ ]
5	Initial scores	[ ]
6	Initial range	[-10; 10]
7	Scaling function	Rank
8	Selection function	Stochastic uniform
9	Elite count	0.05*Population size
10	Crossover fraction	0.8
11	Mutation function	Constraint dependent
12	Mutation rate	0.01
13	Crossover function	Constraint dependent
14	Migration direction	Forward
15	Migration fraction	0.2
16	Migration interval	20
17	Nonlinear constraint algorithm	Augmented Lagrangian
18	Initial penalty	10
19	Penalty factor	100
20	Hybrid function	None
21	Generations	150
22	Time limit	Inf
23	Fitness limit	Inf
24	Stall generations	50
25	Stall time limit	Inf
26	Stall test	Average change
27	Function tolerance	1e-6
28	Constraint	1e-3
29	Plot interval (Best fitness)	1
30	Level of display	Iterative
31	Evaluate fitness and constraint functions	In serial

### **3.4.1.3 Experimental Design and Optimization Using Response Surface Methodology**

#### **3.4.1.3.1 Response Surface Methodology**

Response surface methodology (RSM) is a collection of mathematical and statistical techniques useful in modeling and analysis of problems in which a response of interest is

influenced by several variables and the objective is to optimize this response (Vicente *et al.*, 1998; Jeong & Don-Hee Park, 2009; Montgomery, 2013). RSM is used for design and collection of experimental data which allows fitting a general quadratic equation for data smoothing and prediction, regression analysis, and examination of fitted data which is usually done graphically through response surface plots.

### 3.4.1.3.2 Experimental Design

A Box-Wilson Central Composite Design (CCD), commonly called a ‘Central Composite Design’, contains an imbedded factorial or fractional factorial design with centre points that is augmented with a group of ‘star points’ that allow estimation of curvature. If the distance from the center of the design space to a factorial point is  $\pm 1$  unit for each factor, the distance from the center of the design space to a star point is  $\pm\alpha$  with  $|\alpha| > 1$ . The precise value of  $\alpha$  depends on certain properties desired for the design and on the number of factors involved. Similarly, the number of centre point runs, the design is to contain also depends on certain properties required for the design. A central composite design always contains twice as many star points as there are factors in the design. The star points represent new extreme values (low and high) for each factor in the design. The number of experimental runs is given by the formula

$$N = 2^n + 2n + n_c \quad \text{Equation 3.2}$$

where  $N$  is the number of runs

$n$  is the number of factors

$n_c$  is the number of centre points usually between 2 and 5.

To maintain rotatability, the value of  $\alpha$  depends on the number of experimental runs in the factorial portion of the central composite design:  $\alpha = [\text{number of factorial runs}]^{1/4}$ . If the factorial is a full factorial, then  $\alpha = [2^k]^{1/4}$ . For a 3 factor design,  $k = 3$ ,  $\alpha = [2^3]^{1/4} = 1.682$  (Engineering Statistics Handbook, 2006).

Box and Behnken have proposed some three-level designs for fitting response surfaces. These designs are formed by combining  $2k$  factorials with incomplete block designs. The resulting designs are usually very efficient in terms of the number of required runs, and they are either rotatable or nearly rotatable. Box-Behnken design is a spherical design, with all points lying on a sphere of radius  $\sqrt{2}$  (Montgomery, 2013).

From the optimization model, equation 3.1, the independent factors affecting biomass yield are; biomass concentration, growth rate, volume of reactor content, illuminated photobioreactor area and photon flux density. Biomass concentration, specific growth rate, and photon flux density were varied whereas volume of reactor content and illuminated photobioreactor area were kept constant. A five-level, three-factor Central Composite Design (CCD) was used to optimize these 3 independent variables to achieve maximum biomass yield. Table 3.3 gives the independent variables and levels used for experimental design.

**Table 3.3: Independent Variables and Their Levels in CCD**

Independent variable	Code	Variable levels				
		$-\alpha=-1.682$	<b>-1</b>	<b>0</b>	<b>1</b>	$+\alpha=1.682$
Growth rate ( $\text{h}^{-1}$ )	<b>A</b>	0.0055	0.0067	0.0085	0.0102	0.0114
Biomass concentration ( $\text{gL}^{-1}$ )	<b>B</b>	-0.0327	0.001	0.0505	0.1	0.1337
Photon flux density ( $\mu\text{molphotonsm}^{-2}\text{s}^{-1}$ )	<b>C</b>	31.8207	100	200	300	368.179

From Table 3.3, the  $-\alpha$  value for biomass concentration is -0.0327, which is not logical as concentration cannot be negative, hence it was replaced by 0.0005. Table 3.4 was then generated which was used in the experimental design.

**Table 3.4: Independent Variables and Their Levels in CCD with Outlier Removed**

Independent variable	Code	Variable levels				
		$-\alpha=-1.682$	<b>-1</b>	<b>0</b>	<b>1</b>	$+\alpha=1.682$
Growth rate ( $\text{h}^{-1}$ )	<b>A</b>	0.0055	0.0067	0.0085	0.0102	0.0114
Biomass concentration ( $\text{gL}^{-1}$ )	<b>B</b>	0.0005	0.001	0.0505	0.1	0.1337
Photon flux density ( $\mu\text{mol photons m}^{-2}\text{s}^{-1}$ )	<b>C</b>	31.8207	100	200	300	368.179

A total of 20 simulations, including 6 replications at the centre point, were conducted. Replicates at the centre point give pure error. Reactor content and illuminated area were kept constant at 192 L and 2.16 m<sup>2</sup>, respectively. A software program, Design Expert 13.0 (Stat-Ease, Inc., MN, USA), was used for the regression analysis, analysis of variance (ANOVA), drawing of surface plots and model adequacy checking.

### 3.4.2 Isolation and Characterization of Strains of Microalgae

#### 3.4.2.1 Sample Collection

Sampling was done as per Muruga (2015). Four water samples were collected aseptically from sites that appeared to contain algal blooms within Jomo Kenyatta University of Agriculture and Technology, Main campus, Juja (1° 05' 33" S, 37° 00' 46" E, 1526 m) and near Park-Road, Nairobi (1° 16' 22" S 36° 50' 2" E, 1,659 m). Temperature was measured *in situ* with an infrared thermometer (Model: BAFX3783). The pH was measured with a portable pH meter (InLab 738-ISM). Samples were put in sterile one litre bottles, labeled and transported to the laboratory immediately in an ice filled cooler box. Storage was done in a refrigerator at 4 °C.

#### 3.4.2.2 Preparation of the Culture Media

##### 3.4.2.2.1 Nutrient Agar and Peptone Water

Nutrient agar plates and peptone water were prepared according to Cappuccino and Sherman (2014). Distilled water was used to prepare culture media; 15 g of peptone water

and 28 g of nutrient agar were separately weighed by difference using an analytical weighing balance (Model CS 200, OHAUS Corporation, USA) and each dissolved in one litre of distilled water. Each solution was heated to boil with frequent agitation using a magnetic stirrer (Model: HS4T-Pro, Infitek Co., Ltd, Shandong, China) to completely dissolve the medium. Sterilization of the media was done by autoclaving in a vertical pressure steam sterilizer (Model LS-B75L-I, Yancheng, Jiangsu, China) at 121 °C for 15 minutes. It was allowed to cool to 45-50 °C before dispensing in petri dishes placed in the biosafety cabinet (Model: BSC-IIA2-950) to solidify.

#### **3.4.2.2.2 Marine Biological Laboratory (MBL) Medium**

Marine Biological Laboratory (MBL) Medium Woods-Hole (Nichols, 1973) adapted for freshwater microalgae was used and prepared according to Cappuccino and Sherman (2014). It has the following components and their concentration ( $\text{gL}^{-1}$ ) as shown in Table 3.5.



**Table 3.5: Components of the MBL Medium**

Stock solutions	Concentrations per litre of distilled water (gL <sup>-1</sup> )
1. CaCl <sub>2</sub> ·2H <sub>2</sub> O	36.76
2. MgSO <sub>4</sub> ·7H <sub>2</sub> O	36.97
3. NaHCO <sub>3</sub>	12.60
4. K <sub>2</sub> HPO <sub>4</sub>	8.71
5. NaNO <sub>3</sub>	85.01
6. Na <sub>2</sub> SiO <sub>3</sub> ·9H <sub>2</sub> O	28.42
7. Na <sub>2</sub> EDTA	4.36
8. FeCl <sub>3</sub> ·H <sub>2</sub> O	3.15
9. Metal mix	
CuSO <sub>4</sub> ·H <sub>2</sub> O	0.01
ZnSO <sub>4</sub> ·7H <sub>2</sub> O	0.022
CoCl <sub>2</sub> ·6H <sub>2</sub> O	0.01
MnCl <sub>2</sub> ·4H <sub>2</sub> O	0.18
Na <sub>2</sub> MoO <sub>4</sub> ·2H <sub>2</sub> O	0.006
10. Vitamin stock	
Cyanocobalamin(vitamin B12)	0.0005
Thiamine HCL(vitamin B1)	0.10
Biotin	0.0005
11. Tris stock	250.0

The stock solutions produced were then stored at 4 °C in the refrigerator. To prepare MBL medium, 1 mL of each stock solution was added to 1 L of distilled water. The pH was then adjusted to 7.2 using dilute hydrochloric acid (HCl). The medium was sterilized using an autoclave (Model LS-B75L-I, Yancheng, Jiangsu, China) at 121 °C (15 PSI) for 15 minutes (Nichols, 1973) and then allowed to cool to room temperature.

#### 3.4.2.3 Isolation, Purification and Identification of Microalgae

Isolation was done according to Cappuccino and Sherman (2014). Approximately 1 mL of microalgal sample was suspended in 9 mL of sterile distilled water and vortexed thoroughly. From this stock solution of 10 mL, serial dilutions were performed to 10<sup>-8</sup> using peptone water as the culture media as illustrated in Figure 3.9. Aliquots of 100 µL (0.1 mL) from the stock solution were drawn separately, plated on sterile agar medium aseptically, and spread using a glass rod. The plates in triplicates were incubated at 27 °C until visible colonies appeared (Black, 2008). A morphologically distinct colony was pinched with a sterile pin tool and sub cultured in MBL media (Figure 3.10). The incubation at 27 °C, under continuous light intensity of 15 µmol photons m<sup>-2</sup> s<sup>-1</sup> (RS485, BGT Technology Co., Ltd, Beijing, China) supplied by 60 cm fluorescent lamp with the

light and dark cycle of 8:16 h. The tubes were in tube racks that were placed on an orbital shaker (Rotabit, J.P. Selecta, Abrera, Spain) rotating at 85 rpm. Sub culturing in MBL media continued till axenic microalgae cultures were obtained (Duong *et al.*, 2012). Morphological characterization based on shape was done by observing under binocular microscope (Model No. XSZ-107BN, China) at magnification of X4, X40 and X100. Pictures were taken by a smartphone (Infix S4, 23MP).

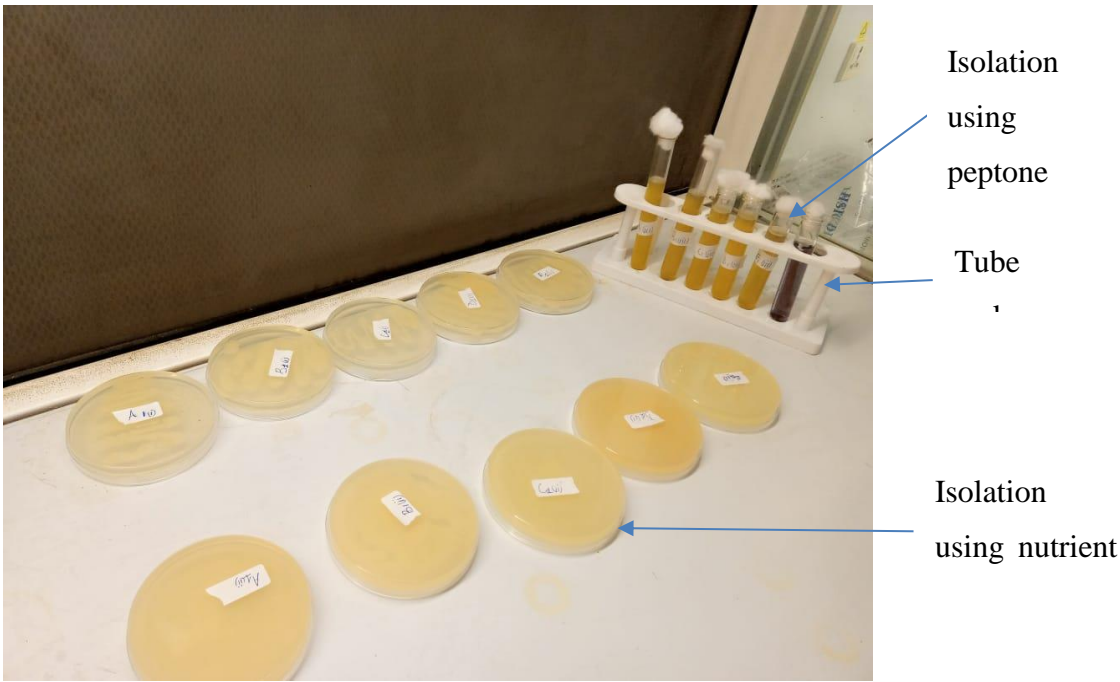


**Figure 3.9: Experimental Setup for Initial Isolation Using Nutrient Agar and Peptone Water**



**Figure 3.10: Experimental Setup for Isolation by Serial Dilution Method in MBL**

#### **3.4.2.4 Maintaining Microalgae Stocks**

Axenic microalgae were obtained from the higher dilution test tubes by withdrawing 1 mL aliquot and diluting in 1 litre liquid MBL medium contained in 2 L polyethylene terephthalate (PET) bottles. Subculturing rounds were done every three months into fresh MBL medium (Alanís, 2013). In this case, media was replaced every month. They were all stored at 26 °C, no agitation, 8:16 h light/dark photoperiod and  $50 \mu\text{mol photons m}^{-2}\text{s}^{-1}$  light intensity supplied by a twin 120 cm white fluorescent tube (T8 TUBE 18 W, Microlite LTD, UK) as shown in Figure 3.11.



**Figure 3.11: Experimental Setup for Maintaining Microalgae Stocks**

#### **3.4.2.5 Screening Microalgae for Biomass Production**

Microalgae cultures were screened for biomass yield considering their specific growth rate, doubling time and dry cell weight. The growth traits of the two isolates cultivated in batch culture were observed gravimetrically and spectrophotometrically (Thangavel *et al.*, 2018). Biomass yield was quantified using dry weight. For quantitative analysis and computation of doubling time as well as the specific growth rate, the optical densities at 680 nm were measured (Abubakar, 2012; Lee *et al.*, 2014; Puspanadan *et al.*, 2018; Vasker *et al.*, 2021 ) (denoted as OD 680) using PD-3000UV spectrophotometer (APEL Co. LTD, Japan). The OD is a simple and effective means of measuring the growth curve.

To determine the growth profile, the isolated microalgae cultures were grown in 1500 mL PET bottles with 1000 mL of autoclaved MBL medium by inoculation with 25 mL starter culture. The bottles were incubated at  $26 \pm 1$  °C under continuous lighting set to a 16:8 h light-dark cycle with a timer for 20 days (Thangavel *et al.*, 2018) (Figure 3.12). A third

bottle with MBL medium only served as a control. A twin 120 cm white LED tube (T8 TUBE 18 W) provided light intensity of between 30-45  $\mu\text{mol photons m}^{-2}\text{s}^{-1}$ . The bottles were placed in reciprocating shaker (Type: OLS 200, Grant Instruments (Cambridge) Ltd, England). About 35 mL of the sample was drawn after every four days and stored in a refrigerator at 4 °C awaiting analysis.

The specific growth rate ( $\mu$ ) and doubling time ( $T_d$ ) of the microalgae were computed according to values of OD 680 nm recorded using equations 3.2 and 3.3 as follows (Ibifubara *et al.*, 2019):

$$\mu = \frac{(\ln OD_t - \ln OD_0)}{\Delta t} \quad \text{Equation 3.2}$$

$$T_d = \frac{\ln 2}{\mu} \quad \text{Equation 3.3}$$

Where  $OD_t$  and  $OD_0$  refer to optical density at time t (day) and time zero, respectively, and  $\Delta t$  is the change in time (days).

For the dry weight measurement, approximately 10 mL of a 20-day old microalgae suspension was filtered using Whatman No. 1 filter paper. The algae pellet was washed twice with distilled water to eradicate the salts and then oven dried (Mitamura Riken Kogyo, INC., Tokyo, Japan) at 105 °C until it attained constant weight and the dry biomass was expressed as  $\text{g L}^{-1}$  (Thangavel *et al.*, 2018).

#### **3.4.2.6 Biomass Growth for Inoculation into Flat PBRs**

For the biomass growth for inoculation, the isolated axenic microalgal cultures were grown in four 2000 mL PET bottles containing each 1000 mL of autoclaved MBL medium by inoculating with 25 mL starter culture of the same strain. The bottles were incubated at  $26 \pm 1$  °C under uninterrupted illumination set on a 16:8 h light and dark cycle with a timer for 10 days (Figure 3.12). Light intensity of between 30-45  $\mu\text{mol photons m}^{-2}\text{s}^{-1}$  was

provided by a twin 120 cm white LED tube (T8 TUBE 18 W). The bottles were placed in an orbital shaker (Rotabit, J.P. Selecta, Abrera, Spain) rotating at 85 rpm.

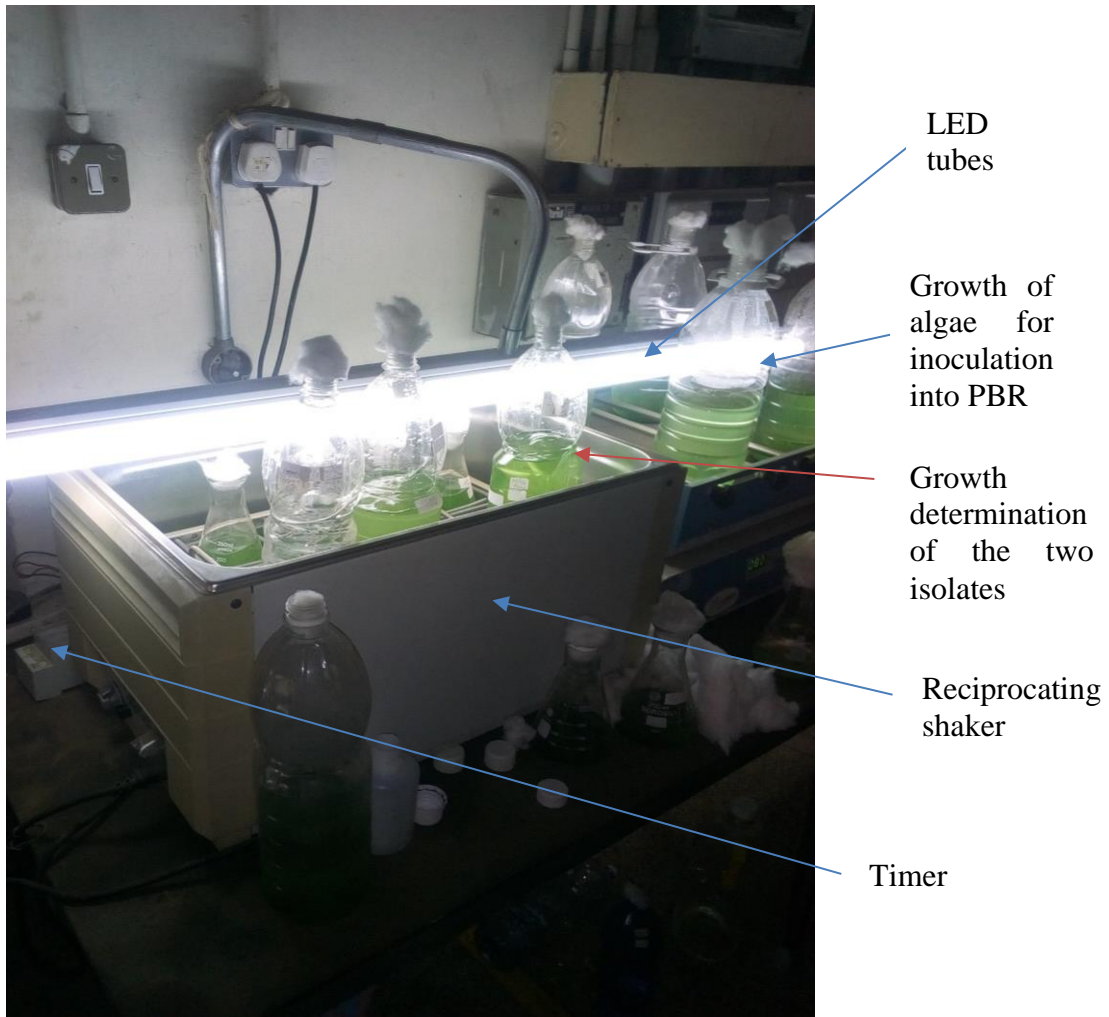


**Figure 3.12: Experimental Setup for the Determination of Growth of the Two Isolated Unialgal Microalgae and for Biomass Growth for Inoculation into PBRs**

#### **3.4.2.7 Optical Density (OD680) Standardization**

Standardization based on the OD680 of isolate stocks was carried out prior to inoculation in the three PBRs with white, red and blue wavelengths for yield test.

Equation 3.4 was used to calculate the proper dilutions needed so that the initial OD680 for both isolates in all conditions tested was the same at the beginning of the yield experiments.

$$m_1v_1 = m_2v_2 \quad \text{Equation 3.4}$$

Where  $m_1$  equals the OD680 measured in the spectrophotometer,  $m_2$  represents the concentration wanted in each PBR at the beginning of the experiment,  $v_2$  represents the total volume that will be used for each PBR during the experiment and  $v_1$  is the unknown, representing the amount of stock volume that needs to be added to accomplish a standard OD680. Finally, the amount of media needed per PBR is calculated by subtracting  $v_1$  from the total reaction volume (Alanís, 2013).

### **3.4.3 Validation of the Performance of the Developed Computer Simulation Model**

#### **3.4.3.1 Microalgae Growth in the FPPPBRs**

The entire PBR system used in this study is located inside a workshop shade in SoBEE where the experimental runs were carried out. This flat-plate perspex PBR was used in batch mode where both the inoculum and the nutrients were loaded into the bioreactor at the beginning, and no inlet nor outlet streams operated during the run, except for the air flow (Figure 3.13).

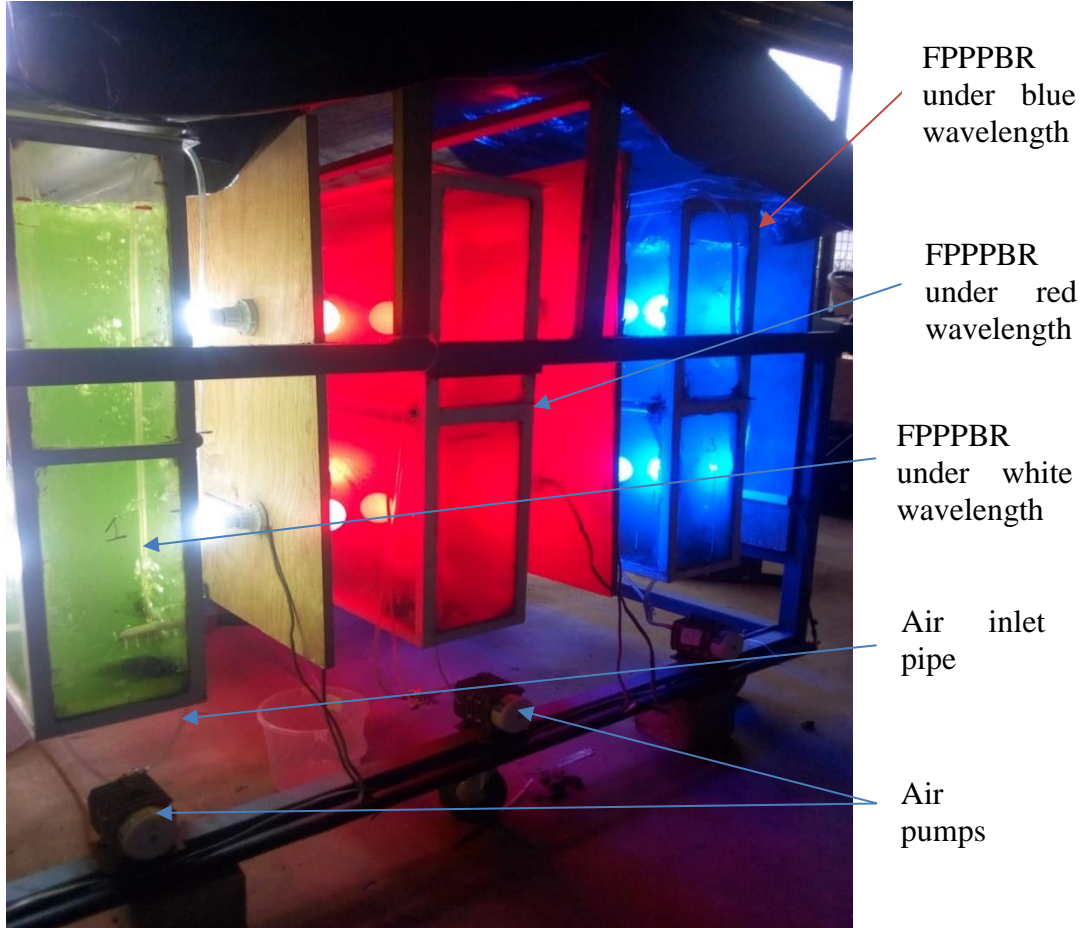


**Figure 3.13: Experimental Set-Up**

The media (MBL) used for isolation was the same one used for the microalgal growth in the PBRs. Once the MBL media was prepared as explained in 3.4.2.2.2, it was autoclaved (WAC-100, DAIHAN Scientific CO, Ltd, Korea) at 121 °C for 15 minutes and stored in hot water sterilized 20 L jerricans at room temperature. When approximately 600 L of MBL had been autoclaved, it was loaded into the PBRs with a working volume of each PBR of 192 L (length: 120 cm, width: 20 cm and height: 80 cm). Two isolates that had been isolated according to 3.4.2.3 and pre-cultured as described in 3.4.2.4 were each separately inoculated into each PBR at a concentration of  $0.1 \text{ gL}^{-1}$  and initial volume of approximately 1 litre. The PBRs were then covered with a black polythene paper to cut off any interference from the natural light. The system was set to operate at optimal



conditions that had been established by the simulation of the optimization model (Equation 3.1). The photoperiod was set at 12:12 hours of light and dark cycle and each incubation/run took 15 days. The measurement of the net irradiance outside and inside of the flat panel without contents was performed by a photosynthetic active radiation sensor (RS485, BGT Technology Co., Ltd, Beijing, China). The measurements were taken at the top, bottom and middle and nine positions in total per PBR. The irradiance inside the PBR was the one used in the research.

#### **3.4.3.2 Growth Monitoring in the FPPPBRs**

The culture growth in the FPPPBRs was estimated by measuring the optical density at 680 nm using PD-3000UV spectrophotometer (APEL Co. LTD, Japan). The samples for OD measurement were taken on 2<sup>nd</sup>, 4<sup>th</sup>, 6<sup>th</sup>, 8<sup>th</sup>, 10<sup>th</sup>, 12<sup>th</sup> and 14<sup>th</sup> day for each experimental run.

#### **3.4.3.3 Harvesting the Microalgae and Drying**

After the incubation period was over, the system was switched off and the contents left to settle overnight. Harvesting was done by filtration using a cheese cloth (46x54 threads per inch) that was folded four times and held firmly in position by a 200 mesh sieve. The cheese cloth was then washed and the resulting microalgae put in 5 L clear pre-weighed plastic buckets and placed in a biomass greenhouse for drying (Figure 3.14). The drying was carried out at a temperature of between 50 to 60 °C until constant weight was attained. The resulting yield (Figure 3.15) was then obtained by subtracting the tare weight of the empty buckets from the weight of buckets plus the dried microalgae.

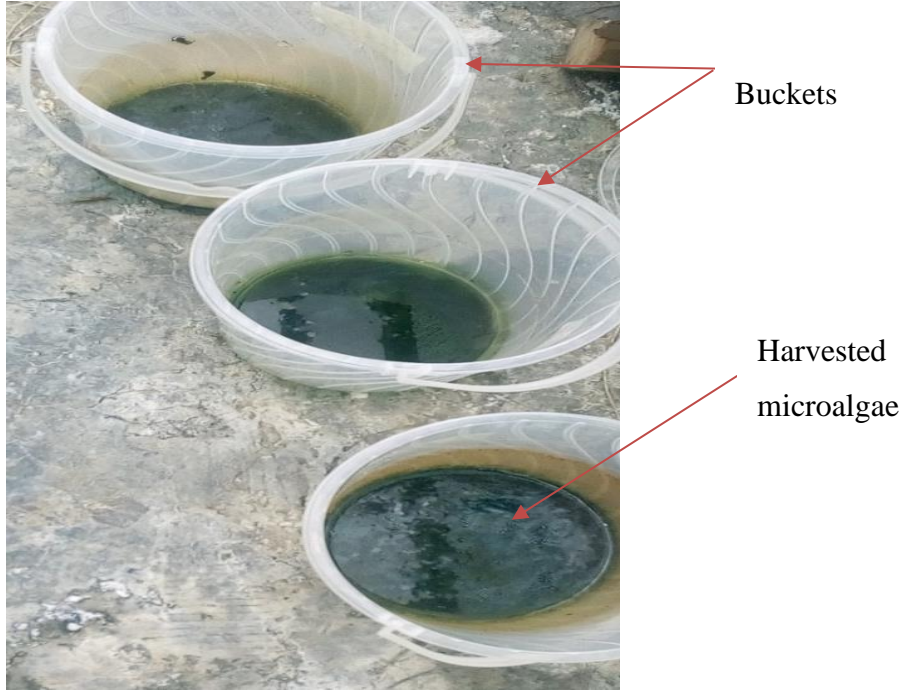


**Figure 3.14: Drying of Harvested Microalgae in a Biomass Greenhouse**



**Figure 3.15: Dried Microalgae Biomass**

### 3.4.3.4 Model Validation

The validation of the performance of the developed computer simulation model was carried out by comparing simulated and experimental data. The statistical tools used in the validation (Equations 3.5–3.8) include; mean square error (MSE), mean absolute percentage error (MAPE), mean absolute error (MAE), root mean square error (RMSE) and correlation coefficient (R). These tools are frequently used to measure the difference between values predicted by a model and the values actually observed from an experimental setup (Zhang, 2003; Zhang, 2007; Hamzacebi, 2008). For a good prediction, the obtained error values should be as small as possible while R should be high (Ibifubara *et al.*, 2019). The expressions are given as follows:

Mean square error:

$$MSE = \frac{\sum_{i=1}^n (X_{obs,i} - X_{model,i})^2}{n} \quad \text{Equation 3.5}$$

Root mean squared error:

$$RMSE = \sqrt{\left( \frac{\sum_{i=1}^n (X_{obs,i} - X_{model,i})^2}{n} \right)} \quad \text{Equation 3.6}$$

Mean absolute error:

$$MAE = \frac{\sum_{i=1}^n (X_{obs,i} - X_{model,i})}{n} \quad \text{Equation 3.7}$$

Mean absolute percentage error:

$$MAPE = \frac{(\sum_{i=1}^n (X_{obs,i} - X_{model,i}) / X_{obs,i})}{n} \times 100 \quad \text{Equation 3.8}$$

Where  $X_{obs}$  is observed values,  $X_{model}$  is modelled values at time/place  $i$ , and  $n$  is the number of experimental data points. Also the student's  $t$ -test was performed on the data.

### **3.4.4 Investigation of the Effect of Light Wavelength and Strain on the Biomass and Lipid Yield**

To investigate the influence of light wavelength and strain on the biomass and lipid yield of microalgae, the system was operated as explained in Section 3.4.3.1 under the following wavelengths; 400-700 nm (white), 430-480 nm (blue) and 610-680 nm (red). Strains used were *C. vulgaris* and *C. emersonii*. This was so because the control and monitoring system is designed to operate the three PBRs concurrently. Thus as the validation of the optimization model was ongoing using white wavelength, the influence of blue and red wavelengths on the biomass and lipid yield of microalgae was happening simultaneously.

#### **3.4.4.1 Lipid Extraction from Microalgae**

Dried microalgae were analyzed for lipid/oil content by a procedure adapted from Bligh and Dyer (1959). About 5 g of the sample, after milling, was weighed and put into centrifuge (falcon tubes) bottles. Approximately 20 mL of methanol - chloroform mixture in the ratio 2:1 v/v was added. This was shaken for about an hour using electronic shaker (KS 250B, IKA LABORTECHNIK, GmbH & CO., Austria). The mixture was then filtered using Whatman filter paper No.1 and 20 mL of pure chloroform added to the filtrate. This was vortexed (TTM-1, Shibata Science Co., Ltd, Hong Kong) for a few seconds, then cold water added and vortexed again to obtain a homogeneous solution. This solution was centrifuged (Werk NC D-78532, Tuttlingen, Germany) at 7000 rpm for 10 minutes. Two layers were formed viz. organic and inorganic. The organic layer containing the fats was transferred into pre-weighed clean and dried reflux flasks. Then dried in an oven (Mitamura Riken Kogyo, INC., Tokyo, Japan) at 105 °C for an hour. It was then

weighed and this weight recorded as  $W_1$ . The contents were evaporated using rotary evaporator (Bibby Sterilin Ltd, RE 100B, UK) to obtain the residue. The residue was transferred back in the oven to dry for another hour at 105 °C and the resulting weight recorded as  $W_2$ . The percent lipid content was then calculated according to equation 3.6 and the dried residue dissolved in 7 ml of 5% methanolic: HCl awaiting fatty acid profiling.

$$\% \text{Lipid content (w/w)} = \frac{(W_2 - W_1)}{\text{sample weight}} * 100 \quad \text{Equation 3.6}$$

### 3.5 Statistical Analysis

Statistical analyses were performed using IBM SPSS statistics 25 software, Design expert 13, Microsoft office excel 2016 and MATLAB R2016a. All data presented in tables and figures are expressed as the mean  $\pm$  standard deviation (SD). The biomass and lipid yields were analyzed using a two-way analysis of variance (ANOVA). Differences were considered significant at  $p < 0.05$ .

## CHAPTER FOUR

### RESULTS AND DISCUSSION

#### 4.1 Introduction

This chapter presents the obtained results and is organized into four sections. The first section presents the results of the optimization model, the second section presents the results on isolation and characterization of strains of microalgae for biomass and lipid production. The third section presents results on validation of the optimization model and finally the fourth section presents the findings on the effect of blue, red and white wavelength and strain of microalgae on the biomass and lipid yield of microalgae.

#### 4.2 Computer Optimization Model for Simulating Microalgae Biomass Yield

From the computer optimization model equation 3.1 and applying Genetic Algorithm (GA) and the limits in Table 3.1 and values for the GA options in Table 3.2, after 87 generations, in a 3.06GHz, 512MB RAM computer, the optimum microalgae yield was  $0.250715 \pm 0.001608 \text{ gmolphotons}^{-1}$  (Figure 4.1) and the optimal cultivation conditions were as in Table 4.1, that is to say, biomass concentration of  $0.1 \text{ gL}^{-1}$ , microalgae growth rate of  $0.0102 \text{ h}^{-1}$  (i.e., is the amount of microalgae created in 1 unit of time divided by the total amount of original microalgae) and photon flux density of  $100 \text{ } \mu\text{molphotonsm}^{-2}\text{s}^{-2}$ .

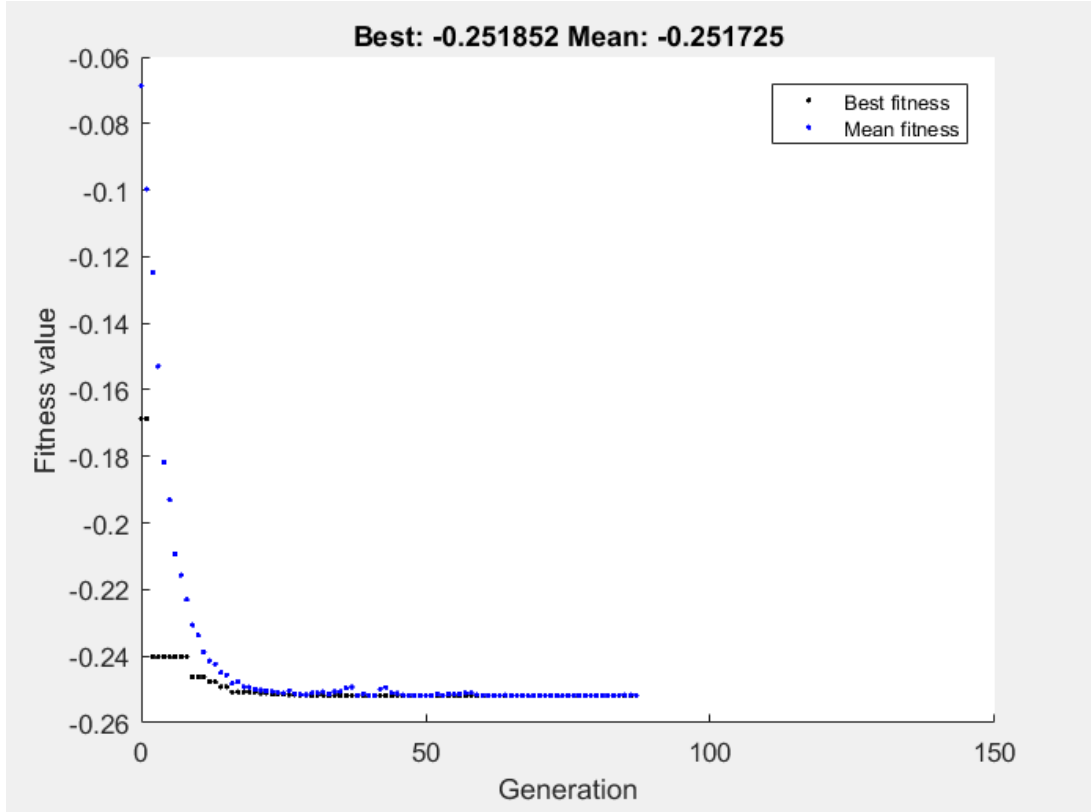


**Figure 4.1: Results of Simulation Model Equation 3.1**

**Table 4.1: Optimal Cultivation Conditions According to Equation 3.1 Using GA**

Symbol	Variable	Optimal value	Units
<b>X1</b>	Biomass concentration	0.1	$\text{gL}^{-1}$
<b>X2</b>	Microalgae growth rate	0.0102	$\text{h}^{-1}$
<b>X3</b>	Volume of reactor content	192	L
<b>X4</b>	Photon flux density	100	$\mu\text{molphotonsm}^{-2}\text{s}^{-1}$
<b>X5</b>	Illuminated reactor surface area	2.16	$\text{m}^2$

**Note:** The physical meaning of the growth rate is the amount of algae created in 1 unit of time divided by the total amount of original algae (growth rate = number of new algae per unit time / number of old algae). The units of growth rate can vary with the experiment or model, growth rate  $\mu$  is found in units of  $\text{s}^{-1}$ ,  $\text{h}^{-1}$  and  $\text{d}^{-1}$  (Arragon, 2014).

According to the best knowledge of the researcher, there was no other research findings to compare with the findings of this research.

#### 4.2.1 Optimization Using Response Surface Methodology and Genetic Algorithm

Table 4.2 gives the details of a set of 20 experiments in terms of actual and coded levels as per CCD, and simulated biomass yields.

**Table 4.2: CCD Matrix with Simulated Biomass Yields**

STD	RUN	Level of factors[actual(coded)]			Simulated yield (gmol/photons)
		Factor 1 A: Growth rate (h <sup>-1</sup> )	Factor 2 B: Biomass concentration (gL <sup>-1</sup> )	Factor 3 C: Photon flux density ( $\mu\text{mol photons m}^{-2}\text{s}^{-1}$ )	
19	1	0.00845 (0)	0.0505 (0)	200 (0)	0.0526821
3	2	0.0067 (-1)	0.1 (1)	100 (-1)	0.165432
7	3	0.0067 (-1)	0.1 (1)	300 (1)	0.055144
1	4	0.0067 (-1)	0.001 (-1)	100 (-1)	0.00165432
17	5	0.00845 (0)	0.0505 (0)	200 (0)	0.0526821
2	6	0.0102 (1)	0.001 (-1)	100 (-1)	0.00251852
16	7	0.00845 (0)	0.0505 (0)	200 (0)	0.0526821
8	8	0.0102 (1)	0.1 (1)	300 (1)	0.0839506
13	9	0.00845 (0)	0.0505 (0)	31.8207 (-1.682)	0.331118
4	10	0.0102 (1)	0.1 (1)	100 (-1)	0.251852
6	11	0.0102 (1)	0.001 (-1)	300 (1)	0.000839506
9	12	0.00550686 (-1.682)	0.0505 (0)	200 (0)	0.0343329
12	13	0.00845 (0)	0.133749 (1.682)	200 (0)	0.139528
10	14	0.0113931 (1.682)	0.0505 (0)	200 (0)	0.0710311
5	15	0.0067 (-1)	0.001 (-)	300 (1)	0.00055144
18	16	0.00845 (0)	0.0505 (0)	200 (0)	0.0526821
11	17	0.00845 (0)	0.0005 (-1.682)	200 (0)	0.000521605
15	18	0.00845 (0)	0.0505 (0)	200 (0)	0.0526821
20	19	0.00845 (0)	0.0505 (0)	200 (0)	0.0526821
14	20	0.00845 (0)	0.0505 (0)	368.179 (1.682)	0.0286177

Data in Table 4.2 were tested for fit for a linear, two-factor interaction (2FI), quadratic and cubic polynomials. The results are as shown in Table 4.3.



**Table 4.3: Summary for Model Fit- Sequential Model Sum of Squares**

Source	Sequential p-value	Lack of Fit p-value	Adjusted R <sup>2</sup>	Predicted R <sup>2</sup>	
Linear	<b>0.0006</b>		<b>0.5867</b>	<b>0.3628</b>	<b>Suggested</b>
<b>2FI</b>	0.3168		0.6085	0.2961	
Quadratic	<b>0.0072</b>		<b>0.8396</b>	<b>0.2791</b>	<b>Suggested</b>
<b>Cubic</b>			1.0000		<b>Aliased</b>

Sequential Model Sum of Squares [Type I]

Source	Sum of Squares	df	Mean Square	F-value	p-value	
<b>Mean vs Total</b>	0.1100	1	0.1100			
Linear vs Mean	<b>0.0937</b>	<b>3</b>	<b>0.0312</b>	<b>9.99</b>	<b>0.0006</b>	<b>Suggested</b>
<b>2FI vs Linear</b>	0.0115	3	0.0038	1.30	0.3168	
Quadratic vs 2FI	<b>0.0264</b>	<b>3</b>	<b>0.0088</b>	<b>7.24</b>	<b>0.0072</b>	<b>Suggested</b>
<b>Cubic vs Quadratic</b>	0.0121	5	0.0024			<b>Aliased</b>
<b>Residual</b>	0.0000	5	0.0000			
<b>Total</b>	<b>0.2537</b>	<b>20</b>	<b>0.0127</b>			

Looking at R<sup>2</sup> values, Cubic model had the highest value (R<sup>2</sup> = 1.0000) but it is aliased, so should not be selected. Next highest R<sup>2</sup> was for a Quadratic model (R<sup>2</sup> = 0.8396), which was the suggested model. Criterion of p-value, Prob > F, was less than 0.0500, indicating that the Quadratic model terms were significant. Therefore, the Quadratic model was selected as it had the highest order polynomial where the model terms were significant and the model was not aliased.

A full quadratic model for yield (Equation 4.1) was tested.

$$Y = b_0 + b_1A + b_2B + b_3C + b_{12}AB + b_{13}AC + b_{23}BC + b_{11}A^2 + b_{22}B^2 + b_{33}C^2 \quad \text{Equation 4.1}$$

Table 4.4 gives Analysis of Variance (ANOVA) for the Response Surface Quadratic model.

**Table 4.4: ANOVA for Response Surface Quadratic Model**

Source	Sum of Squares	df	Mean Square	F-value	p-value	
Model	0.1316	9	0.0146	12.05	0.0003	Significant
<b>A-Growth rate</b>	0.0023	1	0.0023	1.91	0.1966	
<b>B-Biomass concentration</b>	0.0488	1	0.0488	40.22	< 0.0001	
<b>C-Photon flux density</b>	0.0457	1	0.0457	37.64	0.0001	
<b>AB</b>	0.0016	1	0.0016	1.34	0.2738	
<b>AC</b>	0.0004	1	0.0004	0.3488	0.5679	
<b>BC</b>	0.0095	1	0.0095	7.81	0.0189	
<b>A<sup>2</sup></b>	0.0003	1	0.0003	0.2713	0.6138	
<b>B<sup>2</sup></b>	0.0019	1	0.0019	1.53	0.2445	
<b>C<sup>2</sup></b>	0.0235	1	0.0235	19.36	0.0013	
Residual	0.0121	10	0.0012			
<b>Lack of Fit</b>	0.0121	5	0.0024			
<b>Pure Error</b>	0.0000	5	0.0000			
Cor Total	0.1437	19				
<b>Std. Dev.</b>	0.0348		<b>R<sup>2</sup></b>		0.9156	
<b>Mean</b>	0.0742		<b>Adjusted R<sup>2</sup></b>		0.8396	
<b>C.V. %</b>	46.97		<b>Predicted R<sup>2</sup></b>		0.2791	
			<b>Adeq Precision</b>		12.1133	

The Model F-value of 12.05 implies the model is significant. There is only a 0.03% chance that an F-value this large could occur due to noise. P-values less than 0.0500 indicate model terms are significant. In this case B, C, BC and C<sup>2</sup> are significant model terms. Values greater than 0.1000 indicate the model terms are not significant. In this case A, AB, AC, A<sup>2</sup> and B<sup>2</sup>. Since, there are many insignificant model terms (not counting those required to support hierarchy), model reduction may improve the model.

The **Predicted R<sup>2</sup>** of 0.2791 is not as close to the **Adjusted R<sup>2</sup>** of 0.8396 as one might normally expect; i.e. the difference is more than 0.2. This may indicate a large block effect or a possible problem with the model and/or data. Things to consider are model reduction, response transformation, outliers, etc. When the model was tested for adequacy, run 9 was

found to be an outlier and the PFD was adjusted from 31.8207 to 55 by trial and error method. Table 4.5 shows the CCD matrix with outlier removed.

**Table 4.5: CCD Matrix with Simulated Biomass Yields and Outlier Removed**

STD	RUN	Level of factors[actual(coded)]			Simulated yield (gmol/photons)
		Factor 1 A: Growth rate (h <sup>-1</sup> )	Factor 2 B: Biomass concentration (gL <sup>-1</sup> )	Factor 3 C: Photon flux density ( $\mu\text{mol photons m}^{-2}\text{s}^{-1}$ )	
19	1	0.00845 (0)	0.0505 (0)	200 (0)	0.0526821
3	2	0.0067 (-1)	0.1 (1)	100 (-1)	0.165432
7	3	0.0067 (-1)	0.1 (1)	300 (1)	0.055144
1	4	0.0067 (-1)	0.001 (-1)	100 (-1)	0.00165432
17	5	0.00845 (0)	0.0505 (0)	200 (0)	0.0526821
2	6	0.0102 (1)	0.001 (-1)	100 (-1)	0.00251852
16	7	0.00845 (0)	0.0505 (0)	200 (0)	0.0526821
8	8	0.0102 (1)	0.1 (1)	300 (1)	0.0839506
13	9	0.00845 (0)	0.0505 (0)	55 (-1.682)	0.191571
4	10	0.0102 (1)	0.1 (1)	100 (-1)	0.251852
6	11	0.0102 (1)	0.001 (-1)	300 (1)	0.000839506
9	12	0.00550686 (-1.682)	0.0505 (0)	200 (0)	0.0343329
12	13	0.00845 (0)	0.133749 (1.682)	200 (0)	0.139528
10	14	0.0113931 (1.682)	0.0505 (0)	200 (0)	0.0710311
5	15	0.0067 (-1)	0.001 (-)	300 (1)	0.00055144
18	16	0.00845 (0)	0.0505 (0)	200 (0)	0.0526821
11	17	0.00845 (0)	0.0005 (-1.682)	200 (0)	0.000521605
15	18	0.00845 (0)	0.0505 (0)	200 (0)	0.0526821
20	19	0.00845 (0)	0.0505 (0)	200 (0)	0.0526821
14	20	0.00845 (0)	0.0505 (0)	368.179 (1.682)	0.0286177

Data in Table 4.5 were tested for fit for a linear, two-factor interaction (2FI), quadratic and cubic polynomials. The results are as shown in Table 4.6.

**Table 4.6: Summary for Model Fit- Sequential Model Sum of Squares for Modified Data**

Source	Sequential p-value	Lack of Fit p-value	Adjusted R <sup>2</sup>	Predicted R <sup>2</sup>	
<b>Linear</b>	< 0.0001		0.7308	0.5832	
<b>2FI</b>	0.0111		0.8550	0.7491	
Quadratic	<b>0.0038</b>		<b>0.9478</b>	<b>0.7807</b>	<b>Suggested</b>
<b>Cubic</b>			1.0000		<b>Aliased</b>

Sequential Model Sum of Squares [Type I]

Source	Sum of Squares	df	Mean Square	F-value	p-value	
<b>Mean vs Total</b>	0.0903	1	0.0903			
<b>Linear vs Mean</b>	0.0700	3	0.0233	18.20	< 0.0001	
<b>2FI vs Linear</b>	0.0115	3	0.0038	5.56	0.0111	
Quadratic vs 2FI	<b>0.0065</b>	<b>3</b>	<b>0.0022</b>	<b>8.71</b>	<b>0.0038</b>	<b>Suggested</b>
<b>Cubic vs Quadratic</b>	0.0025	5	0.0005			<b>Aliased</b>
<b>Residual</b>	0.0000	5	0.0000			
<b>Total</b>	0.1808	20	0.0090			

The highest order polynomial (quadratic) was selected where the additional terms were significant and the model was not aliased.

A full quadratic model for yield (Equation 4.1) was tested and the Analysis of Variance (ANOVA) for the Response Surface Quadratic model is as shown in Table 4.7.

**Table 4.7: ANOVA for Response Surface Quadratic Model with Outlier Removed**

Source	Sum of Squares	df	Mean Square	F-value	p-value	
Model	0.0880	9	0.0098	39.36	< 0.0001	Significant
<b>A-Growth rate</b>	0.0023	1	0.0023	9.35	0.0121	
<b>B-Biomass concentration</b>	0.0455	1	0.0455	183.24	< 0.0001	
<b>C-Photon flux density</b>	0.0241	1	0.0241	96.87	< 0.0001	
<b>AB</b>	0.0016	1	0.0016	6.55	0.0284	
<b>AC</b>	0.0004	1	0.0004	1.70	0.2210	
<b>BC</b>	0.0095	1	0.0095	38.16	0.0001	
<b>A<sup>2</sup></b>	0.0000	1	0.0000	0.0718	0.7942	
<b>B<sup>2</sup></b>	0.0004	1	0.0004	1.78	0.2118	
<b>C<sup>2</sup></b>	0.0061	1	0.0061	24.58	0.0006	
Residual	0.0025	10	0.0002			
<b>Lack of Fit</b>	0.0025	5	0.0005			
<b>Pure Error</b>	0.0000	5	0.0000			
Cor Total	0.0905	19				
<b>Std. Dev.</b>	0.0158	<b>R<sup>2</sup></b>			0.9725	
Mean	0.0672	<b>Adjusted R<sup>2</sup></b>			0.9478	
C.V. %	23.46	<b>Predicted R<sup>2</sup></b>			0.7807	
		<b>Adeq Precision</b>			23.8239	

The Model F-value of 39.36 implies the model is significant. There is only a 0.01% chance that an F-value this large could occur due to noise. P-values less than 0.0500 indicate model terms are significant. In this case A, B, C, AB, BC, C<sup>2</sup> are significant model terms. Values greater than 0.1000 indicate the model terms are not significant. In this case AC, A<sup>2</sup> and B<sup>2</sup> are not significant. Hence, these terms were removed to improve the model. Table 4.8 shows the ANOVA results for the reduced quadratic model.

**Table 4.8: ANOVA for Reduced Quadratic Model**

Source	Sum of Squares	df	Mean Square	F-value	p-value	
Model	0.0871	6	0.0145	56.03	< 0.0001	Significant
<b>A-Growth rate</b>	0.0023	1	0.0023	8.96	0.0104	
<b>B-Biomass concentration</b>	0.0474	1	0.0474	182.95	< 0.0001	
<b>C-Photon flux density</b>	0.0240	1	0.0240	92.43	< 0.0001	
<b>AB</b>	0.0016	1	0.0016	6.28	0.0263	
<b>BC</b>	0.0095	1	0.0095	36.59	< 0.0001	
<b>C<sup>2</sup></b>	0.0060	1	0.0060	23.28	0.0003	
Residual	0.0034	13	0.0003			
<b>Lack of Fit</b>	0.0034	8	0.0004			
<b>Pure Error</b>	0.0000	5	0.0000			
Cor Total	0.0905	19				
Std. Dev.	0.0161		<b>R<sup>2</sup></b>		0.9628	
Mean	0.0672		<b>Adjusted R<sup>2</sup></b>		0.9456	
C.V. %	23.96		<b>Predicted R<sup>2</sup></b>		0.8508	
			<b>Adeq Precision</b>		26.7783	

The Model F-value of 56.03 implies the model is significant. There is only a 0.01% chance that an F-value this large could occur due to noise. P-values less than 0.0500 indicate model terms are significant. In this case A, B, C, AB, BC, C<sup>2</sup> are significant model terms. Values greater than 0.1000 indicate the model terms are not significant. All model terms are significant, hence no further model improvement. The Predicted R<sup>2</sup> (a measure of the amount of variation in new data explained by the model) of 0.8508 is in reasonable agreement with the Adjusted R<sup>2</sup> of 0.9456; i.e. the difference is less than 0.2. Adeq Precision measures the signal to noise ratio. A ratio greater than 4 is desirable. The ratio of 26.778 indicates an adequate signal. This model can be used to navigate the design space. Table 4.9 gives the values of coefficients for the Reduced Quadratic Model.

**Table 4.9: Coefficients for the Reduced Quadratic Model in Terms of Coded factors**

<b>Factor</b>	<b>Coefficient Estimate</b>	<b>df</b>	<b>Standard Error</b>	<b>95% CI Low</b>	<b>95% CI High</b>	<b>VIF</b>
<b>Intercept</b>	0.0510	1	0.0047	0.0408	0.0611	
<b>A-Growth rate</b>	0.0130	1	0.0044	0.0036	0.0225	1.0000
<b>B-Biomass concentration</b>	0.0634	1	0.0047	0.0532	0.0735	1.00
<b>C-Photon flux density</b>	-0.0434	1	0.0045	-0.0531	-0.0336	1.02
<b>AB</b>	0.0143	1	0.0057	0.0020	0.0266	1.0000
<b>BC</b>	-0.0344	1	0.0057	-0.0467	-0.0221	1.0000
<b>C<sup>2</sup></b>	0.0226	1	0.0047	0.0125	0.0327	1.02

The coefficient estimate represents the expected change in response per unit change in factor value when all remaining factors are held constant. The intercept in an orthogonal design is the overall average response of all the runs. The coefficients are adjustments around that average based on the factor settings. When the factors are orthogonal the Variance Inflation Factor (VIFs) are 1; VIFs greater than 1 indicate multi-collinearity, the higher the VIF the more severe the correlation of factors. As a rough rule, VIFs less than 10 are tolerable. In the present study, VIF is unity hence there is no multi-collinearity.

The final equation in terms of coded factors (Equation 4.2) was used to make predictions about the response for given levels of each factor (Table 4.10). By default, the high levels of the factors are coded as +1 and the low levels are coded as -1. The coded equation is useful for identifying the relative impact of the factors by comparing the factor coefficients.

$$\begin{aligned}
 \text{Biomass yield} = & +0.0510 + 0.0130A + 0.0634B - 0.0434C + 0.0143AB \\
 & -0.0344BC + 0.0226C^2
 \end{aligned}
 \tag{Equation 4.2}$$

**Table 4.10: CCD Matrix with Simulated and Predicted Biomass Yields**

LEVEL OF FACTORS[ACTUAL(CODED)]						
STD	RUN	Factor 1 A: Growth rate (h <sup>-1</sup> )	Factor 2 B: Biomass concentration (gL <sup>-1</sup> )	Factor 3 C: Photon flux density ( $\mu\text{mol photons m}^{-2}\text{s}^{-1}$ )	Simulated yield (gmol/photons)	Predicted yield (gmol/photons) Equation 4.2
19	1	0.00845 (0)	0.0505 (0)	200 (0)	0.0526821	0.0510
3	2	0.0067 (-1)	0.1 (1)	100 (-1)	0.165432	0.1874
7	3	0.0067 (-1)	0.1 (1)	300 (1)	0.055144	0.0318
1	4	0.0067 (-1)	0.001 (-1)	100 (-1)	0.00165432	0.0203
17	5	0.00845 (0)	0.0505 (0)	200 (0)	0.0526821	0.0510
2	6	0.0102 (1)	0.001 (-1)	100 (-1)	0.00251852	0.0179
16	7	0.00845 (0)	0.0505 (0)	200 (0)	0.0526821	0.0510
8	8	0.0102 (1)	0.1 (1)	300 (1)	0.0839506	0.0864
13	9	0.00845 (0)	0.0505 (0)	55 (-1.682)	0.191571	0.1613
4	10	0.0102 (1)	0.1 (1)	100 (-1)	0.251852	0.2420
6	11	0.0102 (1)	0.001 (-1)	300 (1)	0.000839506	0.0003
9	12	0.00550686 (-1.682)	0.0505 (0)	200 (0)	0.0343329	0.0290
12	13	0.00845 (0)	0.133749 (1.682)	200 (0)	0.139528	0.1575
10	14	0.0113931 (1.682)	0.0505 (0)	200 (0)	0.0710311	0.0729
5	15	0.0067 (-1)	0.001 (-)	300 (1)	0.00055144	0.0024
18	16	0.00845 (0)	0.0505 (0)	200 (0)	0.0526821	0.0510
11	17	0.00845 (0)	0.0005 (-1.682)	200 (0)	0.000521605	0.0130
15	18	0.00845 (0)	0.0505 (0)	200 (0)	0.0526821	0.0510
20	19	0.00845 (0)	0.0505 (0)	200 (0)	0.0526821	0.0510
14	20	0.00845 (0)	0.0505 (0)	368.179 (1.682)	0.0286177	0.0418

Equation 4.3 shows the final equation in terms of actual factors.

$$\begin{aligned}
 \text{Biomass yield} = & 0.100364 - 0.860835 \text{Growth rate} \\
 & + 1.27995 \text{Biomass concentration} \\
 & - 0.000985 \text{Photon flux density} \\
 & + 164.60943(\text{Growth rate})(\text{Biomass concentration}) \\
 & - 0.006955(\text{Biomass concentration})(\text{Photon flux density})
 \end{aligned}$$



$$+2.25586 \times 10^{-6}(\textit{Photon flux density})^2 \quad \text{Equation 4.3}$$

The equation in terms of actual factors can be used to make predictions about the response for given levels of each factor. Here, the levels should be specified in the original units for each factor. This equation should not be used to determine the relative impact of each factor because the coefficients are scaled to accommodate the units of each factor and the intercept is not at the center of the design space. The positive and negative sign in each part of the equation (Equation 4.2) show the increasing and decreasing effects of the parameters on each response, respectively. Therefore, an increase in growth rate (A) and biomass concentration (B) each, has a positive effect whereas an increase in photon flux density (C) has a negative effect on the microalgae yield. Also, simultaneous increase of growth rate and biomass concentration lead to positive increase in yield, whereas simultaneous increases in photon flux density and biomass concentration lead to negative effects on the microalgae yield (note the negative coefficient mark). As shown in Table 4.10, the highest yield of  $0.2420 \text{ gmol photons}^{-1}$  occurred at  $0.0102 \text{ h}^{-1}$  of growth rate,  $0.1 \text{ gL}^{-1}$  of biomass concentration and  $100 \text{ } \mu\text{mol photons m}^{-2}\text{s}^{-1}$  of photon flux density.

#### 4.2.1.1 Model Adequacy Checking

It is important to check the adequacy of the fitted model in order to ascertain its validity. Figure 4.2 shows that the normal plot of residuals (i.e., the difference between simulated and predicted responses) for the response was normally distributed, as they lie approximately on a straight line and shows no deviation of the variance. The same applies to Figure 4.3. The results of all the other plots (Figure 4.4-4.8) indicated that developed model is adequate to describe the response, as all the points lay within the upper and lower limits and were structureless (i.e., did not form any particular pattern).


**Biomass yield**

Color points by value of  
Biomass yield:  
0.000521605  0.251852

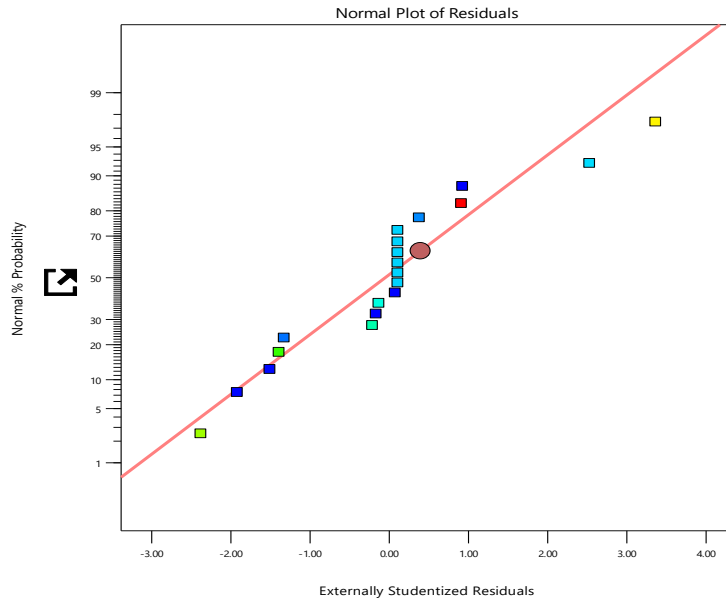


**Figure 4.2: Normal Probability of Externally Studentized Residuals**

**Biomass yield**

Color points by value of  
Biomass yield:  
0.000521605  0.251852

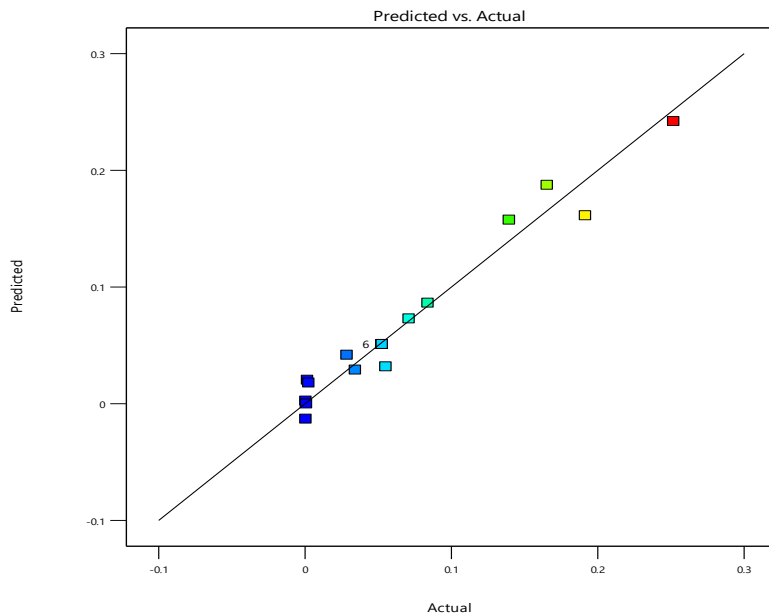


**Figure 4.3: A Graph of Predicted Microalgae Yield against Simulated Microalgae Yield**

**Biomass yield**

Color points by value of  
Biomass yield:

0.000521605  0.251852

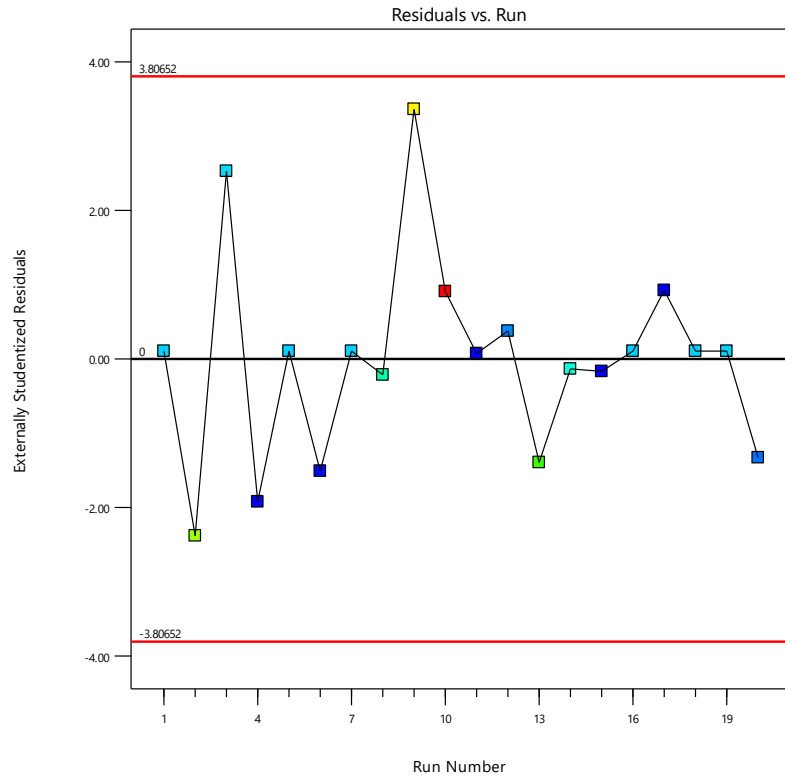


**Figure 4.4: A Graph of Externally Studentized Residuals against Run Number**

**Biomass yield**

Color points by value of  
Biomass yield:

0.000521605  0.251852

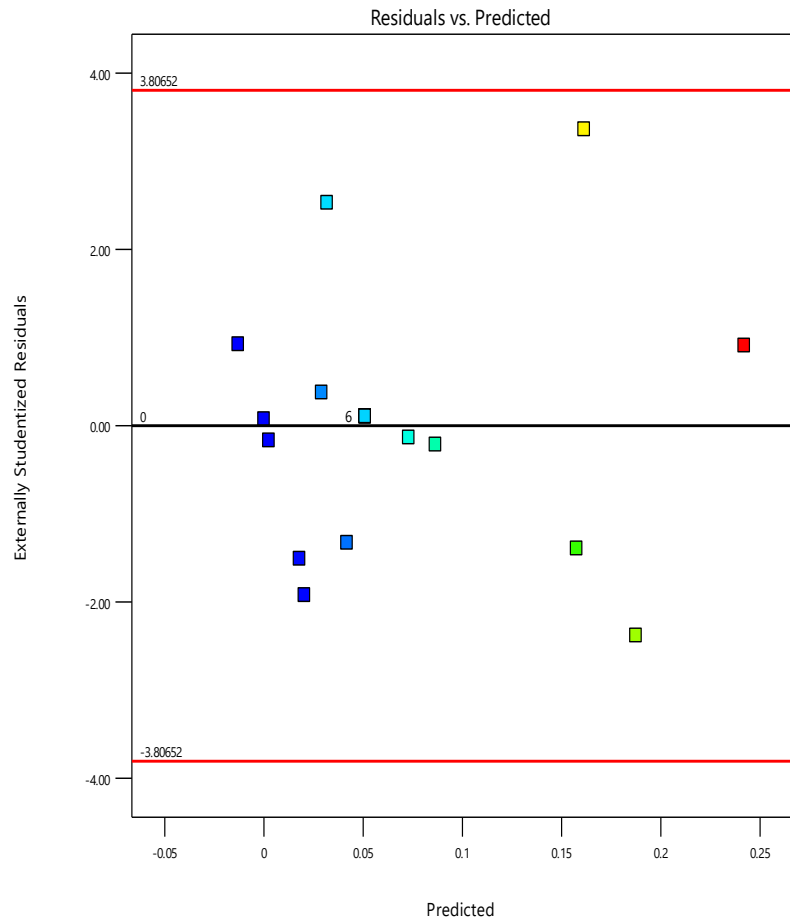


**Figure 4.5: A Graph of Externally Studentized Residuals against Predicted Values**

**Biomass yield**

Color points by value of

Biomass yield:

0.000521605  0.251852

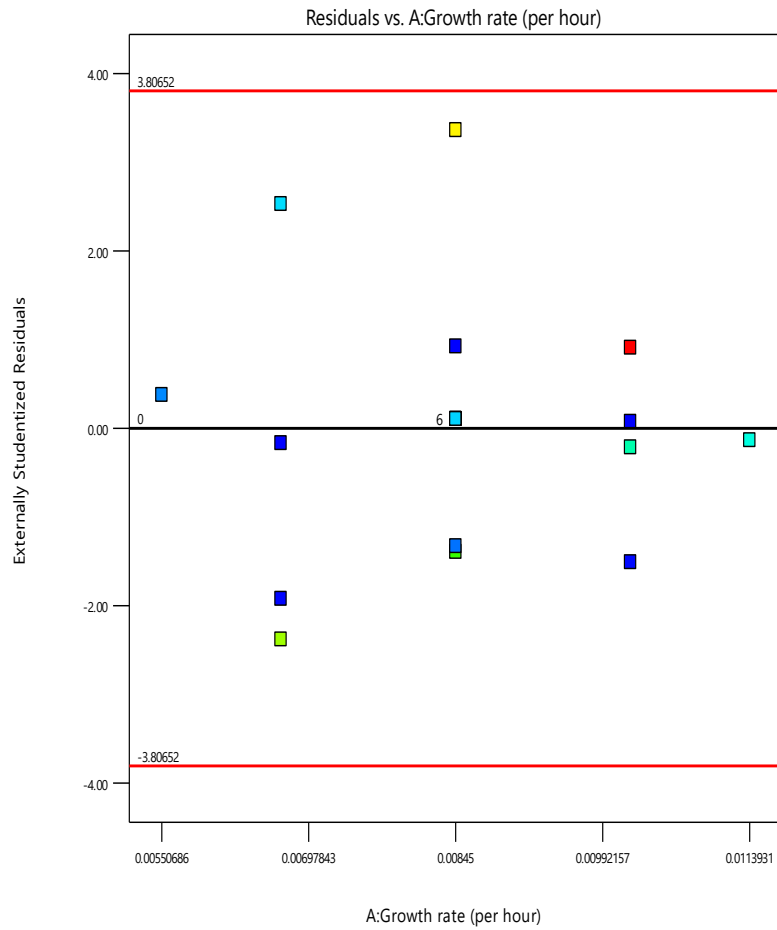


**Figure 4.6: A Graph of Externally Studentized Residuals against Growth Rate**

**Biomass yield**

Color points by value of

Biomass yield:

0.000521605  0.251852

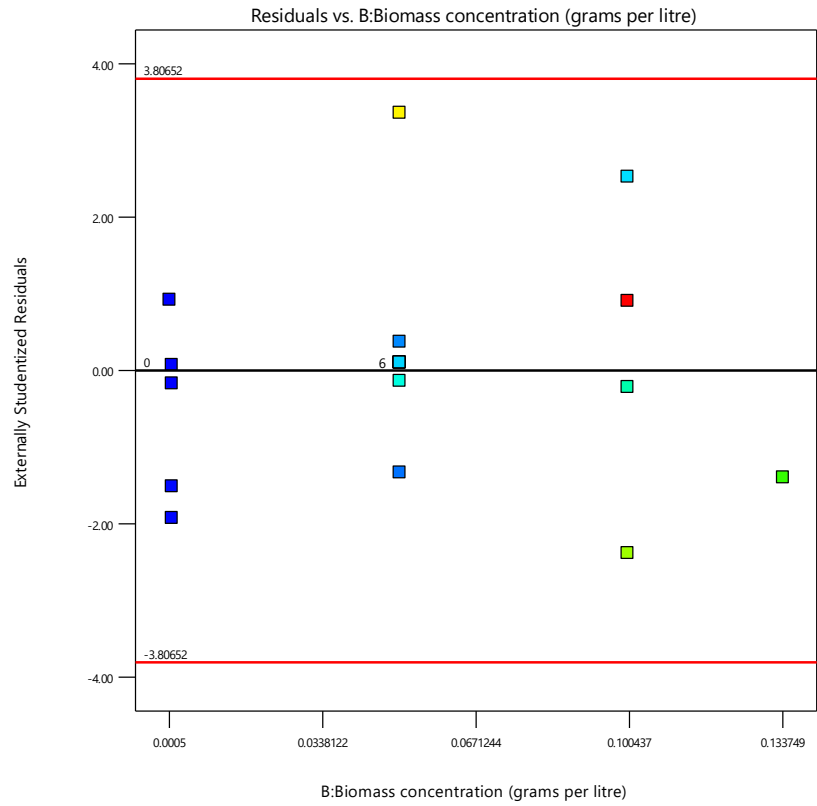


**Figure 4.7: A Graph of Externally Studentized Residuals against Biomass Concentration**

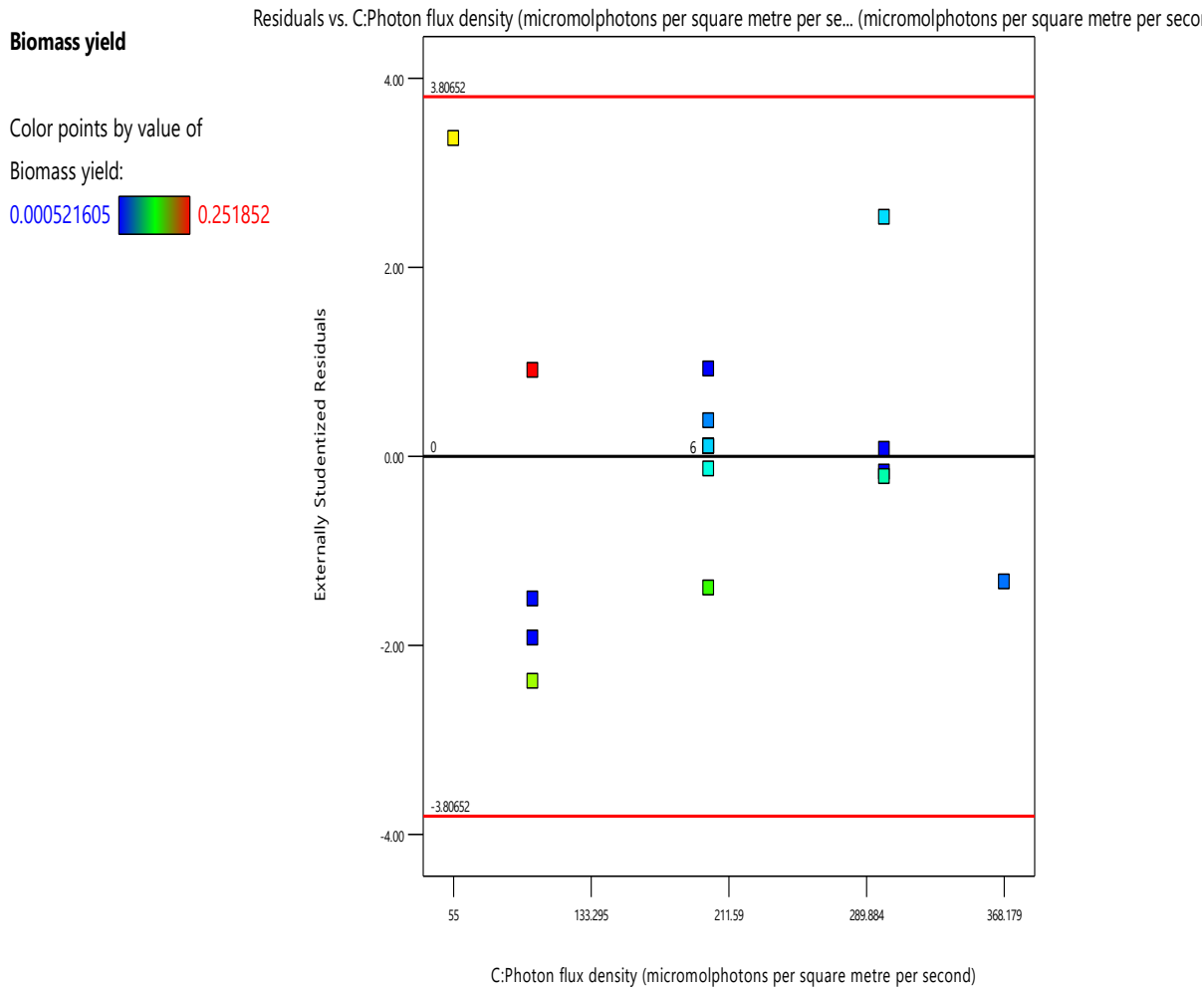


**Figure 4.8: A Graph of Externally Studentized Residuals against Photon Flux Density**

Predicted biomass yield obtained from Equation 4.2 is given in Table 4.10. Equation 4.2 was used to plot response surface plots and contour plots.

**4.2.1.2 Response Surface and Contour Plots**

The diagram of dependent variable response level (microalgae yield) for all the variation of independent variables is shown in Figures 4.9 and 4.10 in contour lines and in Figures 4.11 and 4.12 in 3D. Notice that because the model contains interaction, the contour lines of biomass yield are curves and the response surface is a twisted plane. From Figure 4.9,

it can be observed that the microalgae yield increases with simultaneous increase in biomass concentration and specific growth rate whereas in Figure 4.10 decrease in photon flux density leads to increase in microalgae yield. Figure 4.11 gives a plot for yield as a function of photon flux density and biomass concentration. The optimum lies at a biomass concentration of  $0.1 \text{ gL}^{-1}$  and photon flux density of  $100 \mu\text{mol photons m}^{-2}\text{s}^{-1}$ . Figure 4.12 gives a plot for yield as a function of biomass concentration and growth rate. The observations made in the RSM plots therefore confirm that the simulation values were in good agreement with the predicted values. The optimum lies at a growth rate of  $0.0102 \text{ h}^{-1}$  and biomass concentration of  $0.1 \text{ gL}^{-1}$ . The optimum yield obtained by RSM was  $0.2420 \text{ gmol photons}^{-1}$  whereas the global optimum got by GA was  $0.2507 \text{ gmol photons}^{-1}$ . This was a marginal difference of 3.4%. The results obtained in this study are in agreement with those obtained by Kumar *et al.*, (2015) although the marginal difference was 4.5% and the GA simulated value was higher than the RSM one. The same applies in the present study i.e., the optimum yield obtained by GA is slightly higher than that obtained by RSM. Also, the findings in this study are in agreement with the results of Banerjee *et al.*, (2016). In their study, optimum biomass productivity by GA was  $0.77 \text{ gL}^{-1}$  whereas that by RSM was  $0.75 \text{ gL}^{-1}$ . That is to say a marginal difference of 2.6%.



Factor Coding: Actual

**Biomass yield (gmol per photons)**

● Design Points

0.000521605  0.251852

X1 = A

X2 = B

**Actual Factor**

C = 200

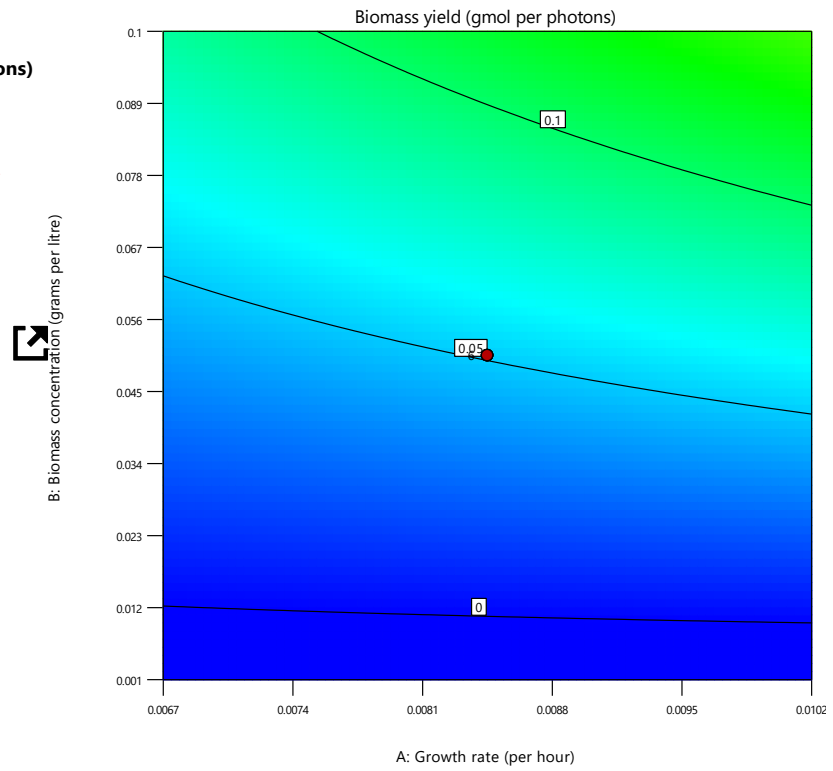


**Figure 4.9: Contour Plot for Biomass Concentration against Growth Rate**

Factor Coding: Actual

**Biomass yield (gmol per photons)**

● Design Points

0.000521605  0.251852

X1 = B

X2 = C

**Actual Factor**

A = 0.00845

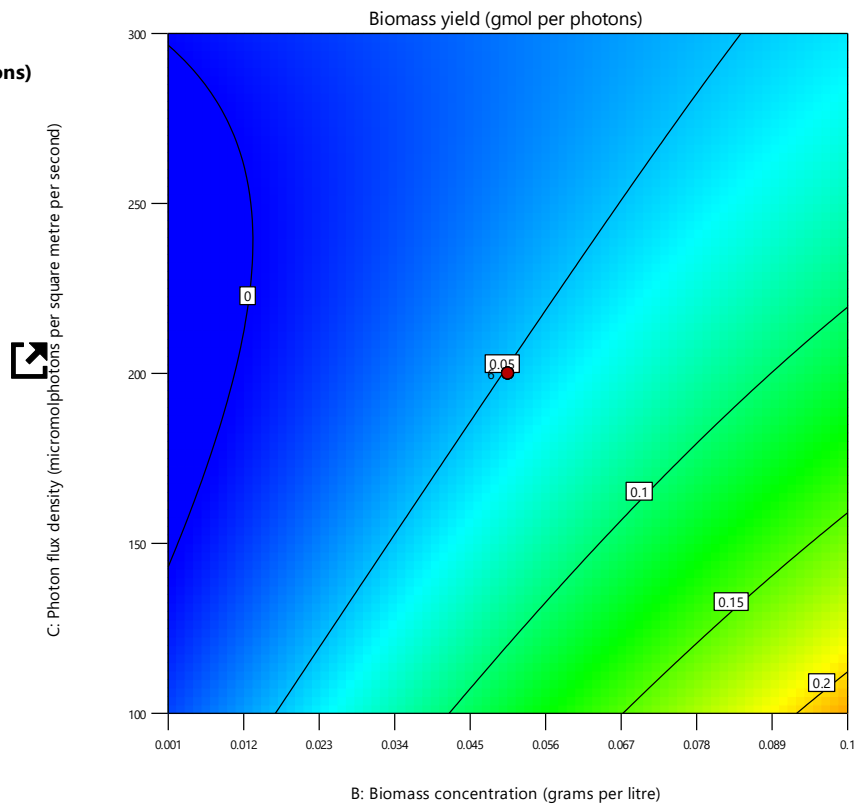


**Figure 4.10: Contour Plot for Photon Flux Density against Biomass Concentration**

Factor Coding: Actual

3D Surface

**Biomass yield (gmol per photons)**

● Design Points

0.000521605  0.251852

X1 = B

X2 = C

**Actual Factor**

A = 0.00845

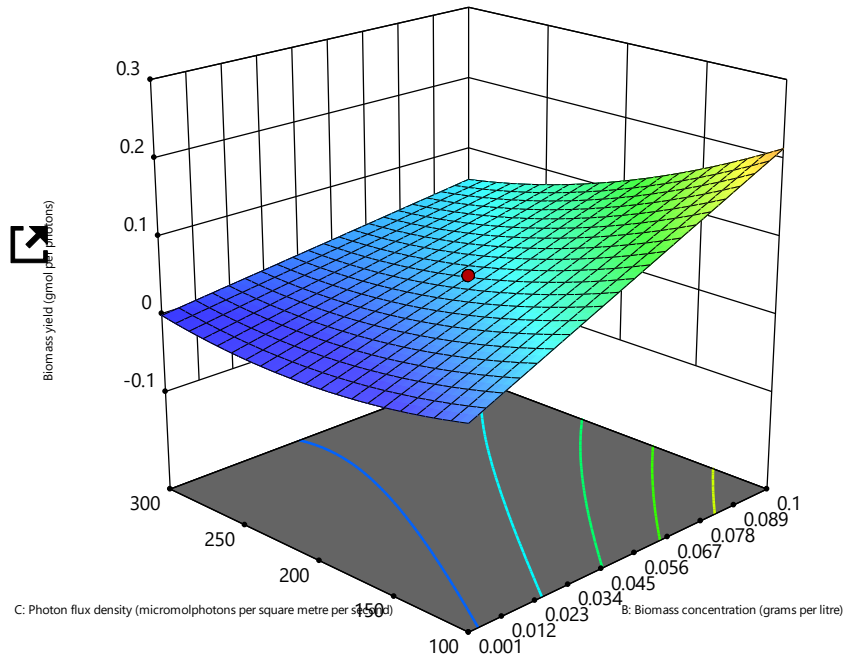


**Figure 4.11: RSM Plot: Effect of Photon Flux Density and Biomass Concentration on Microalgae Yield**

Factor Coding: Actual

3D Surface

**Biomass yield (gmol per photons)**

● Design Points

0.000521605  0.251852

X1 = A

X2 = B

**Actual Factor**

C = 200

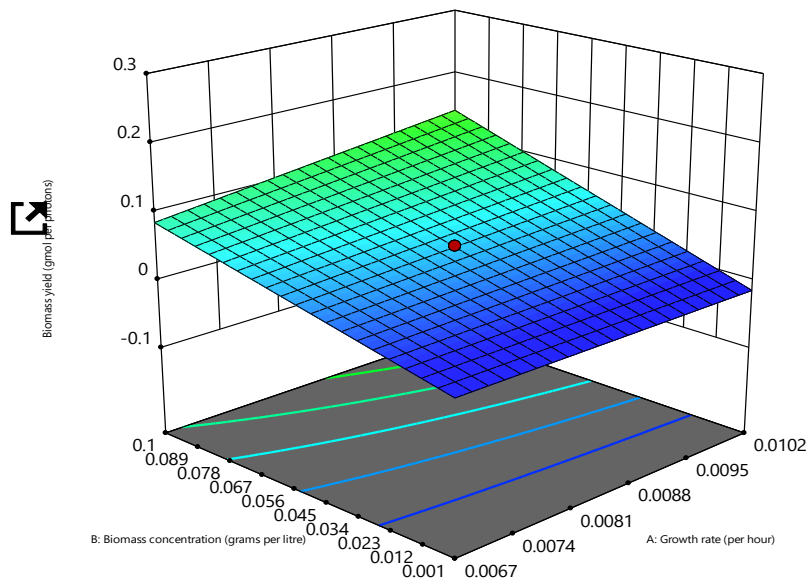


**Figure 4.12: RSM Plot: Effect of Biomass Concentration and Growth Rate on Microalgae Yield**

### 4.3 Isolation and Characterization of Strains of Microalgae

#### 4.3.1 Abiotic Properties of Water Samples Collected

The *insitu* metadata collected for water sample before sampling were temperature and pH. The values were as shown in Table 4.11.

**Table 4.11: Abiotic Properties of Water Samples before Sampling**

Sampling site	GPS coordinate	Temperature (°C)	pH
JKUAT1	1° 5' 38" S 37° 0' 47" E, 1512 m	22.6	7.02
JKUAT2	1° 6' 1" S 37° 0' 50" E, 1518 m	22.6	7.03
JKUAT3	1° 5' 38" S 37° 1' 1" E, 1532 m	22.6	7.03
PARKROAD	1° 16' 22" S 36° 50' 2" E, 1,659 m	23.0	7.05

The sampling sites characterize aquatic environments of temporal and shallow water bodies. The water bodies are shallow with neutral pH and modest temperatures. The shallowness allowed light to infiltrate easily to the bottom of the culture and remain evenly distributed, while the moderate temperature was to avoid overheating which impedes algal growth. Renaud *et al.* (2002) accredited the higher growth rate of *Chaetoceros* sp. to an increase in temperature from 25 to 30 °C. Buck and Smith (1995) and Burja *et al.* (2002) proposed that microalgae can adapt to fluctuating pH conditions, whereas Thornton (2009) reported that the photosynthetic efficiency of some algae decreases as the environment surrounding the cells becomes more acidic. The strains from aquatic environments are expected to be potential starting seed for open system cultivation (Thangavel *et al.*, 2018). The microclimate at these sampling sites regularly varies from conducive (optimal) growth conditions to unconducive conditions (high and low light intensity, high and low temperature, high and low rainfall, and cold, hot, or dry weather). Thus, sampling at these locations was deemed beneficial as the microalgae exposed to unfavorable conditions could accrue more starch or lipid to mitigate the conditions (Thangavel *et al.*, 2018). Thus, the abiotic parameters under which the cultivation is carried out represent an ideal condition that does not have a negative effect on the growth rate of the microalgae.

#### **4.3.2 Isolation**

The isolation protocol by Cappuccino and Sherman (2014) was an efficient method of microalgae isolation and transfer from the natural environment into laboratory conditions. At the same time, the streak plate and serial dilution methods for microalgae enrichment, although slow, proved to be exceptional approaches for the isolation of green phototrophic microorganisms.

At the end of the isolation process (June 2021), 2 slants were produced; each considered to be a different isolate. A representative sample of the isolated microorganisms is shown in Figure 4.13. Microalgae strains were identified using the keys given in (Komarek & Fott, 1983; Hindak, 1988). Morphological comparison of isolated axenic cultures with other described microalgae indicated that these strains belong to the same division,

Chlorophyta. And these strains are, *Chlorella emersonii* (i.e., the oval strain) and *Chlorella vulgaris* (i.e., the round strain), respectively. There was a strain known as filamentous green algae (*Spirogyra* sp.), which could not survive until the end of the isolation process. This could be attributed to decrease in nutrients and fluctuations in pH.

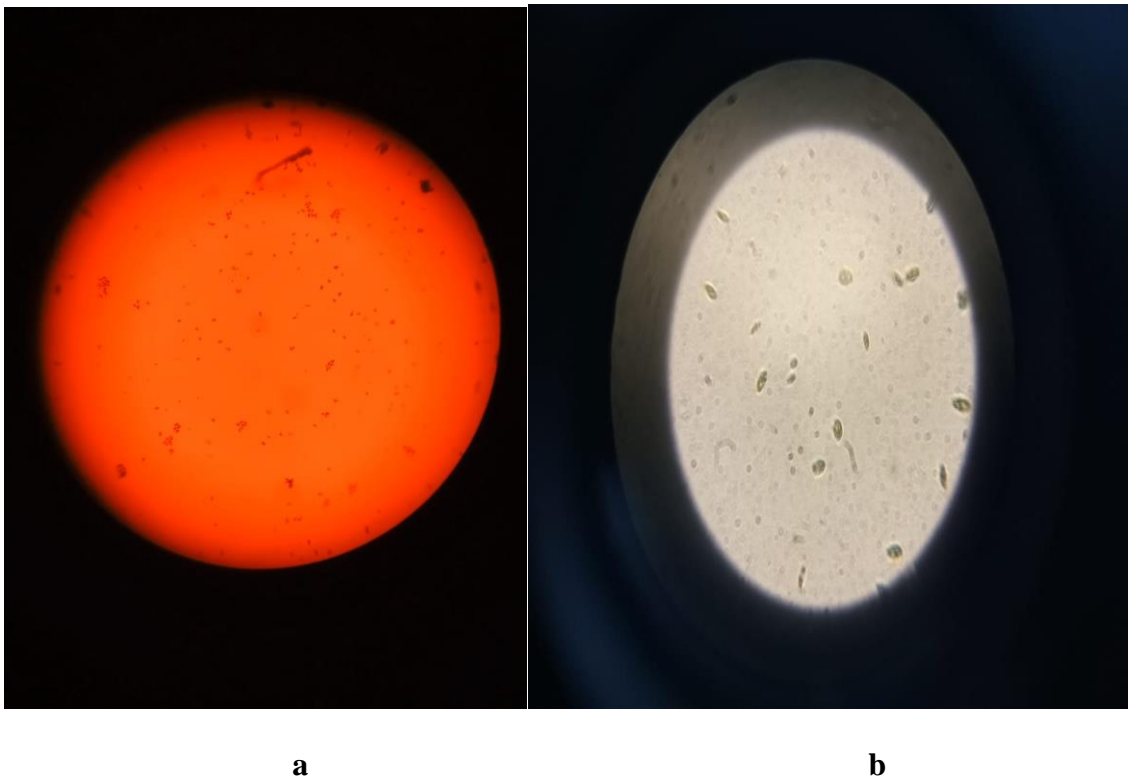


**Figure 4.13: Microscope Images Showing Different Morphologies of the Microalgae Obtained at the End of the Isolation Process (X10-X100)**

**Key:** a) Round one (*C. vulgaris*), b) Oval one (*C. emersonii*)

#### **4.3.3 Comparison of Growth Pattern of Microalgal Isolates**

The microalgal cultures were grown in batch culture for up to 20 days at a temperature of  $26 \pm 1$  °C. This served to ascertain and compare the growth pattern of the isolated strains in terms of; biomass yield, doubling time, and specific growth rate (Thangavel *et al.*,

2018). A typical microbial growth curve, Figure 4.14, showed; the lag, log, stationary and decline phases (Prabuthas *et al.*, 2011).

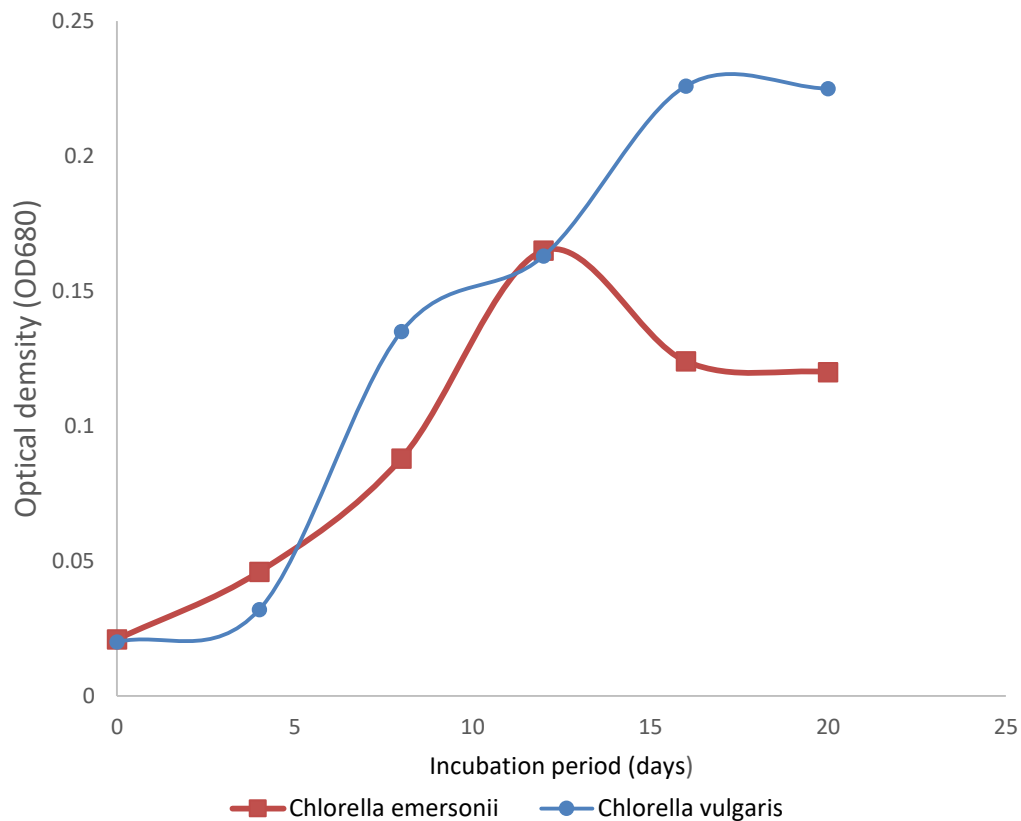


**Figure 4.14: Growth Pattern for Strains: *Chlorella Emersonii* and *Chlorella Vulgaris***

Immediately after the incubation, an exponential growth (log phase) was observed in the oval strain (*Chlorella emersonii*), whereas round strain (*Chlorella vulgaris*) exhibited a lag phase till day 4 when exponential growth commenced. The lag phase may have occurred because microalgae take some times to adapt to the new environmental condition (Rolfe *et al.*, 2012). Normally, an inoculum from a healthy log phase culture exhibits very short lag phase (Thangavel *et al.*, 2018), when transferred into a fresh medium under same growth conditions. Furthermore, the faster adaptability of the *Chlorella emersonii* to a

new environment might be the reason for the absence of lag phase in this culture under study. The exponential growth continued until day 12 for the *Chlorella emersonii* and up to day 16 for the *Chlorella vulgaris*. After day 12, the decline in growth was sharp for the *Chlorella emersonii* whereas for the *Chlorella vulgaris*, the exponential growth continued until around day seventeen when it reached its peak and then stagnated before starting to decline. The decline in growth rate can be attributed to a progressive light limitation by the denser culture, combined with nutrient exhaustion (Mahapatra *et al.*, 2013; Blair *et al.*, 2014). Removing some medium from the photobioreactor and adding the fresh medium may help in regrowth of cyanobacteria and take the peak after some days (Anderson *et al.*, 2016).

The specific growth rate was 0.16 and 0.244 per day (Table 4.12) for the *Chlorella emersonii* and *Chlorella vulgaris* respectively. Therefore, *Chlorella vulgaris* grows almost twice the rate of the *Chlorella emersonii*. The doubling time is 4.30 and 2.84 days respectively, for the *Chlorella emersonii* and *Chlorella vulgaris*. Therefore, *Chlorella vulgaris* accumulates mass faster than *Chlorella emersonii*, about half the time it takes the *Chlorella emersonii* to double its mass.

**Table 4.12: Growth Characteristics of the Microalgal Strains**

Algal strain	Growth rate $\mu$ (day <sup>-1</sup> )	Doubling time (day)	Dry cell weight (20 day old cultures) (gL <sup>-1</sup> )
<i>Chlorella emersonii</i>	0.16±0.000577	4.30±0000	1.1243±0.0073
<i>Chlorella vulgaris</i>	0.244±000000	2.84±0.0000	1.5261±0.0389

Values are presented as Mean ± SD, n=3

The results in Table 4.12, i.e., growth rate, doubling time and dry cell weight, were subjected to Student's *t*-test to determine if there is a significant difference between the results of the two microalgal strains. Results obtained indicate that there was a significant difference in specific growth rate between *Chlorella emersonii* and *Chlorella vulgaris* at  $p < 0.05$ . Therefore, it can be deduced that specific growth rate of microalgae is strain



specific. Moreover, there was significant difference between doubling time and dry cell weight of the two-microalgal strains. Therefore, it can be deduced that doubling time and dry cell weight are tagged to particular strains.

One of the most vital decisions in obtaining biomass and oil from microalgae is the choice of species. Accordingly; both the two purified strains were screened for their mass productivity (Table 4.12). The dry cell weight was  $1.1243 \pm 0.0073$  and  $1.5261 \pm 0.0389 \text{ gL}^{-1}$  respectively, for the *Chlorella emersonii* and *Chlorella vulgaris*. These findings are in agreement with what Mahmoud *et al.* (2015) observed when they screened at laboratory scale *Chlorella vulgaris*, *Scenedesmus quadricauda* and *Trachelomonas oblonga* and obtained 1.23, 1.09 and  $0.9 \text{ gL}^{-1}$  respectively. Also, Thangavel *et al.* (2018) obtained values of between  $1.43 \pm 0.033$  to  $1.55 \pm 0.036 \text{ gL}^{-1}$  for 16 days old cultures when they studied *Chlorella* sp. The doubling time of 2.84 days of *Chlorella* sp. obtained in this study is faster than that obtained by Thangavel *et al.* (2018) of  $4.0 \pm 0.2$  day when studying growth characteristics of the same strain. The increase in doubling time could be attributed to MBL media used in this study, slightly higher temperature of  $26 \text{ }^\circ\text{C}$  and the source of light, i.e., LED tubes instead of fluorescence ones. Hence, the locally isolated autotrophic strains have the potential of biomass production.

#### **4.4 Validation of the Performance of the Developed Computer Simulation Model**

##### **4.4.1 Biomass Yield on Light Energy**

*Chlorella vulgaris* was chosen for model validation because it had a higher growth rate of  $0.244 \text{ day}^{-1}$  and a shorter doubling time of 2.84 days (Table 4.12) compared to the other isolated strain, hence good for microalgae cultivation for biomass and biofuel production.

Table 4.13 shows the yield, both for the experiment and simulation, in grams and in  $\text{gmol photons}^{-1}$  (yield on light energy or photosynthetic efficiency) obtained after incubating *Chlorella vulgaris* in the FPPPBR for 15 days. The microalgal yield obtained on light energy for the experimental run and simulation was  $0.438423 \pm 0.027122$

gmolphotons<sup>-1</sup> and 0.250715±0.001608 gmolphotons<sup>-1</sup> respectively. The corresponding yield in grams is, respectively, 9.30±0.57 and 5.32±0.03. The experimental yield obtained is equal to 20-30% of the theoretical attainable maximum biomass yield on light energy of 1.5 to 1.8 gmolphotons<sup>-1</sup> for growth on nitrate and urea, respectively as calculated in Appendix A1 (Zijffers *et al.*, 2010). The yield on light energy obtained in this study, is almost half of the results obtained by Zijffers *et al.* (2010) of 0.78 and 0.75 gmolphotons<sup>-1</sup> for *Dunaliella tertiolecta* and *Chlorella sorokiniana*, respectively. May be this low yield could be attributed to inadequate mixing and low CO<sub>2</sub> in the air used, since it was atmospheric air.

**Table 4.13: Biomass Yield for the Simulation and Experiment**

	Yield (grams)	Yield (gmolphotons <sup>-1</sup> )
<b>Experimental</b>	9.30±0.57	0.438423±0.027122
<b>Simulation</b>	5.32±0.03	0.250715±0.001608

Values are presented as Mean ± SD, n=3

The yield on light energy of 0.438423±0.027122 gmolphotons<sup>-1</sup> obtained in this study is the same as that achieved by Meiser *et al.* (2004) of maximum yield of 0.5 gmolphotons<sup>-1</sup> for the diatom *Phaeodactylum tricorutum* at a light intensity of 1,000 μmolphotonsm<sup>-2</sup> s<sup>-1</sup>. This low yield could be attributed to high irradiance, since according to the optimization model equation 3.1, when irradiance increases the yield decreases. Furthermore increase in irradiance leads to photoinhibition. The same reasoning applies to Hu *et al.* (1998b) who obtained a yield of 0.5 gmolphotons<sup>-1</sup> cultivating the microalga *Chlorococcum littorale* at a light intensity of 2,000 μmolphotonsm<sup>-2</sup>s<sup>-1</sup>. Richmond *et al.* (2003) obtained a maximum yield of 0.6 gmolphotons<sup>-1</sup> cultivating the microalga *Nannochloropsis* sp. at a light intensity of 2,000 μmolphotonsm<sup>-2</sup>s<sup>-1</sup>. *Monodus subterraneus* showed a maximum yield of 1.0 gmolphotons<sup>-1</sup> (Hu & Richmond, 1996). This productivity was obtained at an increased level of turbulence compared to Meiser *et al.* (2004) and Hu *et al.* (1998b).

Record productivity was obtained during cultivations of the cyanobacterium *Arthrospira platensis* in short light path, 1.3 and 2.8 cm, panel PBRs that were turbulently mixed (Hu & Richmond 1996; Hu *et al.* 1996, 1998a, b). The photosynthetic efficiency exhibited a maximum value of approximately 1.5 g of biomass (dry matter) produced per mole of photons ( $\text{gmolphotons}^{-1}$ ) at incident light intensities of up to  $2,000 \mu\text{molphotons}\cdot\text{m}^{-2}\cdot\text{s}^{-1}$ . This high efficiency was attributed to short exposure times to oversaturating light intensities at the PBR surface due to turbulent mixing. The biomass yield of *Arthrospira platensis* reported by these researchers is close to the theoretical attainable maximum biomass yield on light energy (Appendix A1).

Other researchers (Hu *et al.*, 1996, 1998c; Degen *et al.*, 2001; Richmond & Cheng-Wu 2001; Cuaresma *et al.*, 2009) studied the cultivation of eukaryotic microalgae: *Monodus*, *Chlorococcum*, *Chlorella*, and *Nannochloropsis* in short light path PBRs. Based on the data given, Zijffers *et al.* (2010) estimated the biomass yields for microalgae to be in the range of 0.3 to 1.0  $\text{gmolphotons}^{-1}$ . Therefore, the yield on light energy ( $\text{gmolphotons}^{-1}$ ) obtained in this study augurs well with the findings of other researchers.

The yield obtained in the current study of  $0.438423 \pm 0.027122 \text{ gmolphotons}^{-1}$  differed from the theoretical maximum of 1.5 and 1.8  $\text{gmolphotons}^{-1}$  as calculated in Appendix A1. The difference between the biomass yield and this theoretical maximum could most likely be related to heat dissipation of absorbed light energy in the photosynthetic antenna complex of the microalgae by processes collectively called non-photochemical quenching (Muller *et al.*, 2001; Horton & Ruban, 2005). Furthermore, not attaining the theoretical maximum yield could be explained assuming that a significant fraction of the available light energy is not used for biomass formation but it is used for basic physiological maintenance. These include processes such as; cell motility, osmoregulation, defense mechanisms, and proofreading and internal turnover of macromolecular compounds (van Bodegom, 2007). However, it should be noted that this physiological maintenance term is relatively high in cultures with relatively high biomass concentrations/densities (Zijffers *et al.*, 2010).

#### 4.4.2 Validation of the Optimization Model

In order to validate the model, a comparison of experimental and simulated data for growth of *Chlorella vulgaris* in FPPPBR was done. In order to validate this model, error analyses were carried out on the simulation results using different statistical tools namely RMSE, MSE, MAE and MAPE, as expressed in Equations (3.6–3.9). The results obtained are shown in Table 4.14. The RMSE value for the optimization model was 0.1889, the MSE, MAE and MAPE were 0.0357, 0.2717 and 42.67% respectively. For a good model, the closer the values of MSE, MAE and RSME are to zero, the better and more acceptable is the model (Hyndman & Koehler, 2006; Archontoulis & Miguez, 2015; Ibifubara *et al.*, 2019). The values of RMSE, MSE and MAE for the simulation model were not very small, hence further statistical tests were done to ascertain if the model was valid and was a good predictor of the PBR photosynthetic efficiency.

**Table 4.14: Validation of Model Results**

MSE	RMSE	MAE	MAPE (%)
0.0357	0.1889	0.2717	42.67

**Key:** MSE – Mean Squared Error; RMSE – Root Mean Squared Error; MAE – Mean Absolute Error; MAPE – Mean Absolute Percentage Error.

Further, correlation analysis was done between the experimental and predicted data and the results are as shown in Table 4.15. The model and experimental values have a very low positive coefficient of correlation (R) of 0.231 and two-tailed p-value of 0.852. Although there is a positive correlation between model values and experimental values, the Pearson correlation coefficient between model values and experimental values is statistically insignificant at 5% significance level (R= 0.231, p >0.05). This shows that there is statistical difference between the simulation and experimental values.

**Table 4.15: Correlation Results for the Model and Experimental Values**

	Model values	Experimental values
Model values	1	
Experimental values	0.231	1

\*Correlation is not significant at the 0.05 level (2-tailed),  $p = 0.852$

The model values were further subjected to the student's  $t$ -test and the results in Table 4.16 were obtained. The null hypothesis set was that the mean of the model values was equal to that of the experimental values whereas the alternative hypothesis declared that the two means are not equal.

**Table 4.16: Student's  $t$ -Test Results for Model Values**

One-Sample Test						
Test Value = 0.438423						
	T	Df	Sig. (2-tailed)	Mean Difference	95% Confidence Interval of the Difference	
					Lower	Upper
Model value	-165.091	2	.000	-.187708000	-.19260012	-.18281588

\*Difference is significant at the 0.05 level (2-tailed),  $p = 0.000$

From the results in Table 4.16, the  $t$ -value is -165.091 and the  $p$  value is less than 0.05 i.e.,  $p = 0.000 < 0.05$ . Therefore, since  $p = 0.000$ , the difference in means of the model and experiment is quite significant at 5% significance level, hence the null hypothesis of equality of means between model and experiment values is not accepted. Furthermore, the values of RMSE, MSE and MAE for the simulation model were not very small and coefficient of correlation was not high, and the student's  $t$ -test showed that there was a significant difference between the mean of model and that of the experimental values. Therefore, the model under-predicts the PBR microalgal yield on light (photosynthetic efficiency).

#### 4.4.3 Modification of the Optimization Model

The under-prediction of the yield by the simulation model could be due to the fact that the light that is not utilized in the initial stages when the culture media is dilute was not factored in when the optimization model was being developed (Zijffers *et al.*, 2010). Therefore, the optimization model requires modification for it to predict accurately microalgal yield. After factoring in the unused light when the culture is dilute, and using the experimental yield obtained in the current study of 0.438428 gmolphotons<sup>-1</sup>, a new model was developed (Equation 4.1).

$$Y = \frac{C_x \mu V}{PFD_{in} A \cdot 2070 \times 10^{-6}} \text{ gmolphotons}^{-1} \quad \text{Equation 4.1}$$

where  $Y$  is the microalgal yield ( gmolphotons<sup>-1</sup>)

$\mu$  is the specific growth rate (hour<sup>-1</sup>)

$C_x$  is the biomass concentration (gL<sup>-1</sup>)

$A$  is the illuminated reactor surface area (m<sup>2</sup>)

$PFD_{in}$  is the photon flux density (μmolphotonsm<sup>-2</sup>s<sup>-1</sup>)

$V$  is the volume of the PBR content (L)

#### 4.5 Effect of Light Wavelength and Strain on the Biomass and Lipid Yield of Microalgae

##### 4.5.1 Effect of Light Wavelength and Strain on the Biomass Yield of Microalgae

To investigate the influence of light wavelength and strain on the biomass yield of microalgae, the system was operated as explained in Section 3.4.3.1. The results in Table 4.17 were obtained. *C. vulgaris* yielded; 9.30±0.57 g, 8.32±0.48 g and 7.78±0.67 g under white, blue and red wavelength, respectively. On the other hand, the corresponding values for *C. emersonii* were; 5.88±0.26 g, 5.46±0.20 g and 5.12±0.14 g. For both the strains,

white wavelength produced the highest yield, followed by blue wavelength. The least yield for both strains was produced by the red wavelength.

**Table 4.17: Yield (g) of Microalgae under Different Light Wavelengths**

Strain of microalgae	Light quality		
	White (400-700 nm)	Blue (430-480 nm)	Red (610-680 nm)
<i>C. vulgaris</i>	9.30±0.57	8.32±0.48	7.78±0.67
<i>C. emersonii</i>	5.88±0.26	5.46±0.20	5.12±0.14

Values are presented as Mean ± SD, n=3

#### 4.5.1.1 Growth Profiles of Microalgae in the FPPPBRs

Figures 4.15, 4.16 and 4.17 show the growth patterns of *C. vulgaris* and *C. emersonii* in the FPPPBRs under white wavelength, blue wavelength, and red wavelength, respectively.

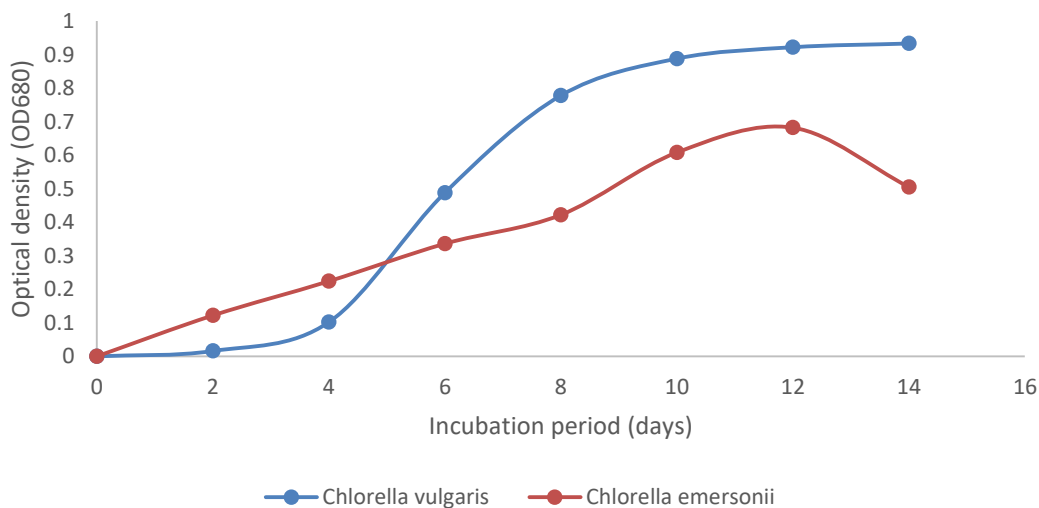


**Figure 4.15: Growth Profile of Microalgae Strains under White Wavelength**

A typical microbial growth curve according to Prabuthas *et al.* (2011), should show; the lag, log, stationary and decline phases. Immediately after the inoculation, an exponential

growth (log phase) was observed in *C. emersonii*, whereas *C. vulgaris* exhibited a lag phase till day 3 when exponential growth commenced. This was the case under all the three wavelengths. The lag phase may have occurred because microalgae take some times to acclimatize to the new environmental condition (Rolfe *et al.*, 2012). Ordinarily, an inoculum from a healthy log phase culture displays very short lag phase (Thangavel *et al.*, 2018), when transferred into a fresh medium under same growth conditions. Furthermore, the faster adaptability of the *C. emersonii* to a new environment might be the reason for the absence of lag phase in this culture under study.

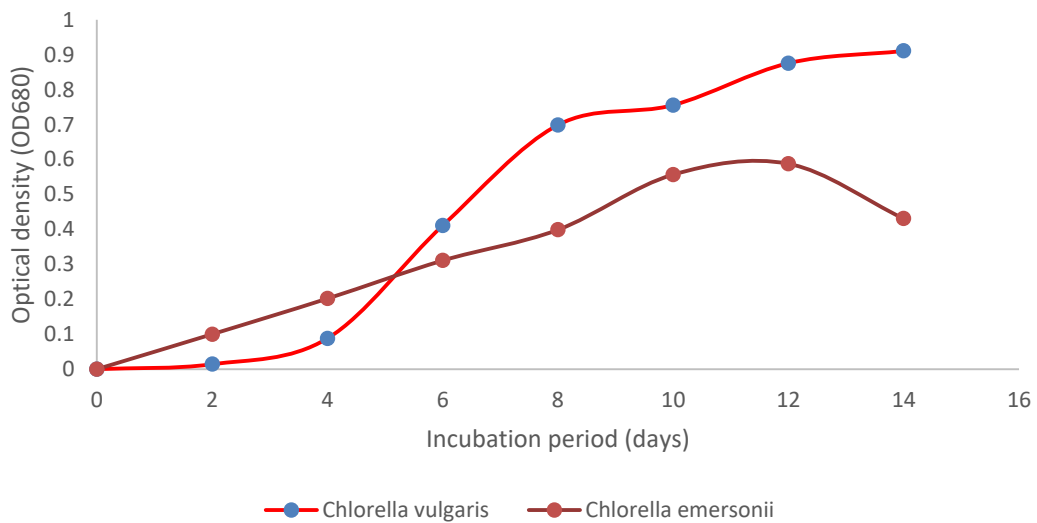


**Figure 4.16: Growth Profile of Microalgae Strains under Blue Wavelength**



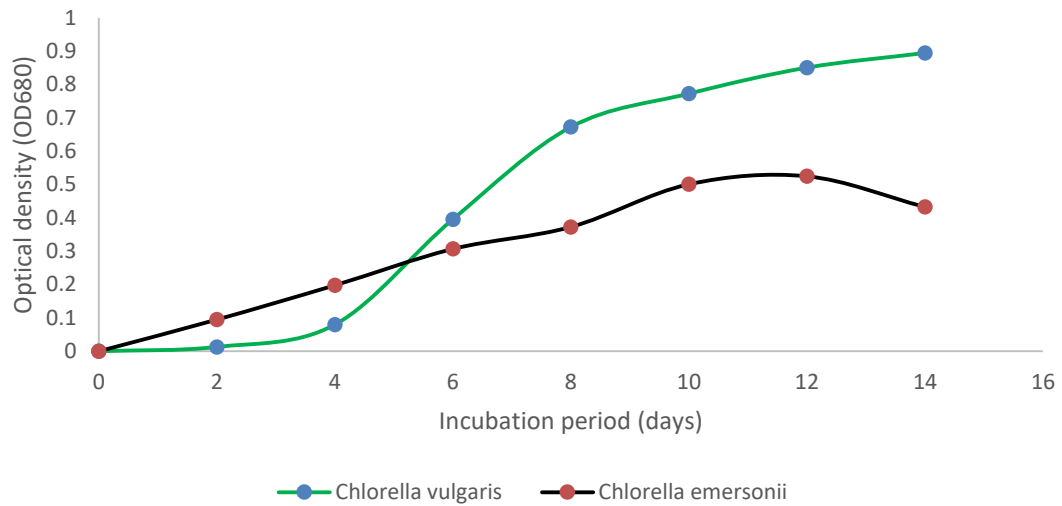


**Figure 4.17: Growth Profile of Microalgae Strains under Red Wavelength**

The exponential growth continued until day 12 for the *C. emersonii* and up to day 10 for the *Chlorella vulgaris* (Figure 4.15). After day 12, the decline in growth was sharp for the *C. emersonii* whereas for the *C. vulgaris*, the stationary phase commenced. The drop in growth rate can be credited to a progressive light limitation by the denser culture, combined with nutrient exhaustion (Mahapatra *et al.*, 2013; Blair *et al.*, 2014). For *C. vulgaris* under blue and red wavelength, by day 14 (Figure 4.16 and 4.17), the stationary phase had not been reached. This implies that the strain was still growing when the process was stopped. This could be attributed to the cultivation conditions favouring its growth.

The mass, nutritional value and growth of microalgae depend on different physico-chemical factors such as CO<sub>2</sub> content, light intensity, temperature, pH, and nutrient composition of culture medium (Sandnes *et al.*, 2005; Patil *et al.*, 2007; Metsoviti *et al.*, 2020). Among them, light intensity is one of the main factors that affect algal physiology and photosynthesis kinetics (Khoeyi *et al.*, 2012). Photoautotrophic algae rely upon light to acquire energy and convert it into synthetic energy such as adenosine triphosphate (ATP) and nicotinamide adenine dinucleotide phosphate (NADP). Photosynthetic light is absorbed via pigments bound chlorophyll and the color of the incident light should match

with the pigment absorption band (Matthijs *et al.*, 1996). Therefore, colors of light quality and quantity demonstrate the energy level in the photosynthetic organisms to carry out their metabolism (Latasa, 1995; Khoeyi *et al.*, 2012). Previous studies suggest that pigment content, proximate composition, and PUFAs content varies in response to different wavelengths of light intensity and color (Brown & Hohmann, 2002; Carvalho & Malcata, 2005; Seyfabadi *et al.*, 2011; Khoeyi *et al.*, 2012). However, the chlorophyll pigments band in microalgae might be obscured by the ordinary fluorescent light source (Matthijs *et al.*, 1996; Seyfabadi *et al.*, 2011; Khoeyi *et al.*, 2012; Wahidin *et al.*, 2013; Metsoviti *et al.*, 2020;). This explains the reason for using LEDs in this study.

Conventionally microalgae are grown under an indoor environmental condition with the presence of direct sunlight or external white light (Devaraja *et al.*, 2017). Some reports mention that at least PAR of  $100 - 276 \mu\text{mol photons.m}^{-2}\text{s}^{-1}$  are needed for proper cultivation of microalgae (Lavens & Sorgeloos, 1996; Alanís, 2013; Atta *et al.*, 2013; Blair *et al.*, 2014; Hultberg *et al.*, 2014) and must be provided to avoid growth inhibition. Many light spectra have a positive influence on microalgal growth (Al-Qasmi *et al.*, 2012). For the cultivation of microalgae, light-emitting diodes (LEDs) have emerged as an appropriate choice with multiple merits over ordinary fluorescence light (Kim & Choi, 2014)). With the advances in LED technology, it can be utilized as suitable light source for indoor mass microalgal cultivation for their specific wavelength, mini chip size, and limited energy consumption as heat (Wang *et al.*, 2007). The LED can efficiently convert electric energy to light energy for the production of microalgae (Pattanaik *et al.*, 2018). It can be used as a promising source of light energy to enhance the economic viability of microalgae-based products. The LED emits monochromatic light with highly saturated colors that is useful for the growth of microalgae (Pattanaik *et al.*, 2018). Green microalgae contain chlorophyll-a and chlorophyll-b (ratio 3:1), which have two identical absorption peaks for blue and red color. Chlorophyll-a absorption peaks are around 430 nm (blue) and 660 nm (red), and chlorophyll-b absorption peaks are 460nm (blue) and 630nm (red) (Devaraja *et al.*, 2017).

According to Max Planck's electromagnetic theory, light, which appears to be in a continuous range of frequencies or wavelengths, is actually emitted in separate packets of energy, called quanta, which can only take on certain discrete values. As such, the energy emitted is inversely proportional to the wavelength of light. This infers that shorter wavelengths have higher energy, whereas longer wavelengths have lower energy per photon (a particle representing a quantum of light). The wavelength of blue light is 470 nm, and that of red light is 660 nm. In effect, a photon of blue light has more energy than one of red light, hence, blue light photons should produce higher microalgal biomass than red light (Ibifubara *et al.*, 2019).

Microalgae absorb different types of wavelength depending on the species (Blair *et al.*, 2014). The intensity of each wavelength of light in this experiment were kept constant at approximately  $100 \mu\text{mol photons}\cdot\text{m}^{-2}\cdot\text{s}^{-1}$  because different light intensities could affect the microalgae cell growth, biomass, lipid production and starch production (Pandey & Tiwari, 2010; Pandey *et al.*, 2011; Blair *et al.*, 2014;). The results obtained indicated that *C. vulgaris* yielded highest biomass under white wavelength ( $9.30\pm 0.57$  g) (Table 4.17) and least biomass ( $7.78\pm 0.67$  g) under red wavelength. On the other hand, *C. emersonii* yielded highest biomass ( $5.88\pm 0.26$  g) under white wavelength and least biomass ( $5.12\pm 0.14$  g) was detected under red wavelength. The results obtained indicated that both the strains grew well with the white illumination. This could be due to the fact that white wavelength has more energy than both blue and red wavelength. Furthermore, of the three wavelengths used, red wavelength has the longest wavelength and hence the least energy. The results obtained in this study on the influence of LED light wavelength on microalgal yield agree with the findings of Puspanadan *et al.* (2018) who found out that microalgae yield was highest under white light followed by blue light. The biomass yield obtained in this study is far much lower than the value obtained by Lam and Lee (2014) of 28 g when they studied cultivation of *Chlorella vulgaris* in 100 L sequential baffled PBR. Therefore, the not so high yield in this study could be due to inadequate CO<sub>2</sub> and mixing.

Mixing can inhibit high-light, free-radical-induced damage by reducing the duration of algal exposure to excessive light. Furthermore, as the microalgae move through the

culture, cells are exposed to fluctuating light that, under certain conditions, could significantly affect photosynthesis (Abu-Ghosh *et al.*, 2015; Abu-Ghosh *et al.*, 2016; Iluz & Abu-Ghosh, 2016; Abu-Ghosh *et al.*, 2018). Mixing also hinders algal sedimentation that causes the settled algae to be in the dark and have no access to nutrients. The settled microalgae thus die and decompose creating a harmful anaerobic layer (Iluz *et al.*, 2008).

Results in Table 4.17 were used for the two-way analysis of variance (ANOVA) with blocking and the findings in Table 4.18 were obtained. From the ANOVA Table 4.18, the differences concerning different light wavelengths are insignificant at 5% level as the calculated F-ratio of 8.521 is less than the table value of 19.00. The biomass yields due to microalgae strain differences are significant as the computed F-ratio of 171.702 is more than the table value of 18.51. This therefore implies that the quality of light used has no significant influence on the amount of biomass yield to be obtained. On the other hand, the strain of microalgae grown has a significant impact on the amount of biomass produced.

**Table 4.18: ANOVA Table for Microalgal Biomass Yield with Blocking**

<b>Source of variation</b>	<b>Sum of squares (SS)</b>	<b>Degrees of freedom (d.f.)</b>	<b>Mean Square (MS)</b>	<b>F-ratio</b>	<b>5% F-limit (Table values)</b>
Between columns (i.e., between lights)	1.322	2	0.661	8.521	F(2,2)= 19.00
Between rows (i.e., between strains)	13.321	1	13.321	171.702	F(1,2)= 18.51
Residual or error	0.155	2	0.077		
<b>Total</b>	<b>14.798</b>	<b>5</b>			

Analysis of variance was also carried out on the biomass yield assuming two factors i.e., light quality and strains of microalgae without blocking, and the results in Table 4.19 were obtained. From the ANOVA Table 4.19, the differences concerning different light wavelengths are significant at 5% level as the calculated F-ratio of 9.822 is more than the table value of 3.88. Also, the microalgae strain differences are significant as the computed

F-ratio of 197.150 is more than the table value of 4.75. Furthermore, interaction between the light quality and the strains is insignificant as the computed F-ratio of 1.227 is less than the table value of 3.88. It can therefore be deduced that when growing microalgae in PBRs, particular strains are not tagged to particular light quality in which they yield best biomass i.e., there is no interaction between strain and light quality as far as microalgae biomass yield is concerned.

**Table 4.19: ANOVA Table for Microalgal Biomass Yield without Blocking**

Source of variation	Sum of squares (SS)	Degrees of freedom (d.f.)	Mean Square (MS)	F-ratio	5% F-limit (Table values)
Between columns (i.e., between lights)	3.988	2	1.994	9.822	F(2,12)=3.88
Between rows (i.e., between strains)	40.021	1	40.021	197.150	F(1,12)=4.75
Interaction	0.498	2	0.249	1.227	F(2,12)=3.88
Within samples or error	2.436	12	0.203		
Total	46.943	17			

#### 4.5.2 Effect of Light Wavelength and Strain on the Lipid Yield of Microalgae

On investigating the influence of light wavelength and strain on the yield of lipids of microalgae, the results obtained are shown in Table 4.20.

**Table 4.20: Lipids (%) Produced by Microalgae under Different Light Wavelengths**

Strain	Light quality		
	400-700 nm (White)	610-680 nm (Red)	430-480 nm (Blue)
<i>C. vulgaris</i>	34.56±3.31	35.87±1.16	43.61±2.23
<i>C. emersonii</i>	28.03±1.60	33.50±1.60	29.80±0.86

Values are presented as Mean  $\pm$  SD, n=3

The *C. vulgaris* produced 43.61, 35.87 and 34.56 % lipids respectively, under blue, red and white wavelengths. On the other hand, *C. emersonii* strain yielded 33.50, 29.80 and 28.03 % lipids under red, blue and white wavelengths, respectively. *C. vulgaris* produced the highest percent lipids of 43.61 under blue wavelength whereas *C. emersonii* produced the highest percent lipids of 33.50 under the red wavelength. Both strains produced the least percent lipids under white wavelength. The values of percent lipids obtained in this study are higher than that obtained by Ren *et al.* (2017) of 23.6% when they grew *Chlorella vulgaris* in a pilot-scale photobioreactor with waste glycerol (i.e., mixotrophic cultivation). The lipid content obtained in this study is lower than that obtained by Park *et al.* (2019) of 60.9 wt% when they were studying photoautotrophic growth of *Nephroselmis* sp. at pilot plant scale in a flat plate/panel PBR under red wavelength. The %lipids obtained in this study is more than double that obtained by Metsoviti *et al.* (2020). The %lipid yield obtained in this study are in agreement with the results of (Manikan *et al.*, 2015; Wen *et al.*, 2016). Arief *et al.* (2009) reported that the content of lipid in microalgae increased with increasing CO<sub>2</sub> concentration. Therefore, the not so high yield of lipid content in this study could be due to inadequate CO<sub>2</sub>, because in this study atmospheric air was used as a source of CO<sub>2</sub> which has 0.03% CO<sub>2</sub>.

Light and temperature are the two most vital factors that affect microalgae biomass productivity. The energy for growing algae is provided by light via photosynthesis. Sufficient light energy must be effectively utilized to achieve higher biomass productivity (Munir *et al.*, 2015). Temperature affects the rates of all chemical reactions related to algal growth and its metabolism (Sandnes *et al.*, 2005). Change in temperature affects the biochemical composition of the cells specifically lipids and proteins. Thus, light and temperature have a significant influence in the metabolism, enzyme activities and cell composition of algae. Algae cultivation also depends on pH levels and optimum pH influences the carbon availability, metabolism and biochemical composition of cells (Richmond, 2000). Furthermore, the effectiveness of the various organic carbons in

supporting cell growth and oil accumulation depends on the strain and other culture conditions (Rodolf *et al.*, 2009; El-Kassas 2013; Eroglu *et al.*, 2015).

A two-way ANOVA with blocking was done to determine if there is a significant difference in percent yields of lipids between lights and between strains and the results in Table 4.21 were obtained.

**Table 4.21: ANOVA Table for Lipid Yield under Different Light Wavelengths with Blocking**

Source of variation	Sum of squares (SS)	Degree of freedom (d.f.)	Mean square (MS)	F-ratio	5% F-limit (Table values)
Between columns (i.e., between lights)	29.8937	2	14.9469	0.8916	F(2, 2)= 19.00
Between rows (i.e., between strains)	85.9573	1	85.9573	5.1272	F(1, 2)= 18.51
Residual or Error	33.5296	2	16.7648		
<b>Total</b>	<b>149.3806</b>	<b>5</b>			

The differences concerning effect of different light wavelengths on lipid yield are insignificant at 5% level as the calculated F-ratio of 0.8916 is less than the table value of 19.00. Also the differences concerning influence of the different strains on lipid yield are not significant at 5% level as the computed F-ratio of 5.1272 is less than the table value of 18.51. Therefore, a logical conclusion is that there is interaction between light quality and strain in relation to yield of microalgae lipids. This therefore implies that the yield of microalgal lipids depends both on microalgal strain and light quality simultaneously and not in isolation on these independent variables.

Analysis of variance was also carried out on the percent lipid yield assuming two factors i.e., light quality and strains of microalgae without blocking, and the results in Table 4.22 were obtained. From the ANOVA Table 4.22, the differences concerning different lights are significant at 5% level as the calculated F-ratio of 11.6089 is more than the table value

of 3.88. Also, the microalgae strain differences are significant as the computed F-ratio of 66.8223 is more than the table value of 4.75. Furthermore, interaction between the light quality and the strains is significant as the computed F-ratio of 128.9870 is more than the table value of 3.88. It can therefore be concluded that when growing microalgae in FPPPBRs, the effect of light quality and the type of strain on the percent lipid yield is significant. Also, there is a significant interaction between light quality and type of strain in affecting the percent lipid yield of microalgae. From these findings, it can be deduced that type of strain and light quality influence lipid yield, hence each microalgae strain should be optimized with light quality. This contradicts the results for biomass yield where there is no interaction between light quality and type of strain in determining biomass yield, thus optimum design of photobioreactors should be based on lipid yield and not on the biomass quantity.

All microalgae contain carbohydrates, proteins, lipids, and nucleic acids in varying proportions. Many microalgae are very rich in lipids, which can be converted into biodiesel. The lipid and fatty acid content of microalgae varies depending on culture conditions. Lipid content in microalgae can exceed 70% by weight of dry biomass (Mata *et al.*, 2010). Lipid content of between 20 and 50% is quite common. However, low lipid



**Table 4.22: ANOVA Table for Lipid Yield under Different Light Wavelengths without Blocking**

Source of variation	Sum of squares (SS)	Degree of freedom (d.f.)	Mean square(MS)	F-ratio	5% F-limit
Between columns (i.e., between lights)	89.5730	2	44.7865	11.6089	F(2,12)=3.88
Between rows (i.e., between strains)	257.7964	1	257.7964	66.8230	F(1,12)=4.75
Interaction	995.2488	2	497.6244	128.9884	F(2,12)=3.88
Within samples (Error)	46.2953	12	3.8579		
Total	1,388.9135	17			

productivity is often associated with high lipid content of microalgae. Lipid productivity is the mass of lipids produced per unit volume of the culture per unit time; it depends on the algal growth rate and the lipid content of the biomass (Chen *et al.*, 2014). Several factors affect the lipid content of microalgae, including light (quality and quantity), temperature, nutrient concentration, O<sub>2</sub>, CO<sub>2</sub>, pH, salinity, and toxic chemicals. Light and temperature are the major cultivation factors that influence overall biomass productivity and biochemical composition of microalgae (Carvalho & Malcata, 2003; Carvalho *et al.*, 2009). The effects of light and temperature are synergistic in nature. Sandnes *et al.* (2005) observed that growth rates of *Nannochloropsis oceanica* increased with higher light intensity at temperatures of up to 28 °C. At low light intensity, the growth rate is less influenced by temperature. Renaud *et al.* (2002) studied the growth and nutritional content of four tropical Australian microalgal species and reported that the optimum temperature for growth was 25–27 °C for *Rhodomonas* sp. and 27– 30 °C for *Prymnesiophyte* NT19, *Cryptomonas* sp., *Chaetoceros* sp., and *Isochrysis* sp. *Chaetoceros* sp. had the highest percentage of lipid when cells were cultured at 25 °C, whereas *Rhodomonas* sp., *Cryptomonas* sp., *Prymnesiophyte* NT19, and *Isochrysis* sp. had significantly higher amounts of lipid at temperatures within the range of 27–30 °C. Therefore, the optimum

lipid content and growth rate of microalgae may vary from species to species (Chen *et al.*, 2014).

From this study, *C. vulgaris* is better than *C. emersonii* in yielding percent lipids because it had higher percent lipids under blue, red and white wavelengths. Furthermore, its growth rate and doubling time were higher than those of *C. emersonii*. When considering light quality, blue wavelength produced the highest percent lipids for *Chlorella* sp. and red wavelength produced the highest percent lipids for the *C. emersonii*. Therefore, *C. vulgaris* absorbs better the blue wavelength compared to the other wavelengths. On the other hand, *C. emersonii* absorbs better the red wavelength compared to the other wavelengths. This could be due to the fact that the pigments bound chlorophyll and the colour of the incident light match with the pigment absorption band (Matthijs *et al.*, 1996; Devaraja *et al.*, 2017).

## CHAPTER FIVE

### CONCLUSIONS AND RECOMMENDATIONS

#### 5.1 Conclusions

1. A computer optimization model to simulate the yield of microalgae in a flat plate photobioreactor was developed and the optimum microalgae yield was found to be  $0.250715 \pm 0.001608$  gmolphotons<sup>-1</sup> and the optimal microalgal cultivation conditions were established by the simulation model to be: biomass concentration 0.1 gL<sup>-1</sup>, microalgae growth rate 0.0102 h<sup>-1</sup>, photon flux density 100  $\mu$ molphotonsm<sup>-2</sup> s<sup>-2</sup>, volume of reactor 192 L and illuminated PBR surface area 2.16 m<sup>2</sup>. Also, RSM could be used to optimize microalgae cultivation conditions.
2. A total of two microalgal strains were isolated and characterized from the samples collected from local aquatic ecosystems. These strains were morphologically identified as *C. emersonii* and *C. vulgaris*, and had specific growth rate of 0.16 and 0.244 day<sup>-1</sup>, and a doubling time of 4.30 and 2.84 days, respectively. *C. vulgaris* has a higher growth rate of 0.244 day<sup>-1</sup> and a shorter doubling time of 2.84 days compared to *C. emersonii*, hence good for microalgae cultivation for biomass and biofuel production.
3. The developed computer optimization model was validated. The simulation and experimental yield was  $0.250715 \pm 0.001608$  (5.32 g) and  $0.438423 \pm 0.027122$  (9.30 g) gmolphotons<sup>-1</sup>, respectively. The RMSE value for the optimization model was 0.1889, the MSE, MAE and MAPE were 0.0357, 0.2717 and 42.67% respectively. The model had coefficient of correlation (R) of 0.231 and student's *t*-test ( $p = 0.000 < 0.05$ ) proved that there was a significant difference between model and experimental values. Thus, the model was underpredicting. The simulation model was modified and a new optimization model developed.

4. *Chlorella vulgaris* yielded;  $9.30\pm 0.57$  g,  $8.32\pm 0.48$  g and  $7.78\pm 0.67$  g under white, blue and red wavelengths, respectively whereas, the corresponding values for the *Chlorella emersonii* were;  $5.88\pm 0.26$  g,  $5.46\pm 0.20$  g and  $5.12\pm 0.14$  g. The quality of light used has no significant influence on the amount of biomass yield to be obtained, but, the strain of microalgae grown has. *Chlorella vulgaris* produced 43.61, 35.87 and 34.56 % lipids respectively, under blue, red and white wavelengths. On the other hand, *Chlorella emersonii* yielded 33.50, 29.80 and 28.03 % lipids under red, blue and white wavelengths, respectively. There is interaction between light quality and strain in relation to yield of microalgae lipids.

## 5.2 Recommendations

### 5.2.1 Recommendations from the Study

1. Genetic Algorithm and Response Surface Methodology can be used to optimize microalgae cultivation conditions.
2. *Chlorella vulgaris* should be cultivated for biomass and biofuel production.
3. The developed simulation model should be used to optimize microalgae cultivation conditions.
4. *Chlorella vulgaris* should be grown under blue wavelength whereas *chlorella emersonii* should be grown under red wavelength in order to yield high lipids.
5. If interested in biomass only, then the microalgae should be grown under white wavelength.

### 5.2.2 Recommendations for Further Studies

1. Phylogenetic identification should be done to identify the molecular identity of the two strains isolated.
2. Isolation and characterization of samples from local aquatic ecosystems using multi media/recipes should be explored.

3. An energy balance should be carried out to determine the amount of energy required to produce 1 kg of microalgal biomass and 1 kg of lipids.
4. Explore various methods of enhancing circulation and minimizing dead zones in the flat plate perspex photobioreactor.
5. The impact of other photoperiods like 16:8 and 14:10 on biomass and lipid yields at pilot scale, should be investigated.
6. Other metabolic pathways, like heterotrophic and mixotrophic, of growing microalgae in flat plate perspex photobioreactor should be investigated.
7. The impact of inoculum size (volume) on the microalgae yield should be investigated.
8. Investigations should be carried out on the impact of enriched air with CO<sub>2</sub> on biomass and lipids yield.

## REFERENCES

- ABCAM (2013). Fluorescence activated cell sorting of live cells. <http://www.abcam.com/index.html?pageconfig=resource&rid=12803>.
- Abomohra, A.E., Wenbiao, J., Renjie, T., Hans, S., Eid, M., & Eladel, H. (2016). Microalgal biomass production as a sustainable feedstock for biodiesel: Current status and perspectives. *Renewable and Sustainable Energy Reviews*, *64*, 596-606.
- Abubakar, L.U., Mutie, A.M., Kenya, E.U., & Muhoho, A. (2012). Characterization of algae oil (oilgae) and its potential as biofuel in Kenya. *Journal of Applied Hytotechnology in Environmental Sanitation*, *1*(4), 147 - 153.
- Abu-Ghosh, S., Dubinsky, Z., Banet, G., & Iluz, D. (2018). Optimizing photon dose and frequency to enhance lipid productivity of thermophilic algae for biofuel production. *Bioresource Technology*, *260*, 374–379.
- Abu-Ghosh, S., Fixler, D., Dubinsky, Z., & Iluz, D. (2016). Flashing light in microalgae biotechnology. *Bioresource Technology*, *203*, 357–363.
- Abu-Ghosh, S., Fixler, D., Dubinsky, Z., & Iluz, D. (2015). Continuous background light significantly increases flashing-light enhancement of photosynthesis and growth of microalgae. *Bioresource Technology*, *187*, 144–148.
- Acien, F.G., Fernandez, J.M., Morgan, J.J., & Molina, E. (2012). Production cost of a real microalgae production plant and strategies to reduce it. *Biotechnology Advances*, *30*(6), 1344-1353.
- Ahmad, A. L., Yasin, N.H.M., Derek, C.J.C., & J. K. Lim, J.K. (2011). Microalgae as a sustainable energy source for biodiesel production: A review. *Renewable and Sustainable Energy Reviews*, *15*(1), 584-593.

- Ahuja, D., & Tatsutani, M. (2009). Sustainable energy for Developing Countries. *Surveys and perspectives integrating environment and society*, 21(1). Retrieved from <https://journals.openedition.org/sapiens/823>.
- Aitken, D., & Antizar-Ladislao, B. (2012). Achieving a green solution: Limitations and focus points for sustainable algal fuels. *Energies*, 5, 1613-1647.
- Akter, K., Hossain, A., Islam, M.R., Hossain, M.A., M. Das, M.M. Rahman, Abdel-Tawwab, M. (2021). Effects of spirulina (*Arthrospira platensis*) as a fishmeal replacer in practical diets on growth performance, proximate composition, and amino acids profile of pabda catfish (*Ompok pabda*). *Journal of Applied Aquaculture*, 33(2), 1-14.
- Alanís, P.A.L. (2013). Isolation, characterization and identification of microalgae from the Red Sea. (Master's thesis). King Abdullah University of Science and Technology, Thuwal, Kingdom of Saudi Arabia.
- Al-Qasbi, M., Raut, N., Talebi, S., Al-Rajhi, S., & Al-Barwani, T. (2012). A review of effect of light on microalgae growth. *Proc. Int. Conf. Eng.*, 1(4), 608-610.
- Alvarez, A.L., Weyers, S.L., Goemann, H.M., Peyton, B.M., & Gardner, R.D. (2021). Microalgae, soil and plants: A critical review of microalgae as renewable resources for agriculture. *Algal Research*, 54, 102200.
- Andersen, R.A. (2005). Algal culturing techniques. San Diego: Elsevier Academic Press.
- Anderson, G. A., Katuwal, S., Kommareddy, A., & Gent, S. (2016). Operation of a porous membrane photobioreactor. In ASME 2016 10th International Conference on Energy Sustainability collocated with ASME 2016 Power Conference and the ASME 2016 14th International Conference on Fuel Cell Science, Engineering and Technology. American Society of Mechanical Engineers.

- Andrade, M.R., & Costa, J.A.V. (2007). Mixotrophic cultivation of microalga *Spirulina platensis* using molasses as organic substrate. *Aquaculture*, 264, 130-134.
- Archontoulis, S.V., & Miguez, F.E. (2015). Nonlinear regression models and applications in agricultural research. *Agronomy Journal*, 107, 786–798.
- Arragon, V.T. (2014). Development of an effective process model for algae growth in photobioreactors (Master's thesis). Delft University of Technology, Netherlands.
- Atiqullah, M., & Rao, S.S. (1995). Parallel processing in optimal structural design using simulated annealing. *American Institute of Aeronautics and Astronautics Journal*, 33, 2386–2392.
- Atta, M., Idris, A., Bukhari, A., & Wahidin, S. (2013). Intensity of blue LED light: A potential stimulus for biomass and lipid content in fresh water microalgae *Chlorella vulgaris*. *Bioresource Technology*, 148, 373-378.
- Azaman, S.N.A., Nagao, N., Yusoff, F.M., Tan, S.W., & S.K. Yeap, S.K. (2017). A comparison of the morphological and biochemical characteristics of *Chlorella sorokiniana* and *Chlorella zofingiensis* cultured under photoautotrophic and mixotrophic conditions. *PeerJ*, 5, e3473.
- Bakirtzis, A.G., Bikas, P.N., Zoumas, C.E., & Petridis, V. (2002). Optimal power flow by enhanced genetic algorithm. *IEEE Transactions on Power Systems*, 17(2), 229-236.
- Banerjee, A., Guria, C., & Maiti, S.K. (2016). Fertilizer assisted optimal cultivation of microalgae using response surface method and genetic algorithm for biofuel feedstock. *Energy*, 115, 1272-1290.
- Becker, E.W. (1994). *Microalgae: Biotechnology and microbiology*. Cambridge University Press, England.



- Behera, S., Singh, R., Arora, R., Sharma, N. K., Shukla, M., & Kumar, S. (2015). Scope of algae as third generation biofuels. *Frontiers in Bioengineering and Biotechnology*, 2, 90. doi: 10.3389/fbioe.2014.00090.
- Benemann, J., Koopman, B., Wieissman, J., Eisenberg, D., & Goebel, R. (1980). *Development of microalgae harvesting and high-rate pond technologies in California*. Amsterdam, The Netherlands: Elsevier/North-Holland Biomedical Press.
- Ben-Iwo, J., Manovic, V., & Longhurst, P. (2016). Biomass resources and biofuels potential for the production of transportation fuels in Nigeria. *Renewable and Sustainable Energy Reviews*, 63, 172–192.
- Berke, L & Hajela, P. (1992). Applications of artificial neural nets in structural mechanics. *Structural Optimization*, 4, 90–98.
- Bhatnagar, A., Chinnasamy, S., Singh, M., & Das, K.C. (2011). Renewable biomass production by mixotrophic algae in the presence of various carbon sources and wastewaters. *Applied Energy*, 88, 3425-3431.
- Bilad, M.R., Discart, V., Vandamme, D., Foubert, I., Muylaert, K., & Vankelecom, I.F.J. (2012). Simultaneous cultivation and pre-harvesting of microalgae in lab-scale membrane photobioreactor (MPBR). *Procedia Engineering*, 44, 712-713
- Biosciences, B. (2000). Introduction to flow cytometry: A learning guide. Manual Part, (11-11032):01.
- Black, J. G. (2008). *Microbiology: Principles and explorations*. Wiley.
- Blair, M. F., Kokabian, B., & Gude, V. G. (2014). Light and growth medium effect on *Chlorella vulgaris* biomass production. *Journal of Environmental Chemical Engineering*, 2, 665-674.

- Bligh, E.G., & Dyer, W.J. (1959). A rapid method of total lipid extraction and purification. *Canadian Journal of Biochemistry and Physiology*, 37, 911–917.
- Bonner, W., Hulett, H., Sweet, R., & Herzenberg, L. (1972). Fluorescence activated cell sorting. *Review of Scientific Instruments*, 43(3), 404–409.
- Brennan, L., & Owende, P. (2010). Biofuels from microalgae – A review of technologies for production, processing, and extractions of biofuels and co-products. *Renewable and Sustainable Energy Reviews*, 14, 557-577.
- Brown, M.R., & Hohmann, S. (2002). Effects of irradiance and growth phase on the ascorbic acid content of *Isochrysis* sp. T. ISO (Prymnesiophyta). *Journal of Applied Phycology*, 14(3), 211-214.
- Buck, D.P. & Smith, G.D. (1995). Evidence for a Na<sup>+</sup>/H<sup>+</sup> electrogenic antiporter in an alkaliphilic cyanobacterium *synechocystis*. *FEMS Microbiology Letters*, 128, 315–320.
- Burja, A.M., Abou-Mansour, E., Banaigs, B., Wright, P.C., Burgess, J.G., & Payri, C. (2002). Culture of marine cyanobacterium, *Lyngbya majuscula* (Oscillatoriaceae), for bioprocess intensified production of cyclic and linear lipopeptides. *Journal of Microbiological Methods*, 48, 207–219.
- Cappuccino, J.G., & Sherman, N. (2014). *Microbiology: A laboratory manual*, (10<sup>th</sup> ed.). Menlo Park, CA: Benjamin/Cummings.
- Carvalho, A.P., & Malcata, F.X. (2003). Kinetic modeling of the autotrophic growth of *Pavlova lutheri*: Study of the combined influence of light and temperature. *Biotechnology Progress*, 19, 1128–1135.

- Carvalho, A.P., & Malcata, F.X. (2005). Optimization of  $\omega$ -3 fatty acid production by microalgae: Crossover effects of CO<sub>2</sub> and light intensity under batch and continuous cultivation modes. *Marine Biotechnology*, 7(4), 381-388.
- Carvalho, A.P., Meireles, L.A., & Malcata, F.X. (2006). Microalgal reactors: A review of enclosed system designs and performances. *Biotechnology Progress*, 22(6), 1490-506.
- Carvalho, A.P., Cristina, M., Monteiro, F., & Malcata, X. (2009). Simultaneous effect of irradiance and temperature on biochemical composition of the microalga *Pavlova lutheri*. *Journal of Applied Phycology*, 21, 543–552.
- Chen, F. (1996). High cell density culture of microalgae in heterotrophic growth. *Trends Biotechnology*, 14, 421-426.
- Chen, C.Y., Yeh, K.L., Aisyah, R., Lee, D.J., & Chang, J.S. (2010). Cultivation, photobioreactor design and harvesting of microalgae for biodiesel production: A critical review. *Bioresource Technology*, 102, 71–81.
- Chen, J.J., Wong, S.L., Li, Y.R., Lai, W.L., & Liao, S.W. (2014). Optimization of microalgae cell conditions for lipid production. *Energy Sources, Part A: Recovery, Utilization, and Environmental Effects*, 36(14), 1596-1603.
- Cheng, L.H., Zhang, L., Chen, H.L., & Gao, C.J. (2006). Carbon dioxide removal from air by microalgae cultured in a membrane-photobioreactor. *Separation and Purification Technology*, 50, 324-329.
- Cheng, J.J. (2010). Advanced biofuel technologies: Status and barriers. Development Research Group. The World Bank.

- Cherng-Yuan, L., & Yi-Wei, L. (2012). Fuel characteristics of biodiesel produced from a high-acid oil from soybean soapstock by supercritical-methanol transesterification. *Energies*, *5*, 2370-2380.
- Chisti, Y. (2007). Biodiesel from microalgae. *Biotechnology Advances*, *25*, 294-306.
- Chisti, Y. (2008). Biodiesel from microalgae beats bioethanol. *Trends in Biotechnology*, *26*, 126–131.
- Chojnacka, K., & Noworyta, A. (2004). Evaluation of *Spirulina sp.* growth in photoautotrophic, heterotrophic and mixotrophic cultures. *Enzyme and Microbial Technology*, *34*, 461-465.
- Christenson, L., & Sims, R. (2011). Production and harvesting of microalgae for wastewater treatment, biofuels, and bioproducts. *Biotechnology Advances*, *29*, 686–702.
- Colorni, A., Dorigo, M., & Maniezzo, V. (1992). Distributed optimization by ant colonies, In *Proceedings of the First European Conference on Artificial Life*, F. J. Varela and P. Bourguin, Eds., MIT Press, Cambridge, 134–142.
- Cuaresma, M., Janssen, M., Vilchez, C., & Wijffels, R.H. (2009). Productivity of *Chlorella sorokiniana* in a short light-path (SLP) panel photobioreactor under high irradiance. *Biotechnology and Bioengineering*, *104*, 352–359.
- Darzins, A. (2008). Recent and Current Research & Roadmapping Activities: Overview. National Algal Biofuels Technology Roadmap Workshop, University of Maryland, December 9,
- Divakaran, R., & Pillai, V.N.S. (2002). Flocculation of algae using chitosan. *Journal of Applied Phycology*, *14*, 419–422.

- De Bhowmick, G., Subramanian, G., Mishra, S., & Sen, R. (2014). Raceway pond cultivation of a marine microalga of Indian origin for biomass and lipid production: A case study. *Algal Research*, 6, 201–209.
- Degen, J., Uebele, A., Retze, A., Schmid-Staiger, U., & Trosch, W. (2001). A novel airlift photobioreactor with baffles for improved light utilization through the flashing light effect. *Journal of Biotechnology*, 92, 89–94.
- De Godos, L., Gonzalez, C., Becares, E., Garcia-Encina, P.A., & Munoz, R. (2009). Simultaneous nutrients and carbon removal during pretreated swine slurry degradation in a tubular biofilm photobioreactor. *Applied Microbiology and Biotechnology*, 82, 187–194.
- Del Río, E., Armendáriz, A., García-Gómez, E., García-González, M., & Guerrero, M.G. (2015). Continuous culture methodology for the screening of microalgae for oil. *Journal of Biotechnology*, 195, 103-107.
- Demirbas, A. (2008). Biofuels Sources, Biofuel Policy, Biofuel Economy and Global Biofuel Projections. *Energy Conversion and Management*, 49, 2106-2116.
- Demirbas A. (2009). Progress and recent trends in biodiesel fuels. *Energy Conversion Management*, 50, 14 - 34.
- Demirbas, A. (2010). Microalgae as a feedstock for biodiesel. *Energy Education Science and Technology*, 25, 31–43.
- Devaraja, S., Bharath, M., Deepak, K., Suganya, B., Vishal, B.S., Swaminathan, D., & Meyyappan, N. (2017). Studies on the effect of red, blue and white LED lights on the productivity of *Chlorella vulgaris* to treat dye industry effluent. *Advances in Biotechnology and Microbiology*, 6(2), 27-32.

- Dhingra, A.K., Rao, S.S., & Kumar, V. (1992). Nonlinear membership functions in the fuzzy optimization of mechanical and structural systems, *American Institute of Aeronautics and Astronautics Journal*, 30(1), 251–260.
- Donovan, J., & Stowe, N. (2009). Is the future of biofuels in algae? Renewable EnergyWorld.com/rea/news/article/2009/06/is-the-future-of-biofuels-in-algae.
- Dorigo, M., Maniezzo, V., & Coloni, A. (1996). The ant system optimization by a colony of cooperating agents, *Institute of Electrical and Electronics Engineers Transactions on Systems, Man, and Cybernetics—Part B*, 26(1), 29–41.
- Doucha, J., & Lívansky, K. (2012). Production of high-density *Chlorella* culture grown in fermenters. *Journal of Applied Phycology*, 24, 35-43.
- Duboc, P., Marison, I., & Von Stockar, U. (1999). *Handbook of thermal analysis and calorimetry*. Elsevier, Amsterdam.
- Dutta, K., Daverey, A., & Lin, J.G. (2014). Evolution retrospective for alternative fuels: First to fourth generation. *Renewable Energy*, 69(Supplement C), 114-122.
- Duong, V.T., Li, Y., Nowak, E., & Schenk, P.M. (2012). Microalgae isolation and selection for prospective biodiesel production. *Energies*, 5, 1835-1849.
- Edmundson, S. J., & Huesemann, M. H. (2015). The dark side of algae cultivation: Characterizing night biomass loss in three photosynthetic algae, *Chlorella sorokiniana*, *Nannochloropsis salina* and *Picochlorum* sp. *Algal Research*, 12, 470–476.
- El-Kassas, H.Y. (2013). Growth and fatty acid profile of the marine microalga *Picochlorum* sp. grown under nutrient stress conditions. *Egyptian Journal of Aquatic Research*, 39(4), 233–239.

Engineering Statistics Handbook, Chapter 5. Retrieved from <http://www.itl.nist.gov/div898/handbook/pri/section1/pri1.htm>

Eroglu, E., Smith, S.M., & Raston, C. (2015). Application of various immobilization techniques for algal bioprocesses, In N. Moheimani, M. McHenry, K. de Boer, & P. Bahri (Eds.), *Biomass and biofuels from microalgae: Advances in engineering and biology* (pp. 19-44). Cham: Springer.

Fonseca, L., & Carvalho, F. (2019). The Reporting of SDGs by Quality, Environmental, and Occupational Health and Safety-Certified Organizations. *Sustainability, 11*, 5797.

Fonseca, L., Domingues, J., & Dima, A. (2020). Mapping the Sustainable Development Goals relationships. *Sustainability, 12*, 3359.

Francisco, É.C., Neves, D.B., Jacob-Lopes, E., & Franco, T.T. (2010). Microalgae as feedstock for biodiesel production: Carbon dioxide sequestration, lipid production and biofuel quality. *Journal of Chemical Technology and Biotechnology, 85*(3), 395-403.

Garbowski, T., Pietryka, M., Pulikowski, K., & Richter, D. (2020). The use of a natural substrate for immobilization of microalgae cultivated in wastewater. *Scientific Reports, 10*(1), 1-9.

Georgianna, D.R., & Mayfield, S.R. (2012). Exploiting diversity and synthetic biology for the production of algal biofuels. *Nature, 488*, 329-35.

Gheewala, S., Damien B., & Shi, X. (2013). Biofuels: Economic, Environmental and Social Benefits, and Costs for Developing Countries in Asia. *Wiley Interdisciplinary Reviews: Climate Change* (Q1), *4*(6), 497-511.

- Gilio, L., & Moraes, M. (2016). Sugarcane industry's socioeconomic impact in Sao Paulo, Brazil: A spatial dynamic panel approach. *Energy Economics*, 58, 27–37.
- Giwa, S., Abdullah, L.C., & Adam, N.M. (2010). Investigating “egusi” (*Citrullus colcyntis* L.) seed oil as potential biodiesel feedstock. *Energies*, 3, 607-618.
- Gordon, J.M. (2002). Tailoring optical systems to optimized photobioreactors. *International Journal of Hydrogen Energy*, 27, 1175–1184.
- Golueke, C.G., & Oswald, W.J. (1963). Power from solar energy-via algae-produced methane. *Solar Energy*, 7, 86–92.
- Golueke, C.G., & Oswald, W.J. (1965). Harvesting and processing sewage-grown planktonic algae. *Water Pollution Control Federation*, 37(4), 471-498.
- Gutzeit, G., Lorch, D., Weber, A., Engels, M., & Neis, U. (2005). Biofloculent algal-bacterial biomass improves low-cost wastewater treatment. *Water Science and Technology*, 52, 9–18.
- Greenwell, H.C., Laurens, L.M.L., Shields, R.J., Lovitt, R. W., & Flynn, K.J. (2010). Placing microalgae on the biofuels priority list: A review of the technological challenges. *Journal of the Royal Society Interface*, 7, 703-726.
- Grima, E.M., Belarbi, E.H., Fernandez, F.G.A., Medina, A.R., & Chisti, Y. (2003). Recovery of microalgal biomass and metabolites: Process options and economics. *Biotechnology Advances*, 20, 491-515.
- Grobbelaar, J.U. (2010). Microalgal biomass production: Challenges and realities. *Photosynthesis Research*, 106, 135–144.
- Grobbelaar, J. U. (2013). Mass production of microalgae at optimal photosynthetic rates. In D. Dubinsky (Ed.), *Photosynthesis* (pp. 357–371). Croatia: INTECH.



- Haggkvist, K., Andersson, C., & Taesler, R. (2012). Numerical simulation of fluid flow and heat/mass transfer processes. *Swedish Meteorological and Hydrological Institute, 18*, 122.
- Hamzacebi, C. (2008). Improving artificial neural networks performance in seasonal time series forecasting. *Information Sciences, 178*(23), 4550–4559
- Heredia-Arroyo, T., Wei, W., Ruan, R., & Hu, B. (2011). Mixotrophic cultivation of *Chlorella vulgaris* and its potential application for the oil accumulation from non-sugar materials. *Biomass Bioenergy, 35*, 2245-2253.
- Hindak, F. (1988). *Studies on the Chlorococcales, Algae (Chlorophyceae), IV, Slovak Academy of Science*. Bratislava: VEDA publishing house.
- Hoekman, S.K., Broch, A., Robbins, C., Cenicerros, E., & Natarajan, M. (2012). Review of biodiesel composition, properties, and specifications. *Renewable and Sustainable Energy Reviews, 16*, 143–169.
- Höök, M., & Tang, X. (2013). Depletion of fossil fuels and anthropogenic climate change: A review. *Energy Policy, 52*, 797-809.
- Horton, P., & Ruban, A. (2005). Molecular design of the photosystem II light-harvesting antenna: Photosynthesis and photoprotection. *Journal of Experimental Botany, 56*(411), 365–373.
- Hu, Q., & Richmond, A. (1996). Productivity and photosynthetic efficiency of *Spirulina platensis* as affected by light intensity, algal density and rate of mixing in a flat plate photobioreactor. *Journal of Applied Phycology, 8*, 139–145.
- Hu, Q., Guterman, H., & Richmond, A. (1996). A flat inclined modular photobioreactor for outdoor mass cultivation of photoautotrophs. *Biotechnology and Bioengineering, 51*, 51–60.

- Hu, Q., Faiman, D., & Richmond, A. (1998a). Optimal tilt angles of enclosed reactors for growing photoautotrophic microorganisms outdoors. *Journal of Fermentation and Bioengineering*, 85, 230–236.
- Hu, Q., Zarmi, Y., & Richmond, A. (1998b) Combined effects of light intensity, light-path and culture density on output rate of *Spirulina platensis* (Cyanobacteria). *European Journal of Phycology*, 33, 165–171.
- Hu, Q., Kurano, N., Kawachi, M., Iwasaki, I., & Miyachi, S. (1998c). Ultrahigh-cell-density culture of a marine green alga *Chlorococcum littorale* in a flat-plate photobioreactor. *Applied Microbiology and Biotechnology*, 49, 655–662.
- Huerlimann, R., De Nys, R., & Heimann, K. (2010). Growth, lipid content, productivity, and fatty acid composition of tropical microalgae for scale-up production. *Biotechnology and Bioengineering*, 107, 245–257.
- Hultberg, M., Johnson, H.L., Bergstrand, K.J., & Carlsson, A.S. (2014). Impact of light quality on biomass production and fatty acid content in the microalga *Chlorella vulgaris*. *Bioresource Technology*, 159, 465-467.
- Hyndman, R.J., & Koehler, A.B. (2006). Another look at measures of forecast accuracy. *International Journal of Forecasting*, 22(4), 679–688.
- Ibifubara, H., Chendo, M.A.C., Njah, A.N., & Nwankwo, D.I. (2019). *Optimization of microalgae growth for biofuel production using a new empirical dynamic model*, *Biofuels*, DOI: 10.1080/17597269.2019.1608012
- Iluz, D., & Abu-Ghosh, S. (2016). A novel photobioreactor creating fluctuating light from solar energy for a higher light-to-biomass conversion efficiency. *Energy Conversion and Management*, 126, 767–773.

- Iluz, D., Yehoshua, Y., & Dubinsky, Z. (2008). Quantum yields of phytoplankton photosynthesis in the Gulf of Aqaba (Elat), Northern Red Sea. *Israel Journal of Plant Sciences*, *56*, 29–36.
- International Energy Agency (IEA). (2008). Bioenergy, from 1<sup>st</sup>-to 2<sup>nd</sup>-generation biofuel technologies: An overview of current industry and R and D Activities.
- IEA. (2010). *Key world energy statistics 2010*.
- IEA, (2015). *Energy Statistical Manual*. International Energy Agency.
- Islam, M.A., Magnusson, M., Brown, R.J., Ayoko, G.A., Nabi, M.N., & Heinmann, K. (2013). Microalgal species selection for biodiesel production based on fuel properties derived from fatty acid profiles. *Energies*, *6*, 5676-5702.
- Jeong, G., & Don-Hee Park, D.H. (2009). Optimization of biodiesel production from castor oil using response surface methodology. *Applied Biochemistry and Biotechnology*, *156*, 1–11.
- Jo, S., Do, J., Na, H., Hong, J. W., Kim, I., & Yoon, H. (2020). Assessment of biomass potentials of microalgal communities in open pond raceways using mass cultivation. *PeerJ*, *8*, e9418.
- Jorquera, O., Kiperstok, A., Sales, E.A., Embirucu, M., & Ghirardi, M.L. (2010). Comparative energy lifecycle analyses of microalgal biomass production in open ponds and photobioreactors. *Bioresource Technology*, *101*, 1406-1413.
- Juneja, A., Ceballos, R.M., & Murthy, G.S. (2013). Effects of environmental factors and nutrient availability on the biochemical composition of algae for biofuels production: a review. *Energies*, *6*(9):4607-38. doi: 10.3390/en6094607.
- Kalpesh, K.S., Holger, S., & Peer, M.S. (2012). High lipid induction microalgae for biodiesel production. *Energies* *5*, 1532-1553.

- Kamau, A.N., Njogu, P., Kinyua, R., & Sessay, M. (2015). Sustainability Challenges and Opportunities of Generating Biogas from Water Hyacinth in Ndunga Village, Kenya. In *Proceedings of the 2015 Sustainable Research and Innovation (SRI) Conference, Nairobi, Kenya 6 - 8 May, 14-22*.
- Kennedy, J., & Eberhart, R.C. (1995). Particle swarm optimization, In *Proceedings of the 1995 IEEE International Conference on Neural Networks*, IEEE Service Center, Piscataway, NJ.
- Khan, S.A., Rashmi, M., Hussain, Z., Prasad, S., & Banerjee, U.C. (2009). Prospects of biodiesel production from microalgae in India. *Renewable and Sustainable Energy Reviews, 13*, 2361-2377.
- Khatiwada, D. (2013). Assessing the sustainability of bioethanol production in different development contexts: A system approach. (Doctoral Thesis). KTH University, Sweden.
- Khoeyi, Z.A., Seyfabadi, J., & Ramezanpour, Z. (2012). Effect of light intensity and photoperiod on biomass and fatty acid composition of the microalgae, *Chlorella vulgaris*. *Aquaculture International, 20*(1), 41-49.
- Kim, D.G. & Choi, Y.E. (2014). Microalgae cultivation using LED light. *Korean Chemical Engineering Research, 52* (1), 8-16.
- Knothe, G. (2005). Dependence of biodiesel fuel properties on the structure of fatty acid alkyl esters. *Fuel Processing Technology, 86*(10), 1059-1070.
- Knothe, G. (2008). "Designer" biodiesel: Optimizing fatty ester composition to improve fuel properties. *Energy fuels, 22*, 1358-64.
- Knothe, G. (2009). Improving biodiesel fuel properties by modifying fatty ester composition. *Energy and Environmental Science, 2*, 759-766.

- Knothe, G. (2010). Biodiesel and renewable diesel: A comparison. *Progress in Energy and Combustion Science*, 36, 364-373.
- Komarek J., & Fott, B. (1983). Chlorophyceae (Grünalgen), Ordnung, Chlorococcales. In G. Huber-Pestalozzi (Ed.), *Das Phytoplankton des Süßwassers, Die Binnengewässer*, (pp. 1–104). Stuttgart: E. Schweizerbart'sche Verlagsbuchhandlung.
- Kothari, C.R. (Ed.). (2004). *Research Methodology: Methods & techniques*. New Delhi, India: New Age International (P) Ltd.
- Kumar, A. (2015). Transesterification of *Croton megalocarpus* oil by heterogeneous catalysis and microwave irradiation – reaction kinetics and process optimization. (PhD thesis). Moi University, Eldoret, Kenya.
- Kumar, A., Pathak, A.K., & Guria, C. (2015). NPK-10:26:26 complex fertilizer assisted optimal cultivation of *Dunaliella tertiolecta* using response surface methodology and genetic algorithm. *Bioresource Technology*, 194, 117-129.
- Kunjapur, A.M., & Eldridge, R.B. (2010). Photobioreactor design for commercial biofuel production from microalgae. *Industrial and Engineering Chemistry Research*, 49, 3516–3526.
- Lam, M.K., Lee, K.T., & Mohamed, A.R. (2009). Life cycle assessment for the production of biodiesel: A case study in Malaysia for palm oil versus jatropha oil. *Biofuels Bioproducts and Biorefining*, 3(6), 601–612.
- Lam, M.K., & Lee, K.T. (2011). Renewable and sustainable bioenergies production from palm oil mill effluent (POME): Win–win strategies toward better environmental protection. *Biotechnology Advances*, 29, 124–141.

- Lam, M.K., & Lee, K.T. (2012). Microalgae biofuels: A critical review of issues, problems and the way forward. *Biotechnology Advances*, 30, 673-690.
- Lam, M.K., & Lee, K.T. (2014). Cultivation of *Chlorella vulgaris* in a pilot-scale sequential-baffled column photobioreactor for biomass and biodiesel production. *Energy Conversion and Management*, 88, 399-410.
- Lapuerta, M., Rodríguez-Fernández, J., & De Mora, E.F. (2009). Correlation for the estimation of the cetane number of biodiesel fuels and implications on the iodine number. *Energy Policy*, 37, 4337-4344.
- Larson, E. (2008). Biofuel production technologies: Status, prospects and implications for trade and development. United Nations Conference on Trade and Development, New York and Geneva.
- Latasa, M. (1995). Pigment composition of *Heterocapsa* sp. and *Thalassiosira weissflogii* growing in batch cultures under different irradiances. *Scientia Marina*, 59 (1), 25-37.
- Lavens, P., & Sorgeloos, P. (1996). *Manual on the production and use of live food for aquaculture*.
- Lee, J.Y., Yoo, C., Jun, S.Y., Ahn, C.Y., & Oh, H.M. (2010). Comparison of several methods for effective lipid extraction from microalgae. *Bioresource Technology*, 101, S75-S77.
- Lee, K., Eisterhold, M.L., Rindi, F., Palanisami, S., & Nam, P.K. (2014). Isolation and screening of microalgae from natural habitats in the Midwestern United States of America for biomass and biodiesel sources. *Journal of Natural Science, Biology and Medicine*, 5(2), 333-339.

- Li, X.F., Xu, H., & Wu, Q.Y. (2007). Large-scale biodiesel production from microalga *Chlorella protothecoides* through heterotrophic cultivation in bioreactors. *Biotechnology and Bioengineering*, 98, 764-771.
- Li, Y., Horsman, M., Wu, N., Lan, C. Q., & Dubois-Calero, N. (2008). Biofuels from microalgae. *Biotechnology Progress*, 24, 815- 820.
- Luque, R., Herrero-Davila, L., Campelo, J.M., Clark, J.H., Hidalgo, J.M., Luna, D., Marinas, J.M., & Romero, A.A. (2008). Biofuels: A technological perspective. *Energy and Environmental Science*, 1(5), 542-564.
- Machandi, J.M. (2021). *Life cycle analysis of bioethanol production from sugarcane molasses and sweet sorghum stalk juice in Kenya* (PhD thesis). Jomo Kenyatta University of Agriculture and Technology, Juja, Kenya.
- Mahapatra, D. M., Chanakya, H.N., & Ramachandra, T.V. (2013). *Euglena* sp. as a suitable source of lipids for potential use as biofuel and sustainable wastewater treatment. *Journal of Applied Phycology*, 25(3), 855-865.
- Mahmoud, E.A., Farahat, L.A., Abdel Aziz, Z.K., Fathallah, N.A., & Salah El Din, R.A. (2015). Evaluation of the potential for some isolated microalgae to produce biodiesel. *Egyptian Journal of Petroleum*, 24, 97-101.
- Mandotra, S.K., Kumar, P., Suseela, M. R., & Ramteke, P.W. (2014). Fresh water green microalga *Scenedesmus abundans*: A potential feedstock for high quality biodiesel production. *Bioresource Technology*, 156, 42-47.
- Manikan, V., Kalil, M.S., & Hamid, A.A. (2015). Response surface optimization of culture medium for enhanced docosahexaenoic acid production by a Malaysian thraustochytrid. *Scientific Reports*, 5, 8611.

- Martin, J. (2013). The billion gallon challenge: Getting biofuels back on track. Washington, DC: *Union of Concerned Scientists*.
- Masojidek, J., Papacek, S., Sergejevova, M., Jirka, V., Cervený, J., Kunc, J., & Stys, D. (2003). A closed solar photobioreactor for cultivation of microalgae under supra-high irradiance: Basic design and performance. *Journal of Applied Phycology*, *15*, 239-248.
- Mata, T.M., Martins, A.A., & Caetano, N.S. (2010). Microalgae for biodiesel production and other applications: A review. *Renewable and Sustainable Energy Reviews*, *14*, 217–232.
- Matthijs, H.C., Balke, H., Van Hes, U.M., Kroon, B.M., Mur, L.R., & Binot, R.A. (1996). Application of light-emitting diodes in bioreactors: Flashing light effects and energy economy in algal culture (*Chlorella pyrenoidosa*). *Biotechnology and Bioengineering*, *50*(1), 98-107.
- Meiser, A., Schmid-Staiger, U., & Trosch, W. (2004). Optimization of eicosapentaenoic acid production by *Phaeodactylum tricornerutum* in the flat panel airlift (FPA) reactor. *Journal of Applied Phycology*, *16*, 215– 225.
- Metropolis, N., Rosenbluth, A., Rosenbluth, M., Teller, A., & Teller, E. (1953). Equation of state calculations by fast computing machines. *Journal of Chemical Physics*, *21* (6), 1087–1092.
- Metsoviti, M.N., Papapolymerou, G., Karapanagiotidis, I.T., & Katsoulas, N. (2020). Effect of light intensity and quality on growth rate and composition of *Chlorella vulgaris*. *Plants*, *9*, 31.
- Miao, X., & Wu, Q. (2006). Biodiesel production from heterotrophic microalgal oil. *Bioresource Technology*, *97*, 841-846.



- Miguel, A.C., Xiaodong, D., & Govinda, R.T. (2010). Second – generation biofuels: Economics and policies. Development Research Group. The World Bank.
- Mitchell D. (2011). Biofuels in Africa: Opportunities, Prospects and Challenges. Washington, DC: World Bank.
- Mohn, F.M. (1980). Experiences and strategies in the recovery of biomass from mass cultures of microalgae. In *Algal Biomass*; Shelef, G., Soeder, C.J., (Eds.), Elsevier: Amsterdam, The Netherlands.
- Montgomery, D.C. (2013). *Design and Analysis of Experiments*, Chapter 11, John Wiley & Sons, Inc. Singapore.
- Moraes, M., Piedade, B. M., & Caldarelli, C. (2016). Accelerated growth of the sugarcane, sugar, and ethanol sectors in Brazil (2000–2008): Effects on municipal gross domestic product per capita in the South-Central Region. *Biomass Bioenergy*, 91, 116–125.
- Morweiser, M., Kruse, O., Hankamer, B., & Posten, C. (2010). Developments and perspectives of photobioreactors for biofuel production. *Applied Microbiology and Biotechnology*, 87, 1291–1301
- Mukabane, B.G. (2015). Utilization of sweet sorghum: Production of bioethanol from non-edible part and evaluation of the juice crystallization potential (Master's thesis). Jomo Kenyatta University of Agriculture and Technology, Juja, Kenya.
- Muller, P., Li, X.P., & Niyogi, K.K. (2001). Non-photochemical quenching. A response to excess light energy. *Plant Physiology*, 125, 1558–1566.
- Munir, N., Imtiaz, A., Sharif, N., & Naz, S. (2015). Optimization of growth conditions of different algal strains and determination of their lipid contents. *The Journal of Animal and Plant Sciences*, 25(2), 546-553.

- Munoz, R., & Guieysse, B. (2006). Algal–bacterial processes for the treatment of hazardous contaminants: A review. *Water Research*, 40(15), 2799-2815.
- Muruga, B.N. (2015). Effect of phage infection and selected physico-chemical factors on growth patterns of proteobacteria and cyanobacteria in Lake Magadi, Kenya. (PhD thesis). The University of Nairobi, Kenya.
- Mwakabuta N., & Sekar, A. (2008). “Study of the application of evolutionary algorithms for the solution of capacitor deployment problem in distribution systems” in Proc. The 40th Southern Symposium on System Theory, USA.178-182, March 2008.
- Nichols, H.W. (1973). Growth Media-Freshwater. In J. Stein (Ed.), *Handbook of Phycological methods, culture methods and growth measurements* (pp. 7-24). Cambridge University Press: Cambridge, UK.
- Ojo, E.O., Auta, H., Baganz, F., & Lye, G.J. (2015). Design and parallelisation of a miniature photobioreactor platform for microalgal culture evaluation and optimization. *Biochemical Engineering Journal*, 103, 93-102.
- Ondimu, S., Raude, J.M., & Wanjala, G. (2019). Personal computer-based control and monitoring system for biodiesel algae photobioreactor. *Journal of Engineering in Agriculture and the Environment*, 5(1), 31-40.
- Oswald, W.J. (2003). My sixty years in applied algology. *Journal of Applied Phycology*, 15, 99–106.
- Panahi, Y., Khosroshahi, A.Y., Sahebkar, A., & Heidari, H.R. (2019). Impact of cultivation condition and media content on *Chlorella vulgaris* Composition. *Advanced Pharmaceutical Bulletin*, 9(2), 182-194.
- Pandey, J. P., & Tiwari, A. (2010). Optimization of biomass production of *Spirulina maxima*. *Journal of Algal Biomass*, 1, 20-32.

- Pandey, J., Tiwari, A., Singh, S., & Tiwari, D. (2011). Potential of different light intensities on the productivity of *Spirulina maxima*. *Journal of Algal Biomass Utilization*, 2, 9-14.
- Park, K.C., Whitney, C., McNichol, J.C., Dickinson, K.F., MacQuarrie, S., Skrupski, B.P., & McGinn, P.J. (2012). Mixotrophic and photoautotrophic cultivation of 14 microalgae isolates from Saskatchewan, Canada: Potential applications for wastewater remediation for biofuel production. *Journal of Applied Phycology*, 24, 339-348.
- Park, S., Ahn, Y., Pandi, K., Ji, M., Yun, H., & Choi, J. (2019). Microalgae cultivation in pilot scale for biomass production using exhaust gas from thermal power plants. *Energies*, 12, 1-10.
- Patil, V., T. Källqvist, T., Olsen, E., Vogt, G., & Gislerød, H.R. (2007). Fatty acid composition of 12 microalgae for possible use in aquaculture feed. *Aquaculture International*, 15(1), 1-9.
- Patil, P.D., Gude, V.G., Mannarswamy, A., Deng, S.G., Cooke, P., S. Munson-McGee, S., & Nirmalakhandan, N. (2011). Optimization of direct conversion of wet algae to biodiesel under supercritical methanol conditions. *Bioresource Technology*, 102, 118–122.
- Pattanaik, A., Sukla, L.B., & D. Pradhan, D. (2018). Effect of LED lights on the growth of microalgae. *Inglomayor*, 14, 17-24.
- Perez-Garcia, O., Escalante, F. M. E., De-Bashan, L. E., & Bashan, Y. (2011). Heterotrophic cultures of microalgae: Metabolism and potential products. *Water Research*, 45, 11–36.
- Perez-Lopez, P., De Vree, J.H., Feijoo, G.D., Bosma, R., Barbosa, M.J., Moreira, M.T., Wijffels, R.H., Van Boxtel, A.J.B., & Kleinegris, D. (2017). Comparative life

- cycle assessment of real pilot reactors for microalgae cultivation in different seasons. *Applied Energy*, 205, 1151–1164.
- Pertoft, H., Laurent, T. C., Låås, T., & Kågedal, L. (1978). Density gradients prepared from colloidal silica particles coated by polyvinylpyrrolidone (percoll). *Analytical biochemistry*, 88(1), 271–282.
- Pienkos, P.T., & Darzins, A. (2009). The promise and challenges of microalgal derived biofuels. *Biofuels, Bioproducts and Biorefining*, 3, 431-440.
- Prabuthas, P., Srivastav, P.P., & Mishra, H.N. (2011). Optimization of environmental factors using RSM for *Spirulina platensis* cultivation. *Nutrition and Food Science*, 41(3), 175-182.
- Priyadarshani, I., & B. Rath, B. (2012). Commercial and industrial applications of micro algae: A review. *Journal of Algal Biomass Utilization*, 3(4), 89-100.
- Puspanadan, S., Wong, X.J., & Lee, C.K. (2018). Optimization of freshwater microalgae, *Arthrospira* sp. (*Spirulina*) for high starch production. *International Food Research Journal*, 25(3), 1266-1272.
- Ramadhas, A.S., Jayaraj, S., Muraleedharan, C., & Padmakumari, K. (2006). Artificial neural networks used for the prediction of the cetane number of biodiesel. *Renewable Energy*, 31(15), 2524-2533.
- Rao, S.S. (1987). Description and optimum design of fuzzy mechanical systems, *American Society of Mechanical Engineers Journal of Mechanisms, Transmissions, and Automation in Design*, 109, 126–132.
- Rao, S.S. (2009). *Engineering optimization: Theory and practice*. (4<sup>th</sup> ed.). Hoboken, New Jersey: John Wiley & Sons.

- Rao, S.S., Sundararaju, K., Prakash, K.B.G., & Balakrishna, C. (1992). A fuzzy goal programming approach for structural optimization, *American Institute of Aeronautics and Astronautics Journal*, 30(5), 1425–1432.
- Rawat, I., Kumar, R.R., Mutanda, T., & Bux, F. (2011). Dual role of microalgae: Phycoremediation of domestic wastewater and biomass production for sustainable biofuels production. *Applied Energy*, 88(10), 3411-3424.
- Ren, H., Tuo, J., Addy, M.M., Zhang, R., Lu, Q., Anderson, E., Chen, P., & Ruan, R. (2017). Cultivation of *Chlorella vulgaris* in a pilot-scale photobioreactor using real centrate wastewater with waste glycerol for improving microalgae biomass production and wastewater nutrients. *Bioresource Technology*, 245, 1130-1138.
- Renaud, S.M., Thinh, L.V., Lambrinidis, G., & Parry, D.L. (2002). Effect of temperature on growth, chemical composition and fatty acid composition of tropical Australian microalgae grown in batch cultures. *Aquaculture*, 211, 195–214.
- Richmond, A. (2000). Microalgal biotechnology at the turn of the millenium: A personal view. *Journal of Applied Phycology*, 12, 441–451.
- Richmond, A. (2008). *Handbook of microalgal culture: biotechnology and applied phycology*. Wiley-Blackwell.
- Richmond, A., & Cheng-Wu, Z. (2001). Optimization of a flat plate glass reactor for mass production of *Nannochloropsis* sp. outdoors. *Journal of Biotechnology*, 85, 259–269.
- Richmond, A., Zhang, C.W., & Zarmi, Y. (2003). Efficient use of strong light for high photosynthetic productivity: Interrelationships between the optical path, the optimal population density and cell-growth inhibition. *Biomolecular Engineering*, 20, 229–236.

- Rodolf, L., Zittelli, G.C., Bassi, N., Padovani, G., Biondi, N., Bonini, G., & Tredici, M.R. (2009). Microalgae for oil: strain selection, induction of lipid synthesis and outdoor mass cultivation in a low-cost photobioreactor. *Biotechnology and Bioengineering*, *102*, 100–112.
- Rolfe, M. D., Rice, C.J., Lucchini, S., Pin, C., Thompson, A., Cameron, A.D.S., Alston, M., Stringer, M.F., Betts, R.P., & Baranyi, J. (2012). Lag phase is a distinct growth phase that prepares bacteria for exponential growth and involves transient metal accumulation. *Journal of Bacteriology*, *194*(3), 686-701.
- Ruffing, A. M. (2011). Engineered cyanobacteria: Teaching an old bug new tricks. *Bioengineered bugs*, *2*(3), 136-149.
- Salim, S., Bosma, R., Vermue, M.H., & VWijffels, R.H. (2011). Harvesting of microalgae by biofloculations. *Journal of Applied Phycology*, *23*, 849–855.
- Sandnes, J.M., Källqvist, T., Wenner, D., & Gislerød, H.R. (2005). Combined influence of light and temperature on growth rates of *Nannochloropsis oceanica*: Linking cellular responses to large-scale biomass production. *Journal of Applied Phycology*, *17*(6), 515-525.
- Schenk, P.M., Thomas-Hall, S.R., Stephens, E., Marx, U.C, Mussgnug, J.M., Posten, C., & Hankamer, B. (2008). Second generation biofuels: High-efficiency microalgae for biodiesel production. *Bioenergy Research*, *1*, 20-43.
- Seyfabadi, J., Ramezanpour, Z., & Khoeyi, Z.A. (2011). Protein, fatty acid, and pigment content of *Chlorella vulgaris* under different light regimes. *Journal of Applied Phycology*, *23*(4), 721-726.
- Sforzaa, E., Bertucco, A., Morosinotto, T., & Giacometti, G.M. (2012). Photobioreactors for microalgal growth and oil production with *Nannochloropsis salina*: From lab-

- scale experiments to large-scale design. *Chemical engineering research and design*, 90, 1151–1158.
- Shah, V., Jurjevic, M., & Badia, D. (2007). Utilization of restaurant waste oil as a precursor for sophorolipid production. *Biotechnology Progress*, 23(2), 512-515.
- Sheehan, J., Dunahay, T., & Benemann, J. (1998). A look at the U.S. Department of Energy's Aquatic Species Program: Biodiesel from algae; National Renewable Energy Laboratory: Golden, Colorado, USA.
- Shelef, G., Sukenick, A., & Green, M. (1984). Microalgae harvesting and processing: A literature review; report number: SERI/STR-231-2396: Solar Energy Research Institute, US Department of Energy: Oak Ridge, TN, USA.
- Shi, Y., & Eberhart, R.C. (1998). Parameter selection in particle swarm optimization, Proceedings of the Seventh Annual Conference on Evolutionary Programming, V. W. Porto, N. Saravanan, D. Waagen, and A. Eibe, Eds., Springer-Verlag, 591–600, Berlin, Germany.
- Sierra, E., Acien, F.G., Fernandez, J.M., Garcia, J.L., Gonzalez, C., & Molina, E. (2008). Characterization of a flat plate photobioreactor for the production of microalgae. *Chemical Engineering Journal*, 138, 136–147.
- Singh, J., & Gu, S. (2010). Commercialization potential of microalgae for biofuels production. *Renewable and Sustainable Energy Reviews*, 14(9), 2596–2610.
- Singh, A., Nigam, P.S., & Murphy, J.D. (2011). Renewable fuels from algae: An answer to debatable land based fuels. *Bioresource Technology*, 102(1), 10-16.
- Singh, A., Nigam, P.S., & Murphy, J.D. (2011). Mechanism and challenges in commercialization of algal biofuels. *Bioresource Technology*, 102, 26-34.

- Slade, R., & Bauen, A. (2013). Micro-algae cultivation for biofuels: Cost, energy balance, environmental impacts and future prospects. *Biomass Bioenergy*, *53*, 29-38.
- Soratana, K. & Landis, A.E. (2011). Evaluating industrial symbiosis and algae cultivation from a life cycle perspective. *Bioresource Technology*, *102*, 6892–6901.
- Spilling, K., Seppala, J., & Tamminen, T. (2009). A potential low-cost method for harvesting microalgae using high pH and regulation of particle encounter rate. *Water Science and Technology*, *52*, 9-18.
- Stephens, E., Ross, I.L., Mussnug, J.H., Wagner, L.D., Borowitzka, M.A., Posten, C., Kruse, O., & Hankamer, B. (2010). Future prospects of microalgal biofuel production systems. *Trends in Plant Science*, *15*, 554–564
- Sukenik, A., Bilanovic, D., & Shelef, G. (1988). Flocculation of microalgae in brackish and sea waters. *Biomass*, *15*, 187–199.
- Tan, J.S., Lee, S.Y., Chew, K.W., Lam, M.K., Lim, J.W., Ho, S., & Sow, P.L. (2020). A review on microalgae cultivation and harvesting, and their biomass extraction processing using ionic liquids. *Bioengineered*, *11*(1), 116-129.
- Taufiqurrahmi, N., & Bhatia, S. (2011). Catalytic cracking of edible and non-edible oils for production of biofuels. *Energy & Environmental Science*, *4*, 1087-1112.
- Thangavel, K., Krishnan, P.R., Nagaiah, S., Kuppasamy, S., Chinnasamy, S., Rajadorai, J.S., Olaganathan, G.N., & Dananjeyan, B. (2018). Growth and metabolic characteristics of oleaginous microalgal isolates from Nilgiri biosphere Reserve of India. *BMC Microbiology*, *18*, 1-17.
- Thornton, D.C.O. (2009). Effect of low pH on carbohydrate production by a marine planktonic diatom (*Chaetoceros muelleri*). *Research Letters in Ecology*, 2009. 1–4.



- Ting, H., Haifeng, L., Shanshan, M., Zhang, Y., Zhidan, L., & Na, D. (2017). Progress in microalgae cultivation photobioreactors and applications in wastewater treatment: A review. *International Journal of Agricultural and Biological Engineering*, 10(1), 301-310.
- Tredici M.R. (2010). Photobiology of microalgae mass cultures: understanding the tools for the next green revolution. *Biofuels*, 1, 143–162.
- Tredici, M.R., & Zittelli, G.C. (1998). Efficiency of sunlight utilization: Tubular versus photobioreactors. *Biotechnology and Bioengineering*, 57, 187– 197.
- Uduman, N., Qi, Y., Danquah, M.K., Forde, G.M., & Hoadley, A. (2010). Dewatering of microalgal cultures: A major bottleneck to algae-based fuels. *Journal of Renewable and Sustainable Energy*, 2, 012701.
- Vasker, B., Ben-Zion, M., Kinel-Tahan, Y., Dubinsky, Z., Grobbelaar, J., Yudkin, H., & Yehoshua, Y. (2021). Computerized optimization of microalgal photosynthesis and Growth. *Applied Phycology*, 2(1), 22-30.
- Van Bodegom, P. (2007). Microbial maintenance: A critical review on its quantification. *Microbial Ecology*, 53, 513–523.
- Verawaty, M., Melwita, E., Apsari, P., & Mayumi, M. (2017). Cultivation strategy for freshwater macro-and micro-algae as biomass stock for lipid production. *Journal of Engineering and Technological Sciences*, 49(2), 261-274.
- Vicente, G., Coteron, A., Martinez, M., & Aracil, J. (1998). Application of the factorial design of experiments and response surface methodology to optimize biodiesel production. *Industrial Crops and Products*, 8, 29–35.

- Wahidin, S., Idris, A., & Shaleh, S.R.M. (2013). The influence of light intensity and photoperiod on the growth and lipid content of microalgae *Nannochloropsis* sp. *Bioresource Technology*, *129*, 7-11.
- Wang, C.Y., Fu, C.C., & Liu, Y.C. (2007). Effects of using light-emitting diodes on the cultivation of *Spirulina platensis*. *Biochemical Engineering Journal*, *37*(1), 21-25.
- Wang, B., Li, Y., Wu, N., & Lan, C.Q. (2008). CO<sub>2</sub> bio-mitigation using microalgae. *Applied Microbiology and Biotechnology*, *79*, 707–718.
- Wang, B., Lan, C.Q., & Horsman, M. (2012). Closed photobioreactors for production of microalgal biomasses. *Biotechnology Advances*, *30*, 904–912.
- Wang, H.Y., Fu, R., & Pei, G.F. (2012). A study on lipid production of the mixotrophic microalgae *Phaeodactylum tricornutum* on various carbon sources. *African Journal of Microbiology Research*, *6*, 1041- 1047.
- Wen, X., Du, K., Wang, Z., Peng, X., Luo, L., Tao, H., Xu, Y., Zhang, D., Geng, Y., & Li, Y. (2016). Effective cultivation of microalgae for biofuel production: A pilot-scale evaluation of a novel oleaginous microalga *Graesiella* sp. WBG-1. *Biotechnology for Biofuels*, *9*, 123.
- Whitelam, G. C., Lanaras, T., & Codd, G. A. (1983). Rapid separation of microalgae by density gradient centrifugation in percoll. *British Phycological Journal*, *18*(1), 23–28.
- World Watch Institute (WWI), Biofuels for Transport: “Global Potential and Implications for Sustainable Energy and Agriculture.” Eds S. 2007. Hunt. Sterling VA.
- Wu, X., Ruan, R., Du, Z., & Liu, Y. (2012). Current status and prospects of biodiesel production from microalgae. *Energies*, *5*, 2667-2682.

- Wu, Z.Y., & Shi, X.M. (2006). Optimization for high-density cultivation of heterotrophic *Chlorella* based on a hybrid neural network model. *Letters in Applied Microbiology*, *44*, 13-18.
- Xu, L., Weathers, P.J., Xiong, X.R., & Liu, C.Z. (2009). Microalgal bioreactors: Challenges and opportunities. *Engineering in Life Sciences*, *9*, 178–189.
- Yuryevich, J., & Wong, K.P. (1999). Evolutionary programming based power flow algorithm. *IEEE Transactions Power Systems*, *14*(4), 1245-1250.
- Zhang, G.P. (2003). Time series forecasting using a hybrid ARIMA and neural network Model. *Neurocomputing*, *50*, 159–175.
- Zhang, G.P. (2007). A neural network ensemble method with jittered training data for time series forecasting. *Information Sciences*, *177*, 5329–5346.
- Zhang, Y., Dube, M.A., McLean, D.D., & Kates, M. (2003). Biodiesel production from waste cooking oil: Economic assessment and sensitivity analysis. *Bioresource Technology*, *90*, 229–240.
- Zijffers, J.W.F., Janssen, M., Tramper, J., & Wijffels, R.H. (2008). Design process of an area efficient photobioreactor. *Marine Biotechnology*, *10*, 404–41.
- Zijffers, J.F., Schippers, K.J., Zheng, K., Janssen, M., Tramper, J., & Wijffels, R.H. (2010). Maximum photosynthetic yield of green microalgae in photobioreactors. *Marine Biotechnology*, *12*, 708–718.

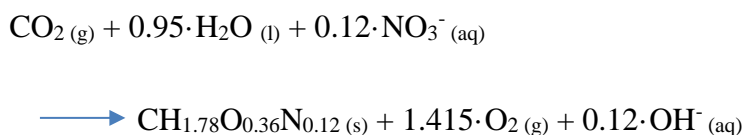
## APPENDICES

### Appendix I: Determination of Photosynthetic Efficiency

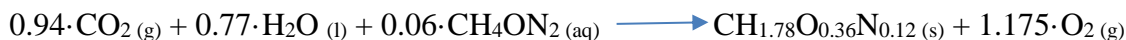
#### Appendix IA: Determination of theoretical biomass yield on light energy

The theoretical biomass yield on light energy was calculated based on the stoichiometric reaction equations for the formation of biomass on carbon dioxide, water, and the nitrogen source used in the cultivation (Duboc *et al.*, 1999):

For growth on nitrate:



For growth on urea:



The yield of the light reactions is assumed to be 0.1 mol of oxygen per mole of photons within the PAR spectrum. This value represents the maximal quantum yield as determined under low light by several independent researchers over the past decades (Zijffers *et al.*, 2010).

Assuming the *Chlorella* sp. (round strain) isolated and used in the model validation has the same elemental composition of  $\text{C}_{1.78}\text{O}_{0.36}\text{N}_{0.12}$  as found for *Chlorella Spain* sp. (Duboc *et al.* 1999), the molecular mass of a C-mol biomass is  $21.22 \text{ gmol}^{-1}$ . To form one C-mol of biomass, 14.15 or 11.75 mol of photons are required to evolve the required amount of oxygen for growth on nitrate and urea, respectively, following the stoichiometric reaction equations. This leads to a theoretical biomass yield of 1.5 and  $1.8 \text{ gmol.photons}^{-1}$  for growth on nitrate and urea, respectively.



## Appendix II: Analysis of Variance

### Appendix IIA: TWO-WAY ANOVA technique in context of two-way design when repeated values are not present

The various steps involved are as follows (Kothari, 2004):

- i. The total number of the values of individual items was taken in all the samples and denoted by  $T$ .
- ii. The correction factor was then worked out as under:

- a. Correction factor =  $\frac{(T)^2}{n}$

- iii. The square of all the item values was calculated one by one and then took its total. Then subtracted the correction factor from this total to get the sum of squares of deviations for total variance. Symbolically, this can be write as:

- a. Sum of squares of deviations for total variance or total SS

- b. 
$$= \sum X_{ij}^2 - \frac{(T)^2}{n}$$

- iv. Took the total of different columns and then obtained the square of each column total and divided such squared values of each column by the number of items in the concerning column and took the total of the result thus obtained. Finally, subtracted the correction factor from this total to obtain the sum of squares of deviations for variance between columns or (SS between columns).
- v. Took the total of different rows and then obtained the square of each row total and divided such squared values of each row by the number of items in the corresponding row and took the total of the result thus obtained. Finally, subtracted the correction factor from this total to obtain the sum of squares of deviations for variance between rows (or SS between rows).

**vi.** Sum of squares of deviations for residual or error variance were worked out by subtracting the result of the sum of (iv)th and (v)th steps from the result of (iii)th step stated above. In other words,

a.  $\text{Total SS} - (\text{SS between columns} + \text{SS between rows}) = \text{SS for residual or error variance.}$

**vii.** Degrees of freedom (d.f.) were worked out as under:

a. d.f. for total variance  $= (c.r - 1),$

b. d.f. for variance between columns  $= (c - 1),$

c. d.f. for variance between rows  $= (r - 1),$

d. d.f. for residual variance  $= (c - 1) (r - 1)$

e. Where  $c = \text{number of columns}$

1.  $r = \text{number of rows}$

**viii.** ANOVA table was then set up in the usual fashion as shown in Table B-1.

**Table B-1: Analysis of Variance Table for Two-way ANOVA**

<b>Source of variation</b>	<b>Sum of squares (SS)</b>	<b>Degrees of freedom (d.f.)</b>	<b>Mean square (MS)</b>	<b>F-ratio</b>
Between columns treatment	$\sum \frac{T_j^2}{n_j} - \frac{T^2}{n}$	$(c-1)$	$\frac{SS \text{ between columns}}{c-1}$	$\frac{MS \text{ between columns}}{MS \text{ residual}}$
Between rows treatment	$\sum \frac{T_i^2}{n_i} - \frac{T^2}{n}$	$r-1$	$\frac{SS \text{ between rows}}{r-1}$	$\frac{MS \text{ between rows}}{MS \text{ residual}}$
Residual or error	Total SS-(SS between columns + SS between rows)	$(c-1)(r-1)$	$\frac{SS \text{ Residual}}{(c-1)(r-1)}$	
Total	$\sum X_{ij}^2 - \frac{(T)^2}{n}$	$c.r-1$		



## **Appendix III: Publications**

### **Appendix IIIA: Publications in peer-reviewed journals**

1. **Mukabane, B.G.**, Gathitu, B., Mutwiwa, U., Njogu, P., Bilhah, E., & Ondimu, S. (2020). Optimization of Microalgae Production Conditions using Genetic Algorithm and Response Surface Methodology. *Journal of Engineering in Agriculture and the Environment*, 6(2), 40-60.
2. **Mukabane, B. G.**, Gathitu, B., Mutwiwa, U., Njogu, P., & Ondimu, S. (2018). Microalgae cultivation systems for biodiesel production: A review. *Journal of Sustainable Research in Engineering*. 4(4), 144-151.

### **Appendix IIIB: Manuscripts in conferences and workshop proceedings**

1. **Mukabane, B.G.**, Gathitu, B., Mutwiwa, U., Njogu, P., Bilhah, E., & Ondimu, S. (2020). Optimization of Microalgae Cultivation Conditions using Genetic Algorithm and Response Surface Methodology. *The International Sustainable Research and Innovation (SRI) virtual Conference; Sub-theme: Linking Industry with Academia through Engineering Research and Innovation, held at Jomo Kenyatta University of Agriculture and Technology (JKUAT), Juja, from 6<sup>th</sup>-7<sup>th</sup> October 2020.*
2. **Mukabane, B.G.**, Gathitu, B., Mutwiwa, U., Njogu, P., & Ondimu, S. (2018). Microalgal biodiesel: Status, Challenges and Prospects: A review. *The 3<sup>rd</sup> Kenya Association of Technical Training Institutions (KATTI) International Conference; Sub-theme: Technical Vocational Education Training (TVET) Agenda in Building Partnerships for Sustainable Development, held at Pride Inn Paradise Hotel, Mombasa, from 10<sup>th</sup> – 15<sup>th</sup> December 2018.*
3. **Mukabane, B.G.**, Gathitu, B., Mutwiwa, U., Njogu, P., & Ondimu, S. (2018). Microalgae Cultivation Systems for Biodiesel Production. *The 2<sup>nd</sup> TVET Fairs Research Conference; Sub-theme: Achieving Sustainable Development*

*through Science, Technology and Innovation, held at The Kisumu National Polytechnic, from 5<sup>th</sup> - 6<sup>th</sup> April 2018.*

4. **Mukabane, B.G.**, Gathitu, B., Mutwiwa, U., Njogu, P., & Ondimu, S. (2018). Microalgal biodiesel: Status, Challenges and Prospects. *The 1<sup>ST</sup> Pan African Society Conference for Agricultural Engineering (PASAE); Sub-theme: Engineering and Technology for Agriculture Transformation in Africa, held at Southern Sun Mayfair Hotel, Nairobi, from 26<sup>th</sup> – 28<sup>th</sup> March 2018.*
5. **Mukabane, B.G.**, Gathitu, B., Mutwiwa, U., Njogu, P., & Ondimu, S. (2018). Microalgae Cultivation Systems for Biodiesel Production. *The KATTI Nairobi region TVET fair/Exhibitions & Robotics contest; Sub-theme: Achieving sustainable development through Science, Technology and Innovations, held at Kajiado, from 8<sup>th</sup>-10<sup>th</sup> March 2018.*
6. **Mukabane, B.G.**, Gathitu, B., Mutwiwa, U., Njogu, P., & Ondimu, S. (2017). Microalgae Cultivation Systems for Biodiesel Production. *The 24<sup>th</sup> Engineers International Conference; Sub-theme: Engineering Innovations and Technical Solutions, held at the Intercontinental hotel, Nairobi, from 10<sup>th</sup>- 12<sup>th</sup> May 2017.*
7. **Mukabane, B.G.**, Gathitu, B., Mutwiwa, U., Njogu, P., & Ondimu, S. (2017). Microalgae Cultivation Systems for Biodiesel Production. *The International Sustainable Research and Innovation (SRI) Conference; Sub-theme: Engineering Innovations for Industrialization, held at Jomo Kenyatta University of Agriculture and Technology (JKUAT), Juja, from 3<sup>rd</sup>-5<sup>th</sup> May 2017.*